Investigating the role of vitamin K in Axl-mediated melanoma progression and chemotherapeutic resistance

Muntequa Ishtiaq Siraji

This dissertation is submitted in partial fulfilment of the requirements for the degree of Master of Science in Biomedical Sciences

Department of Biomedicine
Faculty of Medicine and Dentistry
University of Bergen
Bergen, Norway
2018

Acknowledgement

Foremost, I am grateful to the almighty for all his blessings towards me and for keeping me healthy throughout this study period. The work presented in this dissertation has been accomplished as a part of the Master of Science degree in Biomedical Sciences at the Department of Biomedicine, University of Bergen, in the period August 2016 to June 2018. The laborious work was carried out at CELLNET group.

My sincerest gratitude goes to my supervisors James B. Lorens, Niels Aarsæther and Stacey Ann Nicole D'mello for their excellent scientific guidance and support throughout this work period. I specially would like to thank James B. Lorens for giving me the opportunity to join and to work in his research group, CELLNET. I am very lucky to get the research opportunity in such an interesting and up to date field that fits to my research interest, with highly competent people.

My special appreciation and thanks goes to Niels Aarsæther for always being helpful and supportive, both in the lab and in the writing process. I sincerely thank and grateful to Post doc. Stacey Ann Nicole D'mello for her time and effort to assist me with her valuable suggestion, knowledge and laboratory guidance throughout this research project.

Besides my advisors, I would like to thank rest of my lab members; PhD candidate Kjersti Davidsen for her always encouraging and positive behavior towards me, Sturla Magnus Grøndal for being a great and supportive friend in the lab and also Sissel Vik Berge for supporting me with laboratory consumables. I also want to express my gratitude to rests of the lab members for their stimulating discussion, presentations and co-participations in the long tiring working days.

Last but not the least; I would like to thank my mother Kazi Helena Arju for her unconditional love, dedication and support in my entire life. I want to thank my wife Hanan Ashrafi for loving, supporting and believing in me. I also want to thank my rest of the family members and friends for supporting and encouraging me.

Bergen 2018

Muntequa Ishtiaq Siraji

Abstract

Metastatic melanoma is a highly aggressive cancer with a very poor prognosis and current therapies remain inadequate. Norway is among the top five countries with the highest incidence of melanoma.

Malignant cells carry oncogenic mutations that engender uncontrolled growth and elicit activation of epithelial-to-mesenchymal transition (EMT), an embryonic gene program that induces cancer stem cell features, invasiveness, survival, chemotherapeutic resistance, immune modulation and metastasis. The receptor tyrosine kinase, Axl, is upregulated with this EMT program and overexpressed in several human cancers. Axl is upregulated in a subset of more invasive tumors and thought to be an important facilitator of resistance to therapeutics targeted against oncogenic RTKs. Activation of Axl is dependent on the binding of its ligand Gas6. Gas6 is a vitamin K dependent protein that is modified by the γ-carboxylation of glutamic acid residues in the N-terminal Gla domain. Vitamin K serves as the cofactor for the enzyme γ-glutamyl carboxylase (GGCX) that catalyzes the γ-carboxylation of the glutamic acid residues. BGB324 is an Axl kinase inhibitor currently in ongoing clinical trial against different types of cancers.

Here we first characterized the expression of Axl, Gas6 and vitamin K enzymes such as GGCX in 20 melanoma cell lines and determine their correlation with clinical outcome. Our results suggest that GGCX but not Axl and Gas6 expression correlates with poor patient prognosis. We further evaluated the effect of vitamin K and BGB324 on 5 selected cell lines. We found that the vitamin K increases the expression of Axl and other TAM receptors, GGCX and EMT-related genes while when treated with BGB324 expression reduced or remained unchanged. However, BGB324 was not able to elicit this effect if the cells were cultured in vitamin K suggesting acquisition of a resistant phenotype. We also evaluated the effect of vitamin K on NZM cell proliferation, migration and spheroid formation. Finally, we show that vitamin K upregulated several plasticity markers in presence of vitamin K using mass cytometry (CyTOF).

Abbreviations

Akt	Protein kinase B (PKB)
APC	Adenomatous polyposis coli
BSA	Bovine serum albumin
CIM	Cell invasion/migration
CML	Chronic Myelogenous Leukemia
CTLA4	Anti-cytotoxic T lymphocyte antigen-4
DMSO	Dimethyl sulfoxide
ECM	Extracellular Matrix
EGF	Epidermal Growth Factor
EMT	Epithelial to Mesenchymal Transition
EGFR	Epidermal Growth Factor Receptor
HIF1	Hypoxia-inducible factor 1-alpha
EPHX1	Epoxide Hydrolase 1
GAPDH	Glyceraldehyde 3-phosphate dehydrogenase
GAS6	Growth Arrest-Specific 6
GDP	Guanosine Diphosphate
GGCX	Gamma-Glutamyl Carboxylase
Gla	Gamma-Carboxyglutamic Acid
GTP	Guanosine Triphosphate
Grb2	Growth factor receptor-bound protein 2
HCC	Hepatocellular carcinoma
HER2	Human epidermal growth factor receptor 2
LDH	Lactate dehydrogenase
MAPK	Mitogen Activated Protein Kinase
MITF	Microphthalmia-Associated Transcription Factor
α-MEM	α-modified minimal essential medium
NK	Natural Killer
NZM	New Zealand Melanoma
OS	Overall survival
PBS	Phosphate buffered saline
PD1	Programmed cell death protein 1
PI3K/AKT	Phosphoinositide 3-Kinase/AKT
PIs	Phosphoinositides
Pros 1	Protein S
PTEN	Phosphatase and Tensin homolog
RTKs	Receptor Tyrosine Kinases
RT-PCR	Real Time PCR
SD	Standard Deviation SDS
SDS	Sodium dodecyl sulfate
SHBG	Sex hormone-binding globulin
STAT1	Signal transducer and activator of transcription 1
TAM	Tyro3, Axl and Mer
TKs	Tyrosine Kinases
TLR	Toll Like receptor
VIM	Vimentin
VKORC	Vitamin K Epoxide Reductase

Table of Contents

1. Introduction

1.1 Cancer

Cancer is the second most cause of death after heart disease worldwide. It is characterized by aberrant cell proliferation endangered by multiple genetic modifications and somatic mutations in the cells, lead to the tumor formation. A tumor can achieve the ability to invade neighboring tissue and spread to healthy distant organs, by a process called metastasis [1, 2]. The inherent complexity of cancer makes it difficult to treat and explains why it is as one of the deadliest diseases worldwide. In 2012, the number of new cases of cancer diagnosed was 14.1 million and it was reported that 8.2 million died from this disease. Of all types of cancer, the most common types are epithelial-derived carcinomas of the lung, breast and colon; lung, liver and stomach cancers are the three most common causes of cancer related death worldwide [3].

In Norway, approximately 32827 new cancer cases were reported in 2016, where males contributed 54.1 % and females 45.9%. There were 10 944 deaths reported in Norway owing to cancer in 2015. Almost 50% of the cancer mortality are caused by the lung, colon, rectum, prostate and female breast cancer. The data in 2011 to 2015 from cancer registry in Norway showed that the melanoma is the sixth prevalent cancer in male and fourth in female as well as the mortality rate is high compared to other types of cancers (see Figure 1 & Figure 2) [4].

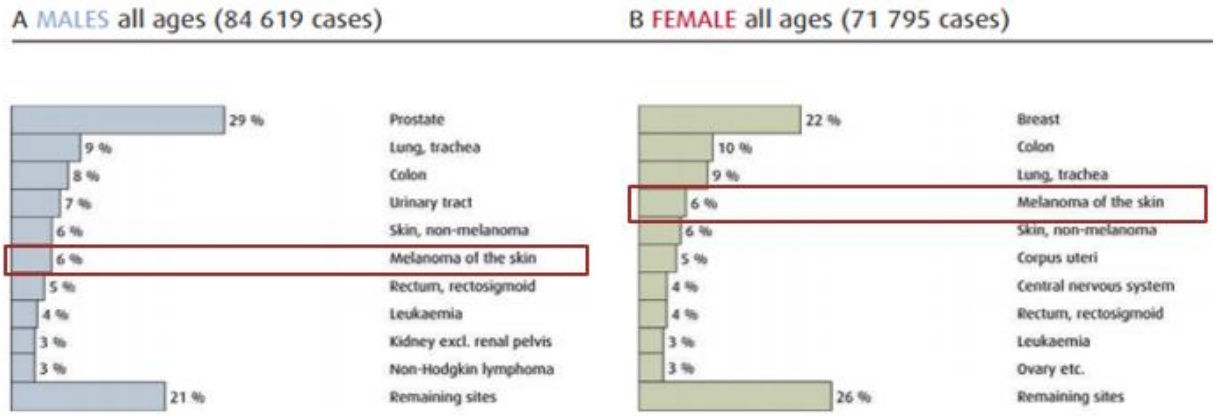

Figure 1: The most frequent types of cancer in Norway by sex, 2011–2015. Adapted from [4].

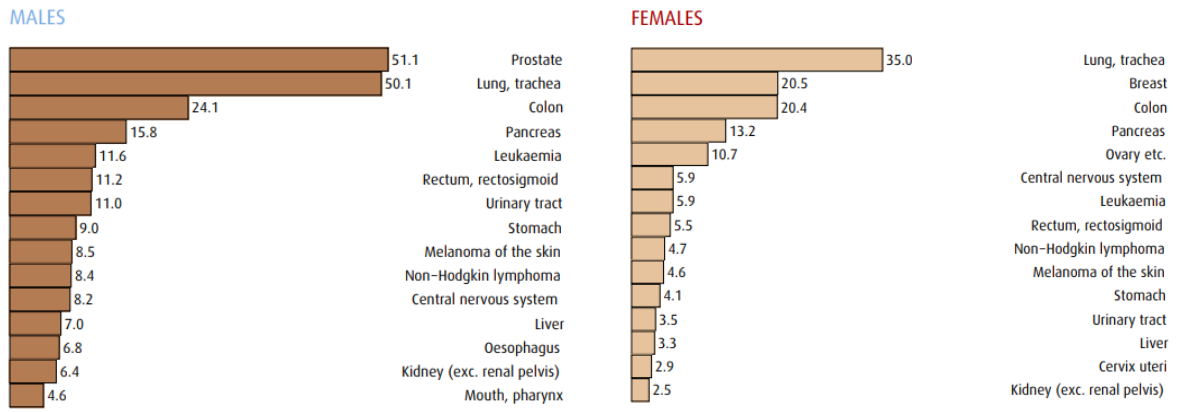

Figure 2: Age-standardized (Norwegian standard) mortality rates per 100 000 person-years for selected cancers, 2015 Adapted from [4].

1.2 Tumor heterogeneity

Cancer is very aggressive and dynamic disease. During progression tumors become increasingly heterogeneous. Different clones with distinct characteristics are found in tumors. The heterogeneity can be spatial and temporal. The spatial heterogeneity exhibits the variation of genetic makeup within and across the cells of a tumor subpopulation; and temporal heterogeneity is the alteration in molecular level in the tumor cell [5]. The genetic differences that are found within a tumor and between tumors are called intratumoral and intertumoral heterogeneity respectively. Tumors from different tissues of one patient and from same tissue of two different patients are phenotypically and genetically distant [6]. Moreover, different sub clones based on epigenetic and genetic differences are found in the same population of a tumor (see Figure 3). The genome of a cancer cell is unstable which leads to increased mutations and generation of diverse sub clones in a bulk tumor [7].

Different cancer types have different recurrent mutations. Colorectal cancer is often caused by the mutation in the tumor suppressor gene *APC*; a form of breast cancer is caused by the gene amplification of the *HER2* gene [8]; the *BRAF(V600E)* oncogenic mutation is common in melanoma as well as in colon cancer [9], and small cell lung cancer frequently exhibits activating EGFR receptor mutations [10]. Subsequent genetic instability and epigenetic reprogramming promotes tumor progression [11].

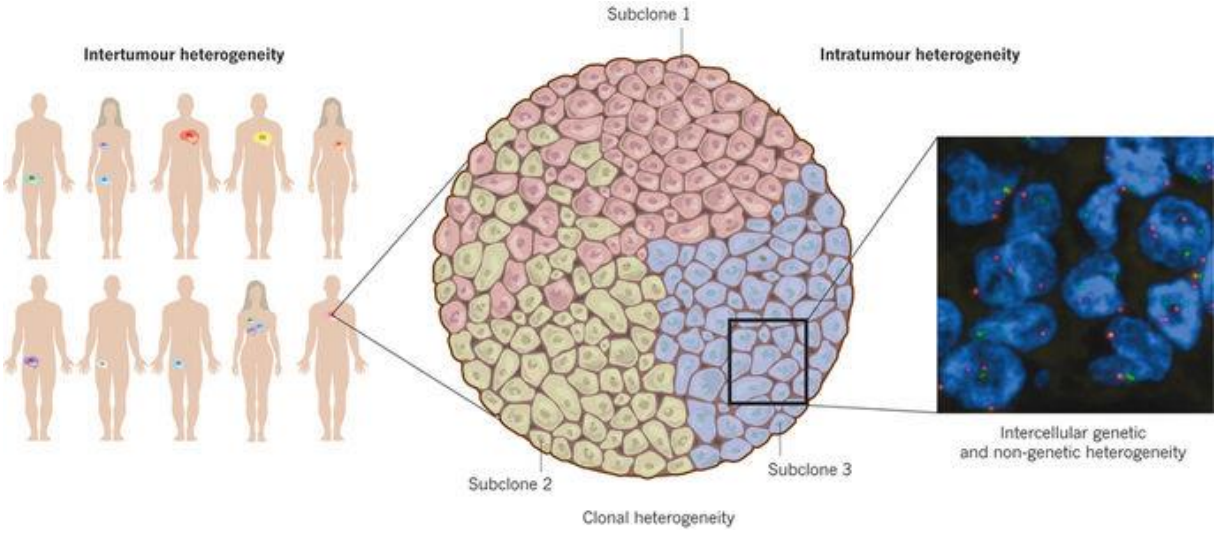

Figure 3: Tumor heterogeneity. Adapted from [7]

1.3 The prevalence of somatic mutation in cancer

Most somatic mutations are caused by incomplete DNA repair following errors in the DNA replication and base damage by reactive oxygen from metabolic reactions or exposure to exogenous mutagens. Several pathogenic viruses (e.g. human papilloma virus, Epstein Barr virus) and some bacteria (*Helicobacter pylori*) are oncogenic.

In lung cancer, somatic mutation can be caused by tobacco smoking; meanwhile ultraviolet exposure can cause melanoma [12]. The prevalence of somatic mutations is approximately 400 per megabase (Mb) in melanoma that is higher than any other classes of cancer, starting from about 0.001 per in pilocytic astrocytoma. The fewest mutations are found in childhood cancer types compared to malignant melanoma that are caused by high ultraviolet (mutagen) exposure (see Figure 4) [6].

In malignant melanoma, somatic mutations are commonly observed mostly in *BRAF*, *NRAS* and *PTEN* genes. Activating mutations in these genes drive cell signaling important for cell proliferation and survival. The most frequent mutation in BRAF is substitution of amino acid glutamic acid for valine leading the *BRAF (V600E)* gene mutation that harbors in 50-60% of all melanomas. *Q61R* mutation in *NRAS* gene is detected in 15% of all type of mutation [13, 14]. Some of the malignant melanoma are caused by mutated *PTEN*, hence the frequency is lot less compared to *BRAF* as well as *NRAS* mutation [15].

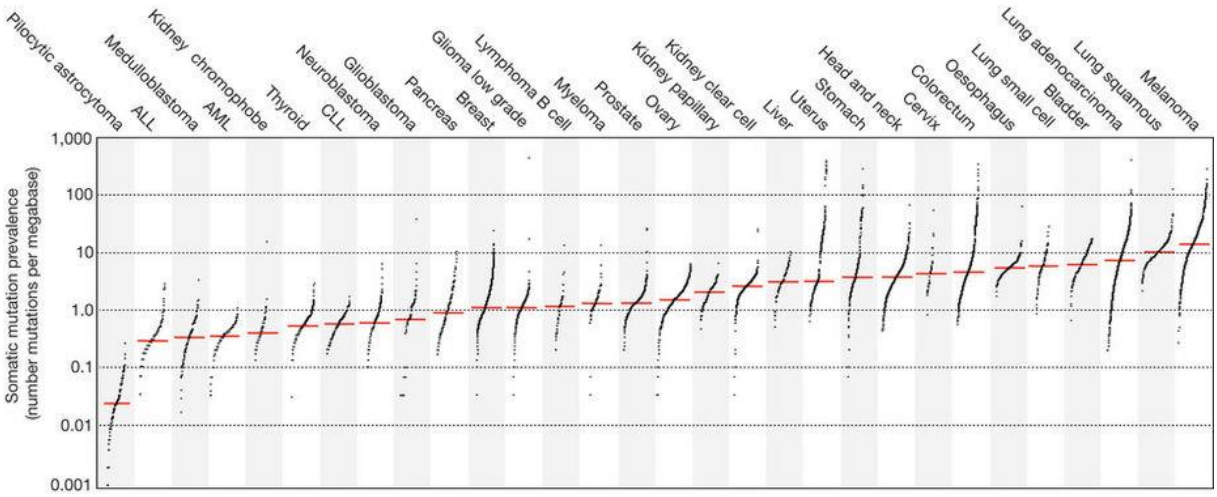

Figure 4: The prevalence of somatic mutations among human cancer types: Each dot shows one single sample. However, red colored horizontal lines are the median frequency of somatic mutations in the various cancer types. The vertical axis (log scaled) represents the frequency of somatic mutations per megabase. The horizontal axis represents different cancer type compared on their prevalence of somatic mutations from lowest 0.001 per megabase (Mb) in pilocytic astrocytoma to highest 400 per Mb in melanoma. Adapted from [6].

1.4 Melanoma

Melanoma is a type of skin cancer that is highly aggressive and responsible for approximately 75% of skin cancer related deaths [4]. The prevalence of melanoma is increasing. In males and females, melanoma is the 5th and 6th most prevalent cancer, respectively in Norway [16]. Every year approximately 132,000 new malignant melanoma cases are identified worldwide, as reported by World Health Organization (WHO), which is higher than any other forms of cancer [17, 18]. The mortality rate is also increasing with the high incidence rate and particularly in the last 10 years. Fair-skinned individuals are more susceptible to melanoma than dark-skinned individuals because of the low production of melanin (a pigment found in hair, skin, eyes, and some internal membranes) that is present in the cells of the epidermis of the skin. Melanin protects against DNA damage (thymidine dimers) by filtering ultraviolet light [19]. Melanin is produced by melanocytes, located in the basal layer of skin epidermis and is transferred to surrounding cells such as keratinocytes [20]. The malignant transformation of the melanocyte causes melanoma. Melanocytes are primarily found in epidermis, some are found in mucous membrane, as well as in eyes and in different body parts. Melanomas that arise in the epidermis are called the cutaneous melanoma and these account for 90% of all types of melanoma. Others include mucosal melanoma from mucous membrane and ocular stroma of the eye termed uveal melanoma, the second most common type of melanoma [21].

Table 1: Melanoma statistics in Norway, 2015. List registered melanoma cases in Norway (2015). Adapted from[22]

Parameter	Total	Men	Female
Incidence	2003	1018	983
Incidence rate in Norway	-	41,2	36,5
Incidence rate in the World	-	23	23,3
5 year survival	-	81,60 %	89,40 %
Prevalence	23393	-	-
Prevalence 10-year	10744	-	-
Mortality	322	178	144

Australia and New Zealand have a higher incidence of melanoma, than western and northern Europe. In comparison to other European countries, Norway has one of the highest melanoma incidences. Although the incidence rate is lower than of Australia, the mortality rate is similar [23]. From the 1950s to date, there has been an alarming increase in the incidence rate of melanoma reported in cancer registry of Norway (see Figure 5).

In the last 60 years, an eight-fold increase in melanoma that is 20% increase in incidence has been observed (from 2007-2011 to 2012-2016) in Norway, which makes melanoma the fifth most prevalent cancer type, accounting for around 6% of all cancer types. For adults aged 25-49 in Norway, it is the second most frequent cancer. Around 2000 new cases of melanoma were reported in 2015 by the cancer registry of Norway [22, 24]. The melanoma incidence and mortality are summarized in Table 1.

The risk factors for developing melanoma are predominantly genetic and environmental. These include exposure to UV radiation, family history of melanoma as well as somatic mutation can contribute to the development of melanoma [25, 26].

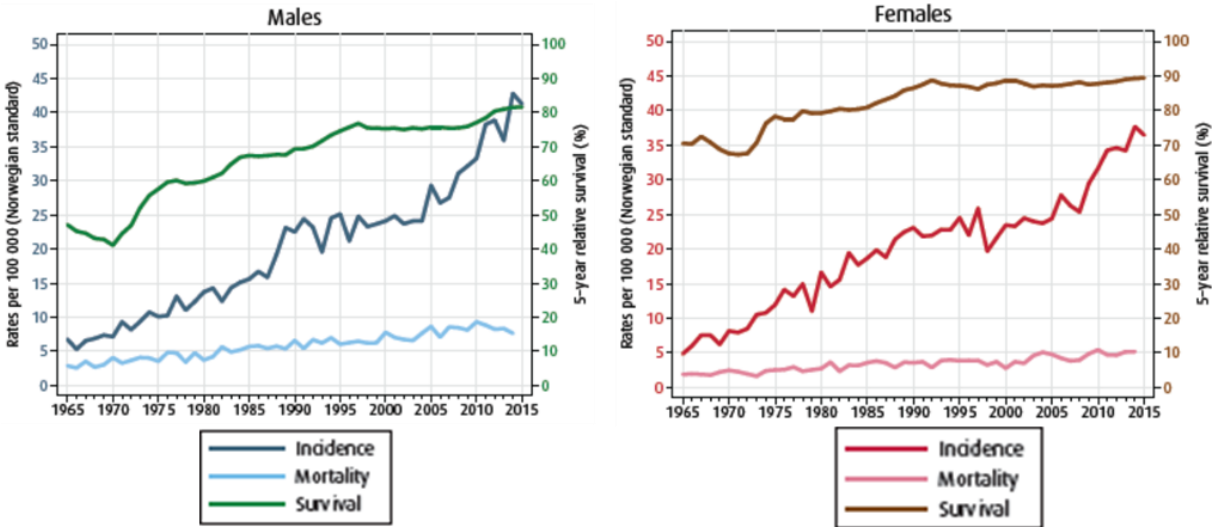

Figure 5: Trends in incidence and mortality rates and 5-year relative survival proportions in male and female melanoma cases from 1995 to 2015 in Norway. Incidence and mortality rates (rates per 100,000) correspond to the data on left Y-axis; 5-year survival rates correspond to the data on right Y-axis. Adapted from [22].

1.4.1 Classification and Staging of Melanoma

Based on the tumor-node-metastases (TNM) classification system, the AJCC (American Joint Committee on Cancer) system of staging melanoma divides patients into several stages of disease progression. The TNM system characterizes the tumor based on the size; nature and dissemination of tumors. Moreover, the characterization also depends on the evolution of primary tumors (T) to their regional lymphatic (N) or distant metastatic (M) spread [27, 28].
A schematic representation of four main stages of melanoma that are associated with the pathological features is presented in (see **Figure 6**) [29].

Melanoma-in-situ patients are categorized (clinical and pathological staging) as Tis and considered to be in stage 0. Tumors up to 2mm in thickness are considered as primary melanoma and do not metastasize regionally or distantly (see **Figure 6**). The subdivisions of Stage I are stage IA without ulceration (T1a) and stage IB that are with ulceration (T1b, T2a) [27, 28]. Tumors > 1.01 mm thick without indication of regional lymphatic or distant metastases are characterized as Stage II patients (see **Figure 6**). Stage II is subdivided into Stage IIA, Stage IIB and Stage IIC depending on size of the tumor and the presence of ulceration (range from T2b, T3a, T3b, T4a and T4b) [27, 28]. If the lesion of a patient spreads regionally and metastasize that patients is staged clinically as Stage III (Any T and N1-N3) (see **Figure 6**). There is no subdivision of Stage III in clinical staging. However, depending on primary tumor

size, types of lymph node and the presence of ulceration in primary or metastatic lesions, the pathological stage III is subtyped into Stage IIIA, Stage IIIB and Stage IIIC [27, 28].

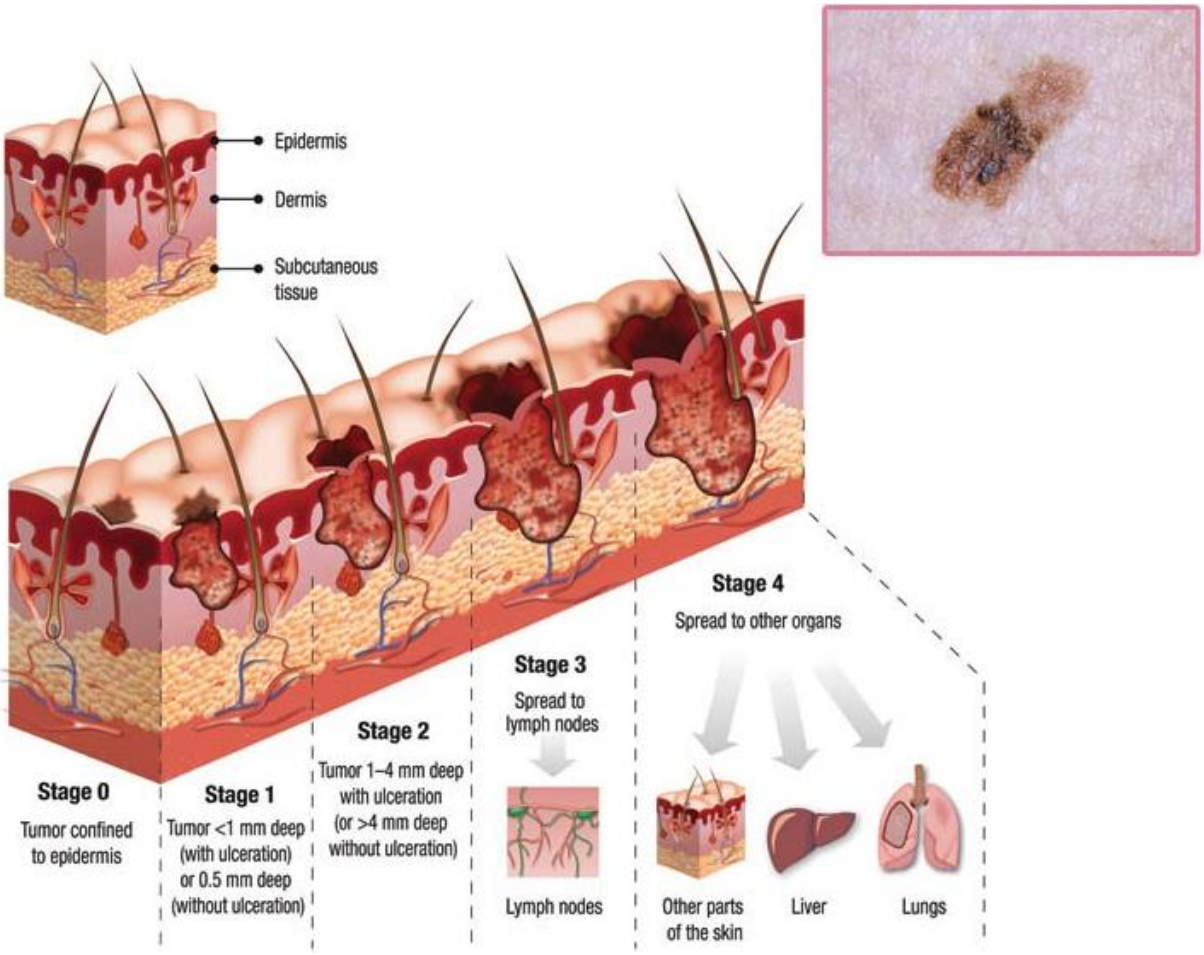

Figure 6: Stages of melanoma progression. Schematic Comparison between healthy skin and malignant melanoma affected skin. During stage 0, the tumor is confined to epidermis and in stage I it penetrates epidermis followed by stage II where the tumors spread into the dermis of the skin. At Stage III, the subcutaneous layer is penetrated by the tumor and it metastasizes to the lymph node. By Stage IV, tumors have metastasized to distant organs. Adapted from [29]

Stage IV patients (clinical and pathological staging) are metastasized to distant organ (**Figure 6**) locations such as skin, lung, lymph nodes, subcutaneous tissue, or other visceral or distant sites followed by elevated serum levels of lactate dehydrogenase (LDH). The metastasis happens very early, from tiny lesions leads to poor prognosis of the patient. The expected median patient survival at stage IV is 6 to 9 months with a 10% to 20% 5-year survival rate [30].

1.4.2 Treatment of metastatic and inoperable melanoma

The past 7 years, the treatment of advanced stage melanoma has changed dramatically. Until 2011, the standard of care with the chemotherapeutic dacarbazine remained unchanged for over 30 years, even though it did not improve the overall survival of patients [31]. The US Food and Drug Administration (FDA) approvals of the immunotherapeutic checkpoint inhibitor Ipilimumab and the targeted BRAF inhibitor Vemurafenib in 2011 for the treatment of metastatic or inoperable melanoma marked the beginning for a new era in the treatment of advanced melanoma [32].

Treatment with immune checkpoint inhibitors improves overall survival, and for both the CTLA-4 targeting checkpoint inhibitor Ipilimumab, and PD-1 targeting checkpoint inhibitors, unprecedented long- lasting responses are seen [33]. However, the majority of patients either do not respond to this treatment, or relapse [34].

The BRAF inhibitor Vemurafenib also improves overall survival in patients with BRAF mutated melanoma [35], but development of resistance is almost inevitable [32]. To improve the survival competing with incidence, new diagnostic techniques and different therapeutic methods are being launched as better options. However, advanced stage melanoma patients have lower survival rates and treatment options are still limited. In addition to that, resistance to the treatment poses a consistent problem [36-38]. Surgery, chemotherapy, radiation therapy, and immunotherapy are currently used to treat melanoma. The understanding of genetic and molecular mechanism of melanoma has improved with increasing research on melanoma. Therefore, new drugs are being approved to treat malignant melanoma. Conventional chemotherapies like treatment with cytokines (5-20%) effect on advance stage melanoma patients. The treatments do not increase survival but rather result in toxicity [35, 39]. Early detection and surgical removal of the primary tumor lesion can increase life expectancy of patient. Novel treatment options, T-cell regulatory immune therapies like the human anti-cytotoxic T lymphocyte antigen-4 monoclonal antibodies (ipilimumab) [31], anti-programmed death-1 (PD-1) antibodies (pembrolizumab, nivolumab) [40] and targeted therapies against MAPK pathway kinases for example BRAF inhibitors, (dabrafenib) [41, 42] show great promise and extended survival. Moreover, MEK inhibitor (trametinib) [43] and their combination with BRAF inhibitors (dabrafenib with trametinib) [44] showed promising effect on melanoma patients with BRAF mutation since several findings show that 50% of melanomas have *BRAF* mutated and approximately 20% of all melanomas have *NRAS* gene mutated.

Table 2: Treatment of malignant melanoma. The FDA approval is set for different stages of melanoma, mainly advanced disease. The NCT: NCT00937937 and BGB324 is an ongoing clinical trial. Adapted from [45, 46]

Drug	Inhibitor target	Pathway	Clinical stage	Response	Therapy
Vemurafenib	BRAF (V600E/K)	MAPK	FDA	50 %	Target drug therapy
Dabrafenib	BRAF (V600E/K)	MAPK	FDA	50-60%	Target drug therapy
Sorafenib	BRAF/c-KIT	MAPK	Phase 3	5-10%	Target drug therapy
Sunitinib	c-KIT	MAPK	Phase 2	7-10%	Target drug therapy
Dasatinib	c-KIT	MAPK	Phase 2	5-13%	Target drug therapy
Imatinib	c-KIT	MAPK	Phase 2	5-16%	Target drug therapy
Trametinib	MEK1/2	RAS-RAF-MEK-ERK	FDA	10 %	Target drug therapy
Selumetinib	MEK1/2	RAS-RAF-MEK-ERK	Phase 2	11 %	Target drug therapy
Rapamycin	mTOR	PI3/AKT/mTOR	Phase 2	-	Target drug therapy
SCH772984	ERK1, ERK2	ATP competative inhibitor	Phase 1	-	Adjuvent therapy
Nivolumab	PD-1	PD-1 receptor	FDA	24 %	Immuno-therapy
Ipilimumab	CTLA-4	CTLA-4 receptor	FDA	10-20%	Immuno-therapy
Interleucin-2	IL-2 receptor	Cytotoxic activity	FDA	10-16%	Immuno-therapy
Dacarbazine	DNA/Guanine	Guanine methylation	FDA	10-15%	Chemotherapy
Interferon-a2b	IFNAR-2 reseptor	JAK-STAT	FDA	5-20%	Adjuvent therapy
LY2835219	CDK4/6	p16-cyclinD-CDK4/6-RB	Preclinical	-	Adjuvent therapy
Dinaciclib	CDK4/6	p16-cyclinD-CDK4/6-RB	Phase 2	-	Adjuvent therapy

Targeted therapy combinations are showing remarkable progress [47]. In Norway, BGB324 (AXL kinase inhibitor) drug is in clinical trial to treat metastatic melanoma patients. Depending on the BRAF mutation status, the BGB324 can be used as combination therapy with pembrolizumab, dabrafenib [46]. However, the patients with both BRAF inhibitors and Axl

inhibitors show promising results [48]. Moreover, wide understanding about other signaling pathways and new biomarker invention has led to more new drug discovery that are approved by the FDA. The new drug development have driven the research on melanoma to target one combination drug therapy with an ambition to overcome drug resistance. However, the acquired resistance negatively influences treatment, which explains why appropriate sequencing and selection of drugs still be a challenge. Currently some FDA approved drugs are being used to treat melanoma as well as some drugs are in ongoing trial in the hospitals (Table 2).

1.5 Receptor tyrosine kinases (RTKs)

Receptor tyrosine kinases (RTKs) are single pass transmembrane receptor proteins expressed on the cell surface that transmitting signals from the outside of the cell to coordinate cellular processes. Ligands bind to the RTK extracellular domain driving dimerization that results autophosphorylation tyrosine residues in the intracellular kinase domain. Phosphotyrosine residues trigger activation of different signaling pathways by recruiting signaling intermediates (e.g. SH2 protein) that bind distinct tyrosine residues. There are 58 RTKs have already been discovered in the human genome, distributed among 20 subfamilies [49-51]. The structure of all members of RTK superfamily are similar, with a large extracellular domain for ligand binding that is connected by a single-chain membrane-spanning transmembrane helix to the cytoplasmic tyrosine kinase domain. The activation of RTKs typically happened by binding of the ligand to the extracellular domain that induces dimerization of the receptor and activation of cytoplasmic kinase domain [51]. In normal cells, RTKs are activated after ligand binding. However, in cancer cells, RTKs can be overexpressed or they can become constitutively activated by activating mutations [52]. Figure 7 shows an overview of the domain structure of 20 RTK families.

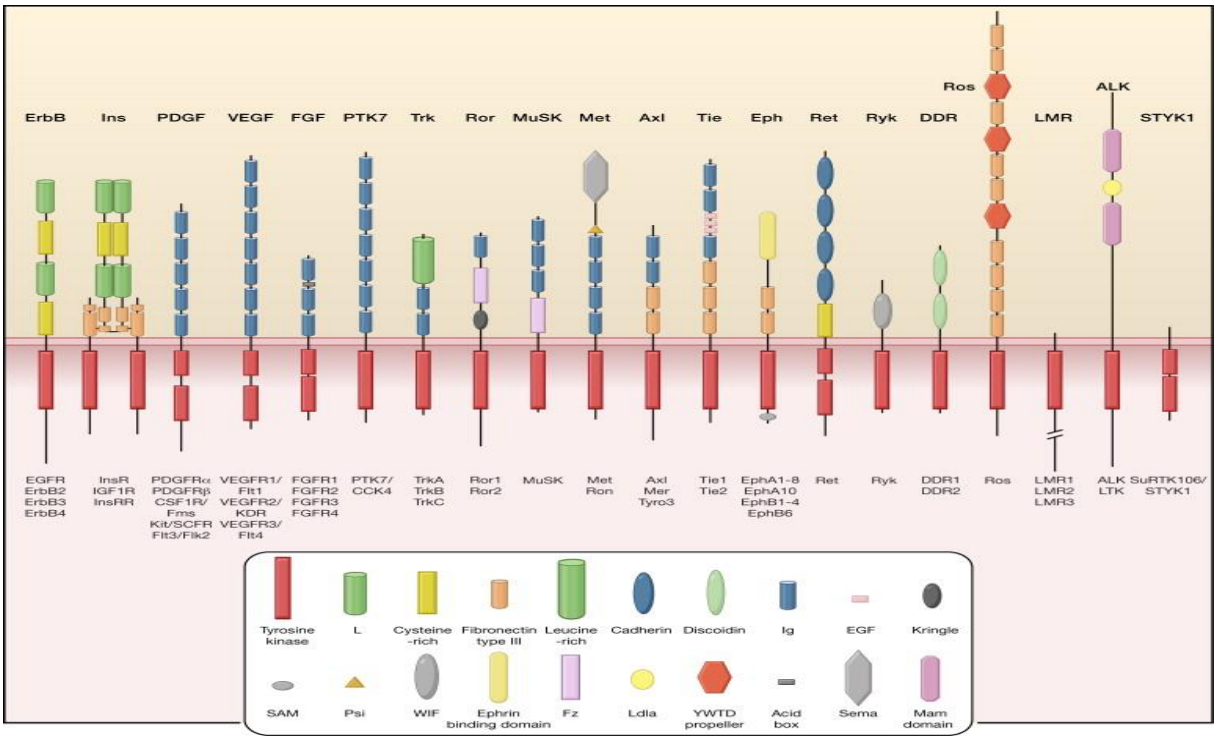

Figure 7: Receptor tyrosine kinases (RTKs) families. Adapted from [51].

1.5.1 Signaling pathway regulated by receptor tyrosine kinases

Signaling through RTKs can be mediated through a canonical and a non-canonical pathway. The canonical pathways were explained previously, as the binding of the ligand to the extracellular domain activates the receptor by dimerization and autophosphorylation of the cytoplasmic kinase domain, facilitates binding of downstream effector protein that activates a particular signaling cascade into the cell. On the other hand, the internalization of RTKs followed by translocation into the cell surface and nucleus carry the signal from outside of the cell to inside, in the non-canonical signaling pathways [53, 54]. The thesis mainly focused on canonical pathway proteins.

There are mainly two main signaling cascade that can be referred as the canonical pathways. After binding of ligand to the RTKs, consequently the dimerization and autophosphorylation of receptor and kinase domain mediate the recruitment of several adaptor proteins to the phosphorylation site. The binding of an adaptor protein can activate the two main downstream signaling cascade, the Growth factor receptor-bound protein 2 (Grb-2) adaptor protein activates the Ras mediated mitogen-activated protein kinase (MAP kinase)/ERK pathway, whereas the regulatory subunit (p85) of phosphoinositide 3-kinase (PI3K), works as an adapter protein to active the PI3K mediated signaling cascade [55-58].

In the MAP kinase/ERK pathway, the Ras is inactive and GDP bound in the absence of a growth factor. However, upon binding with the growth factor, the activated adaptor protein Grb-2 initiates the Ras and a conformational change triggers the exchange of bound guanosine diphosphate (GDP) for guanosine triphosphate (GTP). Meanwhile, activated Ras triggers the downstream signaling protein RAF by phosphorylation that subsequently activates the MEK (MAP kinase kinase), ERK (MAP kinase) proteins in the signaling cascade (see Figure 8). The phosphorylated ERK then activates the transcription factor for cell proliferation AP1 and cell cycle regulatory proteins cyclin D1 that regulates proliferation, survival and differentiation of the cell [55, 56].

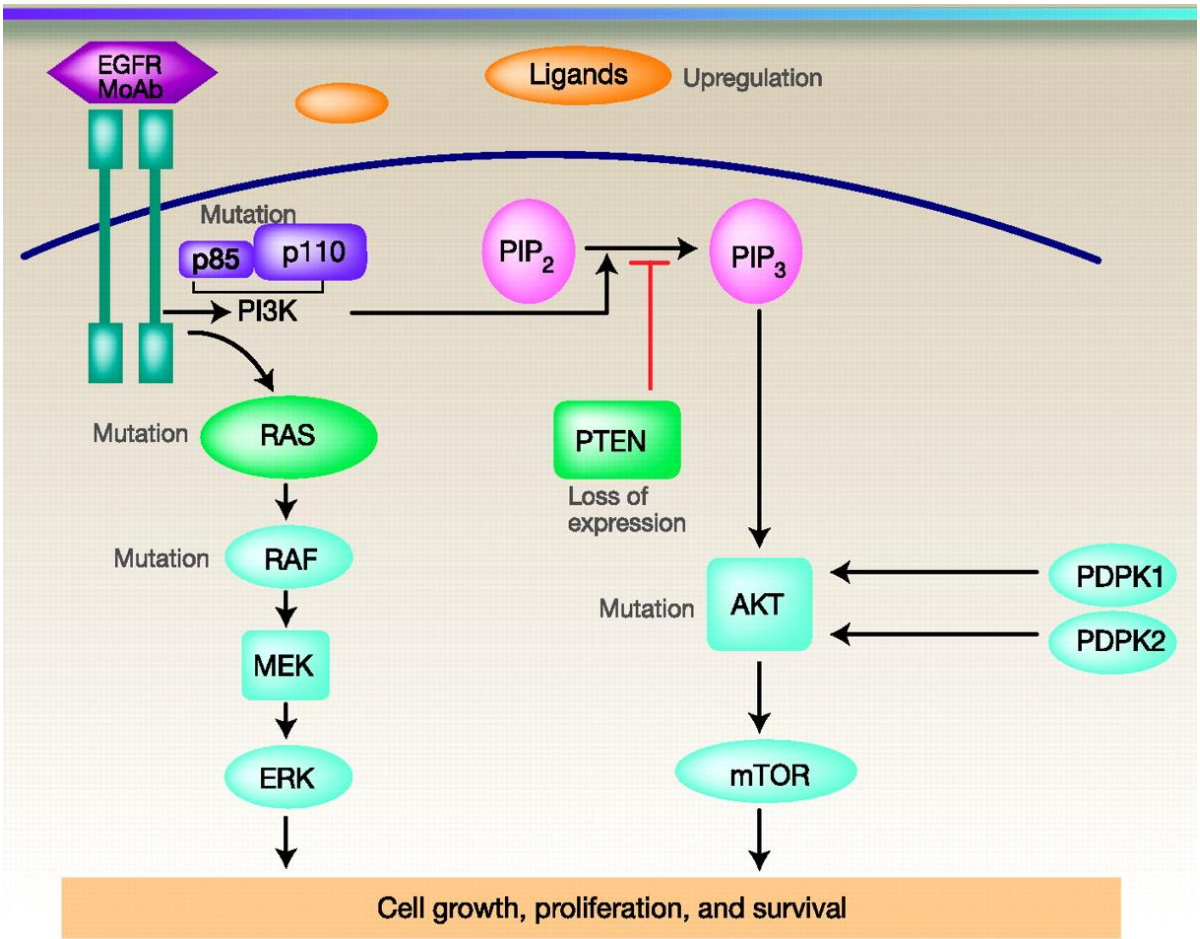

Figure 8: RTK signaling pathways: EGFR is an RTK which is activated by binding of ligand to the receptor that causes dimerization, and subsequent activation of downstream signaling protein by activated adaptor protein. In the MAPK pathway, sequential activation of RAS, RAF, MEK, and ERK by phosphorylation of kinase domain. However, upon activation with p85, the p110 then initiate the conversion of PIP_3 from PIP_2, that trigger the AKT (facilitated by PDPK1 and PDPK2 (mtorC2). The activation of AKT subsequently activates mTOR. PTEN down regulates the pathway. Adapted from [59].

In the PI3K/AKT pathway, the regulatory subunit, p85 of PI3K act as an adaptor protein which binds to the phosphorylated tyrosine domain of activated receptor. The catalytic subunit, p110 of PI3K works as a downstream signal mediator to transmit the signal to protein kinase C (PKC). PKC mediates the formation of Phosphatidylinositol (3, 4, 5)-trisphosphate (PIP3) from Phosphatidylinositol 4, 5-bisphosphate (PIP2) that serves as docking site for Phosphoinositide-dependent kinase-1 (PDK 1) as well as phosphorylated AKT (also known as protein kinase B) [57, 58]. The phosphorylated AKT in turn activates mTOR (a serine threonine kinase) that triggers further cell proliferation and cell survival. On the other hand, AKT also phosphorylates Bcl-2-associated death promoter (BAD) protein, which induces apoptosis in the cell by binding to Bcl-2 in its unphosphorylated state. However, upon phosphorylation by AKT, the pro apoptotic function of BAD is inhibited thereby promoting more cell survival. Phosphatase and Tensin homolog (PTEN) protein downregulates the PI3K/AKT pathway by forming PIP2 from PIP3 [60, 61].

1.5.2 Tyro3, Axl, Mer is the TAM Receptor tyrosine kinases

The TAM family consists of three receptors, tyrosine kinase receptor 3 (Tyro3), Axl, and Mer. All three TAM receptors consist of three domains, the single pass transmembrane domain is α-helical that connects the extracellular adhesion molecule-like domain to the intracellular tyrosine kinase domain which contains a conserved sequence, (KW(I/L)A(I/L)ES). The extracellular domain comprises two immunoglobulin-like (Ig) domains and two fibronectin-type III (FNIII) domains. The receptor forms dimer upon activation by its ligand and these receptors share two types of ligand. First, the growth arrest-specific protein 6 (Gas6) is a vitamin K dependent ligand that can bind to all the three TAM receptors. However, the second one is vitamin K dependent protein, protein S (PROS1) that can only bind to Tyro3 and Mer (see Figure 9) [62]. The receptors form homodimer or heterodimer after binding of ligand [63].

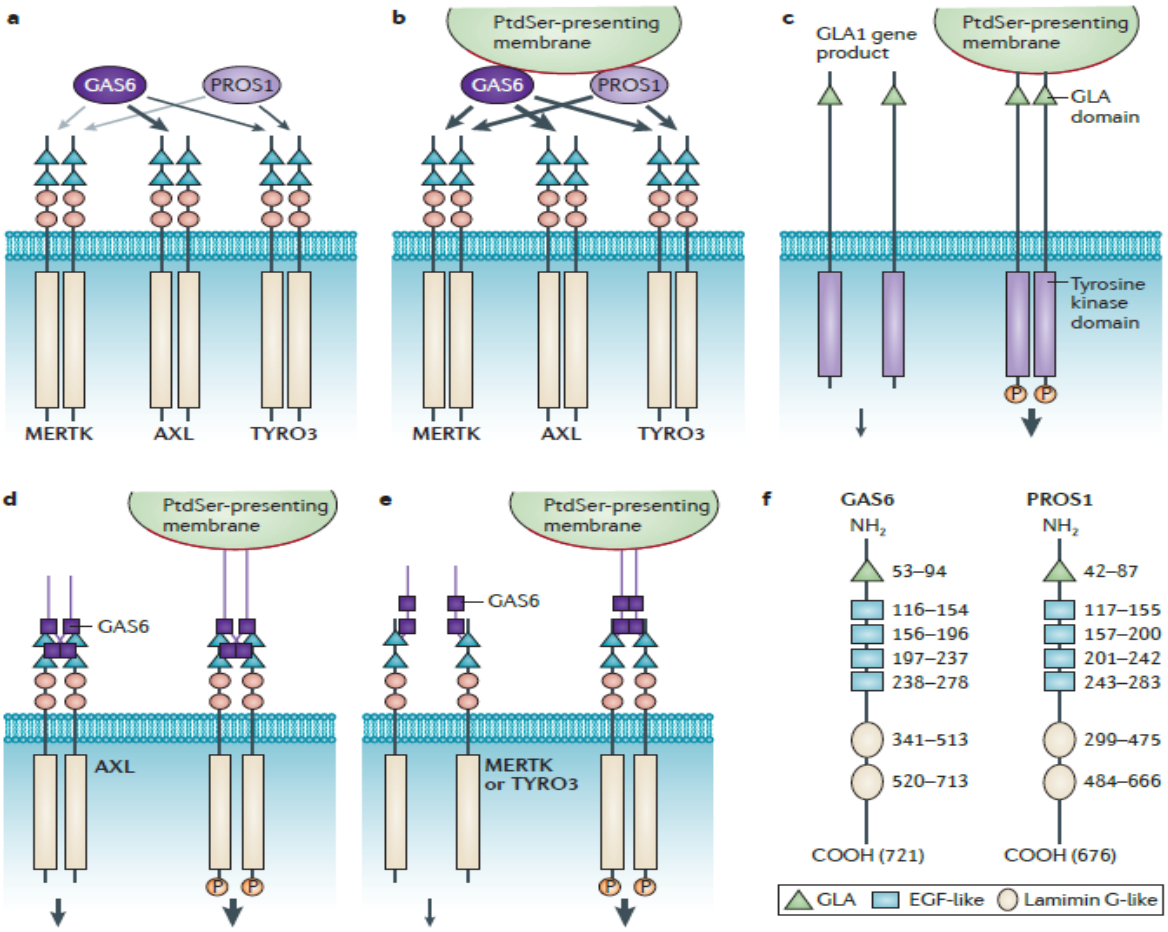

Figure 9: Activation of TAM receptor by ligand Gas6 & protein S.

The ligand acts as bridging factor by vitamin K-dependent γ-carboxylation of glutamic acid residue of the N terminal Gla domain that binds to the phosphatidylserine (PtdSer) and the carboxy-terminal domain bind to the receptor [64].

In normal cellular function, the phosphatidylserine (PtdSer) is located to the inner leaflet of the plasma membrane. Cells that are stressed or apoptotic display phosphatidylserine (PtdSer) on the outer leaflet, which will then bind to the ligand Gas6 and protein S [65]. TAM receptors mediate clearance of apoptotic cells, innate immune control, and differentiation of natural killer cells (NK cells) as well as platelet aggregation [62, 66]. TAM receptors also associated with different types of cancer. Aberrant activation of these receptors promotes tumor cell survival, chemoresistance and invasion [63]. Axl plays an important role in the tumor metastasis and acquired resistance to both conventional cytotoxic drugs, radiation and targeted therapeutics and more recently to immune checkpoint inhibitors. Axl is an important drug target to prevent cancer as well as to overcome the resistance against targeted therapy [67].

1.5.3 TAM family member, Axl receptor tyrosine kinase

Axl is one of the members of the TAM family receptor kinase. It was first identified as a transforming gene with unknown protein function in two patients with chronic myelogenous leukemia (CML) in 1988 [68]. The name Axl comes from Greek "*anexeleto*" that means uncontrolled. The *AXL* gene is highly conserved in vertebrates, located at close vicinity to the *BCL3* oncogene in chromosome 19 (19q13.1-q13.2), which are encoded by 20 exons, and have two different splice variants [69]. The Axl receptor activation depends on binding of the ligand growth-arrest-specific gene 6 (*Gas6*) in a vitamin K dependent manner. The glycosylated receptor is 140kda [68, 70]. Axl is expressed at low levels in myeloid cells, bone marrow stromal osteoblasts, platelets, endothelial cells, and specific cells in skeletal muscle, heart, liver, kidney, testis, hippocampus and cerebellum. Axl activation induces cell survival, migration, cell- cell adhesion and proliferation. [62, 71]. In normal physiological condition, Axl induces cell survival; give stimulation to cell to migrate, cell-cell adhesion and proliferation [72, 73]. However, it has been reported that Axl overexpression is associated with metastasis, invasion, migration and angiogenesis of numerous cancer types like triple negative breast cancer, colon cancer, non-small-cell lung cancer, prostate cancer, pancreatic cancer, ovarian cancer endometrial cancer and sarcomas [74].

1.5.4 Structure of Axl

Since Axl is a receptor tyrosine kinase (RTKs), the structure is like other RTKs. Like other RTKs, Axl receptor is characterized by extracellular (N-terminal) ligand binding domain, consisting of two-fibronectin type III like repeats, and two immunoglobulin (IG)-like domains along with intracellular tyrosine kinase (C-terminal) that encompasses an unusual conserved sequence amino acid sequence, (KW (I/L)A(I/L)ES), like other TAM family receptor (see Figure 10) [69, 75]. The intracellular kinase domain contains an ATP-binding site that includes three autophosphorylation sites (Tyr779, Tyr821, and Tyr866), that can serve as a docking sites for numerous intracellular signaling proteins with s binding sites for phosphorylated tyrosine (src-homology domain-2). Tyr779 exhibits the binding site for PI3K, Tyr866 for PLC and Tyr821 provides docking site for several proteins like PLC, PI3K, c-Src, Grb2, and Lck [76].

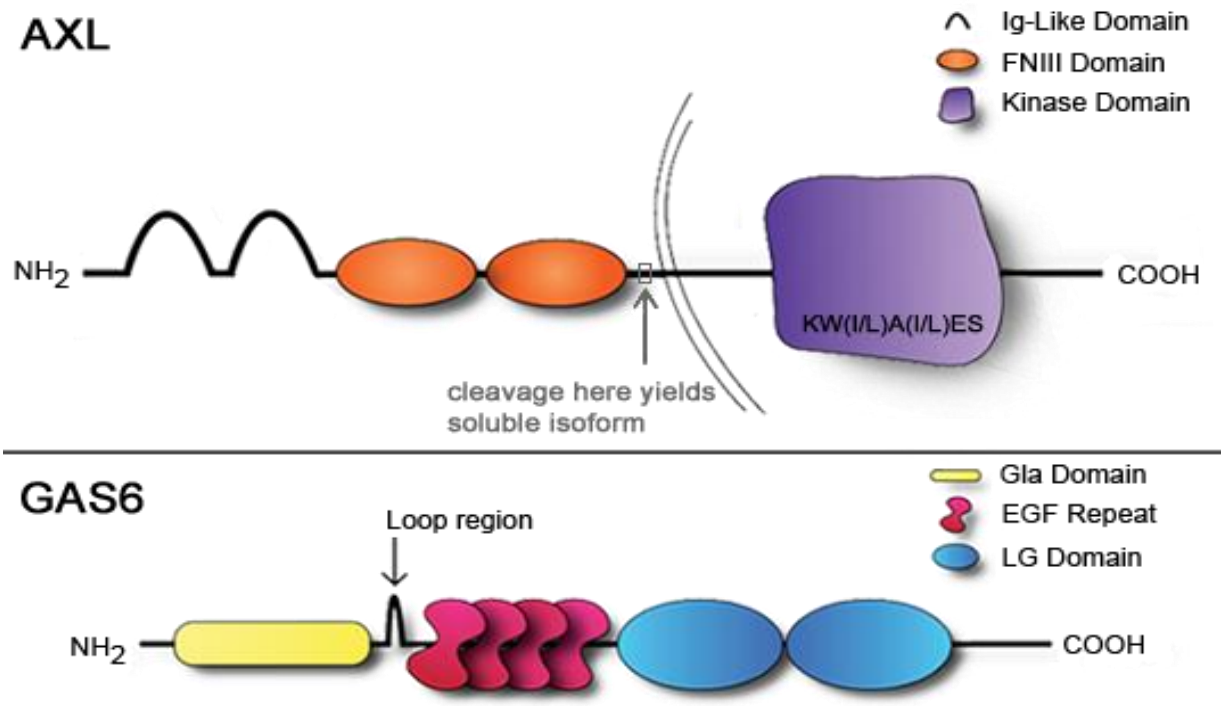

Figure 10: The schematic representation of structure of Axl receptor and its ligand growth-arrest-specific gene 6 (Gas6). Adapted from [75]

1.5.5 Axl activation and signaling

Axl can be activated by two different mechanisms, depending on ligand availability. The most powerful way of activation is ligand dependent activation where the ligand Gas6 binds to the extracellular ligand-binding domain of the Axl receptor and activates it. Apart from the ligand-mediated activation, Axl is reported to activate by homodimerization, which is a ligand independent mechanism. By binding to another Axl receptor, either on a neighboring cell or on the same cell, Axl activation has also been shown to occur. In addition, Axl can also be activated by binding with other TAM receptors, as well as with non-TAM receptors (heterodimer), like epidermal growth factor receptor (EGFR) (see Figure 11) [77, 78].

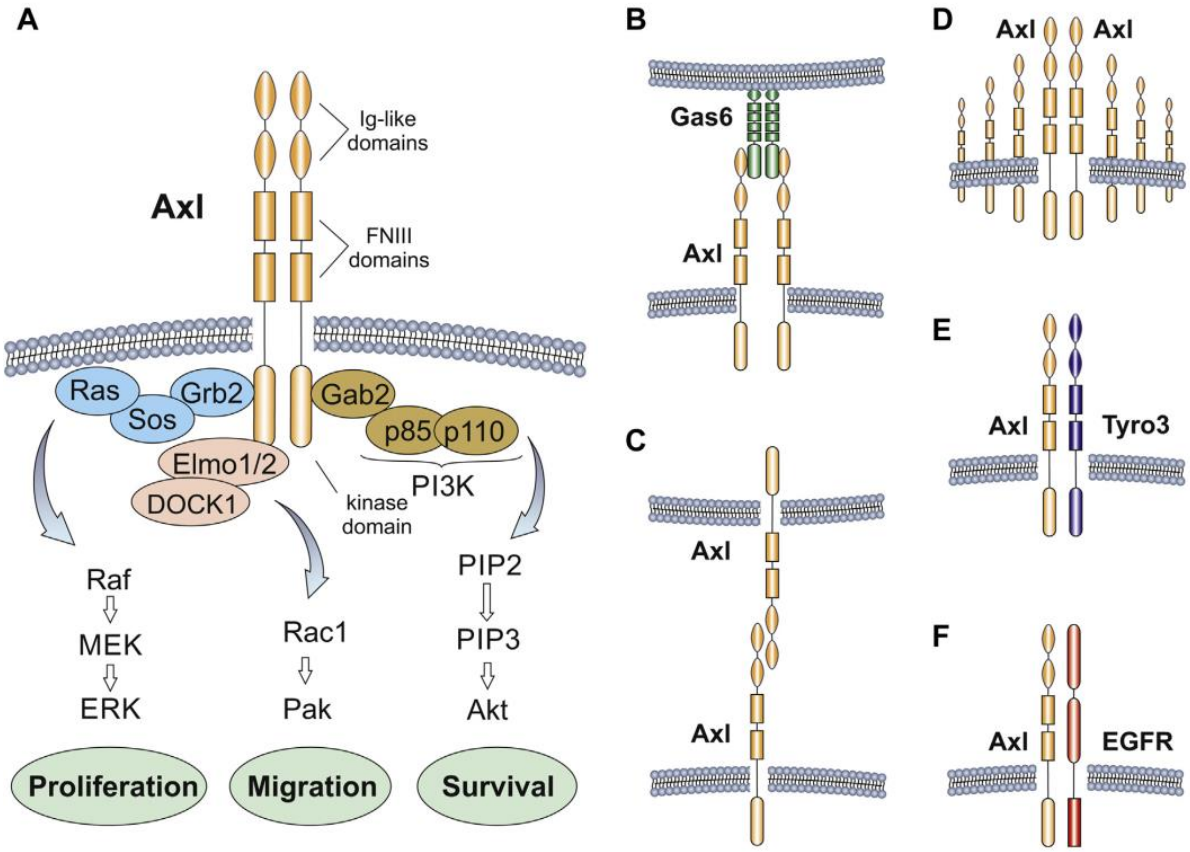

Figure 11: Axl Activation and signaling: A. Three pathways of Axl signaling including (1) Ras/Raf/MEK/ERK, (2) Elmo1/2/DOCK1/Rac1/Pak, and (3) Gab2/PI3K/Akt, that can lead to cell proliferation, migration and survival. **B–F**. Mechanisms of Axl activation, including binding of ligand Gas6 with the receptor in a ligand-dependent manner (**B**) homodimeric interaction of Axl with neighboring cells (**C**), as well as overexpression (**D**), dimerization with another TAM family member receptor (Tyro3) (E), or heterodimerization with a non-TAM family receptor, such as EGFR (**F**) in a ligand independent mechanism (**C-F**). Adapted from [78]

The Axl ligand Gas6 is a 75-kDA vitamin K dependent protein. The amino acid sequence of Gas6 is 43% identical to the other ligand for TAM family, protein S. Gas6 is a 75-kDa vitamin K dependent protein first identified in fibroblasts of embryonic mouse NIH 3T3 in 1995, as a ligand for Axl. The N terminal of the Gas6 protein comprises the gamma-glutamic acid (Gla) domain, followed by four epidermal growth factor-like repeats. The C-terminal regions of Gas6 contains steroid hormone-binding globulin (SHBG) that includes two laminin tandem globular (G) domain (see Figure 11) [79-83].

Each of the Axl receptor molecules contain two sites that have different affinity for distinct ligands, one is high affinity site for ligand binding, Ig1 and other is low affinity site for ligand binding, Ig2. These sites bind to various sites of the two Gas6 to stabilize the receptor-ligand

complex. The high affinity site, Ig1 of one Axl molecule binds to one side of the Gas6, whereas the low affinity site, Ig2 of other Axl molecule binds the opposite side of the same Gas6 and causes dimerization of the receptor (see Figure 12) [84]. However, the Gas6 activation depends on the gamma carboxylation of the Gla domain, which in normal condition converts glutamate to gamma-carboxyglutamate by carboxylation. Upon carboxylation of the Gas6 Gla domain, its binding to phosphatidylserine (PtdSer) is facilitated in a calcium dependent manner on the neighboring cells [79]. Phosphatidylserine is mainly found in the inner leaflet of the plasma membrane that can flipped on the outer surface of the membrane upon activation. Moreover, the platelets and dendritic cells as well as ACs also present PtdSer on the outer surface of the membrane [85].

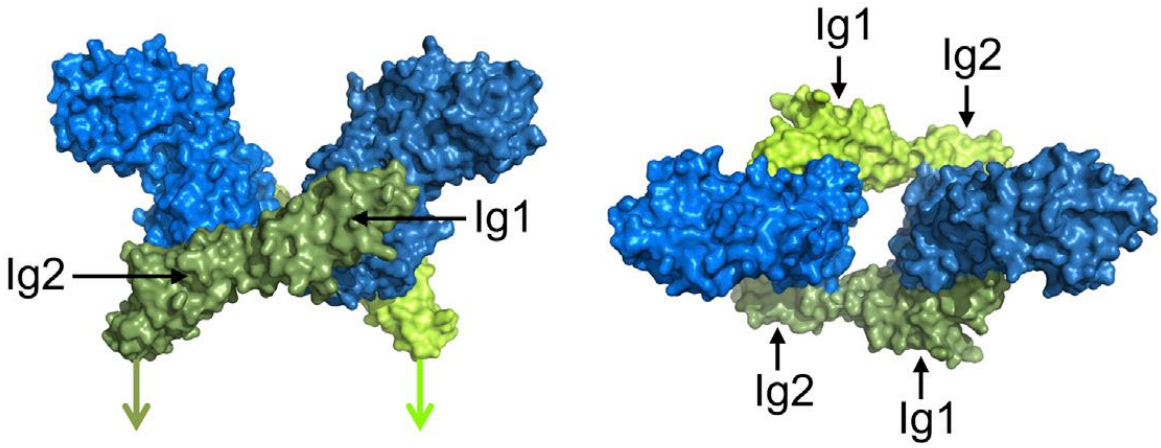

Figure 12: Axl Gas 1:1 complex: Molecular mechanism of binding of Axl to Gas6 by the Ig1 and Ig2 domains of Axl (green) and the C-terminal laminin G-like domains of Gas6 (blue). The left diagram is showing from front and the right one from top. Axl attachment to the membrane are shown using green arrow.

There are several conflicting reports suggest, activation of Axl by Gas6 is dependent or independent of the phosphatidylserine interaction [63]. This was supported by another study that demonstrated that gamma-carboxylation of Gla domain is sufficient for activating the Gas6; there is no need of PtdSer for the signaling of the receptor [64]. On the contrary, one group suggests that the signaling of Axl by the activation of the Gla domain of Gas6 without PtdSer is weaker (see Figure 13) [86]. However, the most common activation of the Axl receptor is carboxylation of the Gla domain, followed by ligand binding of Gas6 to PtdSer [79]. Recent studies suggest that only a small amount of [79].

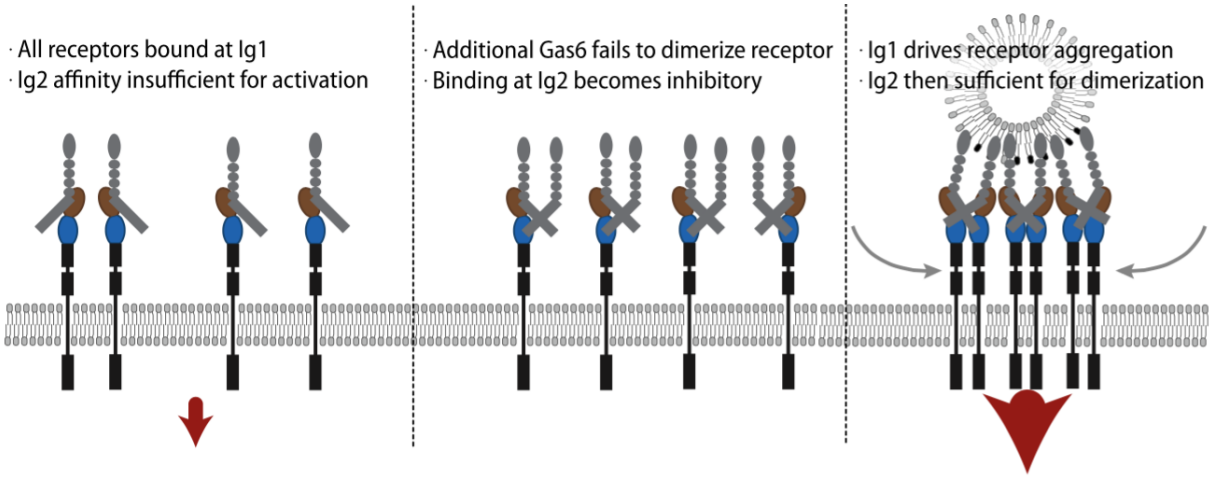

Figure 13: Gas6-PtdSer Interaction for Axl signaling: For increased signal, the Gas6-PtdSer interaction is necessary. PtdSer aggregates the receptor for more extended signal.

The activation of Axl, either with the vitamin K dependent gamma carboxylation of ligand Gas6 and PtdSer or through the ligand independent manner, as a tyrosine kinase receptor, results in dimerization of Axl that transduces a signal from the outside to the inside of the cell. The signal autophosphorylates the tyrosine residues of the C-terminal intracellular kinase domain of Axl receptor at the position Tyr779, Tyr821, and Tyr866 [76, 87]. The phosphorylated tyrosines act as docking sites for several downstream signaling cascade. For Axl, the main activated downstream signaling pathway is PI3K mediated activation of Akt and phosphorylation of nuclear factor κB (NF-κB). The regulatory subunit (P85) of PI3K binds to the phosphorylated Tyr866 docking site on Axl that subsequently phosphorylates Akt and NF-κB. After phosphorylation, the AKT phosphorylates the Bcl-2-associated death promoter (BAD) that blocks the binding of BAD to anti apoptotic protein, reducing apoptosis followed by escalated cell survival [88, 89]. However, PI3K can phosphorylate NF-κB that inhibits the expression of proapoptotic protein caspase 3 and exhibits the formation of two major anti apoptotic protein, B-cell lymphoma-extra large (Bcl-xL) and Bcl-2 (B-cell lymphoma 2) which in turn promotes more cell survival [62]. PI3K can also activate p21 (RAC1) activated kinase 1(PAK1) that leads to increased cell invasion [90]. Heat-shock protein 25 is another downstream signaling protein that is activated by PI3K. Upon activation, this protein stimulates increased cell migration by actin remodeling [91]. As a whole, activation of PI3K signaling pathway by Axl can mediate increased cell proliferation, survival, cell motility and migration (see Figure 14) [92, 93].

Another pathway that is activated by phosphorylation of Axl is MAPK/ERK pathway. In this pathway, the docking protein Grb-2 binds to the autophosphorylation site Tyr821 and activates

Ras that will mediate the phosphorylation of Raf1, followed by Mek1 and Erk1, which will increase cell proliferation [93]. Axl also inhibit the inflammatory response against pathogens in the innate immune system by suppressing the cytokine signaling with Socs1 and Socs3 (suppressor of cytokine signaling 1 and 3) that are activated by the phosphorylation of transcription factor Stat1, followed by inhibition of toll like receptor (TLR), expressed on the sentinel cells such as dendritic cells and macrophages [87, 94]. Axl activation is also related to phosphorylation of the transcription factor Stat3 that is overexpressed in several cancers [95]. Axl also regulates the function of endothelial cell by modulating the angiopoietin/Tie2 and Dickkopf-homologue 3 (DKK3) signaling pathway. The inhibition of angiopoietin/Tie2 and expression of Dickkopf-homologue 3 (DKK3) promotes angiogenesis in the tumor cell [96].

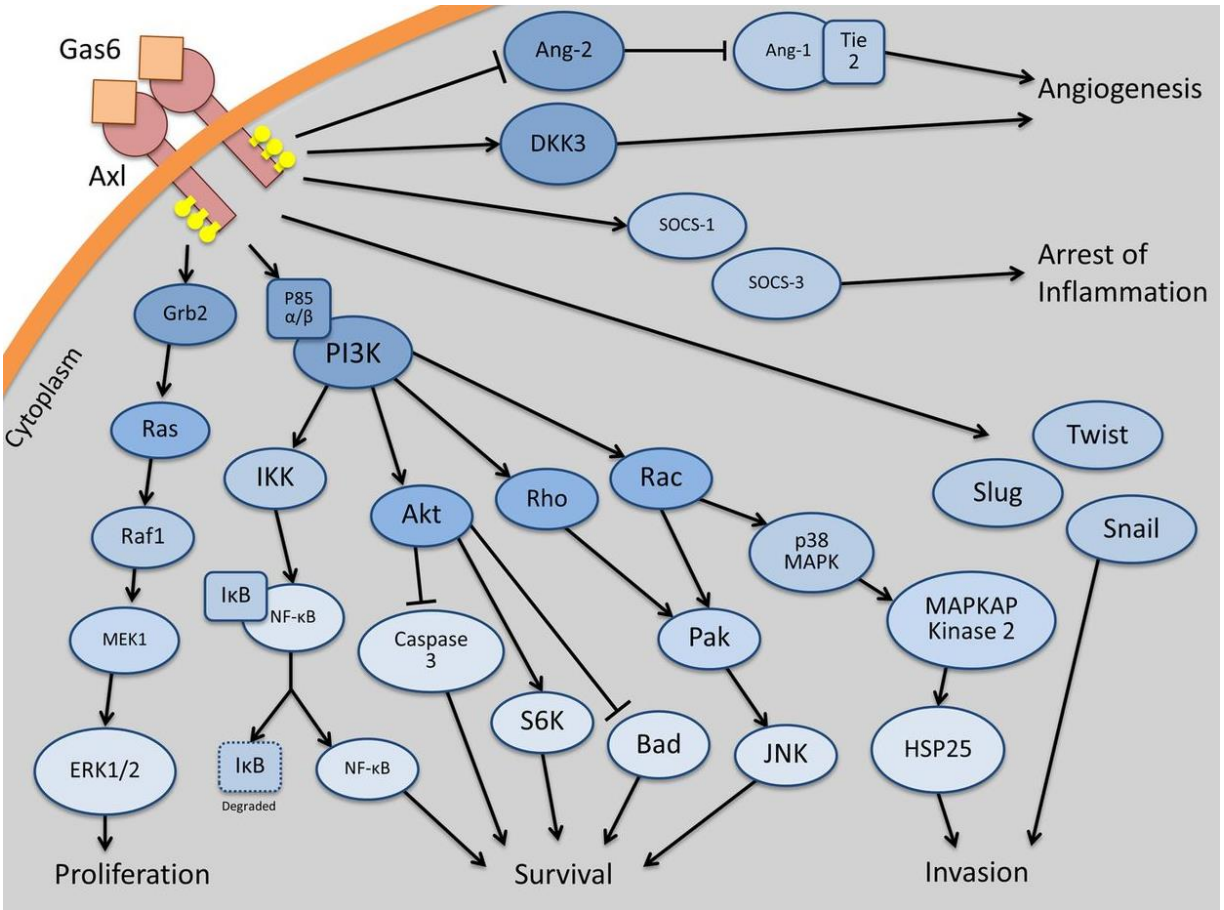

Figure 14: Downstream signaling cascade of Axl after binding with ligand Gas6. Different signaling pathways are activated by Axl that leads to increased cell proliferation, survival, migration, and invasion as well as help tumor cell by mediating angiogenesis. Adapted from [93].

1.5.6 Axl, plasticity and stemness

Stem cells have the ability to self-renew and differentiate into mature cell types. Similarly, cancer stem cell (CSCs) are neoplastic cells with ability to change phenotype, leading to cancer growth, spread and resistance to targeted therapy [97]. In embryonic development, various transcription factors regulate signaling of PI3K/Akt/mTOR, Hedgehog (HH), JAK/STAT, Wnt/β-catenin and Notch pathways control proliferation, differentiation, self-renewal of stem cells. Other transcription factors Twist1, Twist2, Slug, Snail, Zeb1, Zeb2 are characteristic of with epithelial mesenchymal transition (EMT) [97, 98]. Axl is upregulated by the EMT transcription factors that also modulate posttranscriptional and posttranslational modification in the cells that activates N-cadherin and represses E-cadherin [99]. The intermediate filament vimentin, a canonical mesenchymal marker, alters cell morphology and increases the migration capacity of cancer cells [100]. The correlation between Axl expression with the EMT and stemness markers is found in several malignancies, including breast cancer, leukemia, small cell lung cancer, prostate carcinoma, ovarian cancer, gastric carcinoma, chronic myeloid leukemia (CML), and colorectal cancer [101-104].

The expression of Axl is higher in the primary tumor as well as in the metastatic tumor compared to normal cell. Axl overexpression has correlation with increased invasiveness of the tumor cells, development of resistance to drug followed by poor prognosis of patient with different cancer. The invasiveness and metastatic properties of cancer cell in lung adenocarcinoma and glioblastoma can be increased by the overexpression of Axl via PI3K/AKT mediated NF-kB pathway [105, 106]. There is an association between cell proliferation by inhibition of apoptosis and Axl overexpression in osteosarcoma, astrocytoma, and ocular melanoma [107, 108]. Overexpression of Axl also has a correlation with the angiogenesis in cancer (new blood vessel formation) [109].

1.5.7 Axl in cancer

It has been shown in different studies that overexpression of Axl mediated PI3K/AKT signaling enhance the NF-kB pathway and has a correlation with the increased tumor cell invasion in the ovarian, breast, gastric cancer. Downregulation of this signaling leads to the decreased invasive properties of the cells in hepatic carcinoma [110-112]. The activation of Pak1 by Axl mediated PI3K/AKT signaling triggers cell invasion and inhibition of Axl reduces the PAK1 activation that lead to reduced cell invasion [111]. Axl works as a substrate for E3 ubiquitin ligase that

inhibit NK cell to trigger Casitas B lineage lymphoma b metastasis. The inhibition of Axl can downregulate the metastasis of Casitas B lineage lymphoma b [113]. In other different cancer types, Axl overexpression leads to prolonged cell survival. PI3K/AKT signaling activated by Axl receptor inhibits the pro apoptotic BAD protein by phosphorylation and activates the Bcl-2 and Bcl-XL anti apoptotic protein to reduce apoptosis found in breast cancer, osteosarcoma, ocular melanoma and chronic lymphatic leukemia [107, 108, 114]. Axl has role in the VEGF dependent PI3K/AKT activation that promotes vascular angiogenesis. It has been suggested that knockdown of Axl leads to impaired tube formation in endothelial cells and suppresses new blood vessel formation [115]. The tumor microenvironment is also regulated by Axl. Compared to normal tissue, the microenvironment of tumor produces more HIF1α in the hypoxic condition that enhance the transcription of Axl [116]. Axl also increases the expression of MMP-9 (Matrix metallopeptidase 9) that helps cancer cells to degrade the collagen type IV of the basement membrane to penetrate the blood vessel and travel to distant organ for further metastasis [117].

1.5.8 Axl in drug resistance

Axl expression is not only associated with cell proliferation, survival, migration, and metastasis but it is also tightly linked to the development of therapeutic resistance. The malignant melanoma patient carrying B-Raf proto-oncogene serine/threonine kinase (BRAF) mutation treated with BRAF-inhibitors have been found resistant to the inhibitor (see **Figure 15**) [36]. The Axl dimerize with other RTKs to give therapeutic resistance, such as in lung cancer it forms dimer with EGFR to give downstream signal. Thus, Axl supports cancer cells to achieve therapeutic resistance in different cancers [118]. Several studies show overexpression of Axl in different therapy resistant cancers. However, the mechanism is still unclear [119]. In lung cancer treatment, the anti EGFR therapy, cetuximab showed promising effect. Nevertheless, overexpression and dimerization of Axl to the EGFR receptor reduce the treatment effect with anti EGFR therapy, by activating the downstream signaling [118]. There are other studies suggesting that the overexpression of Axl have effect on therapy resistance in breast cancer patients [102].

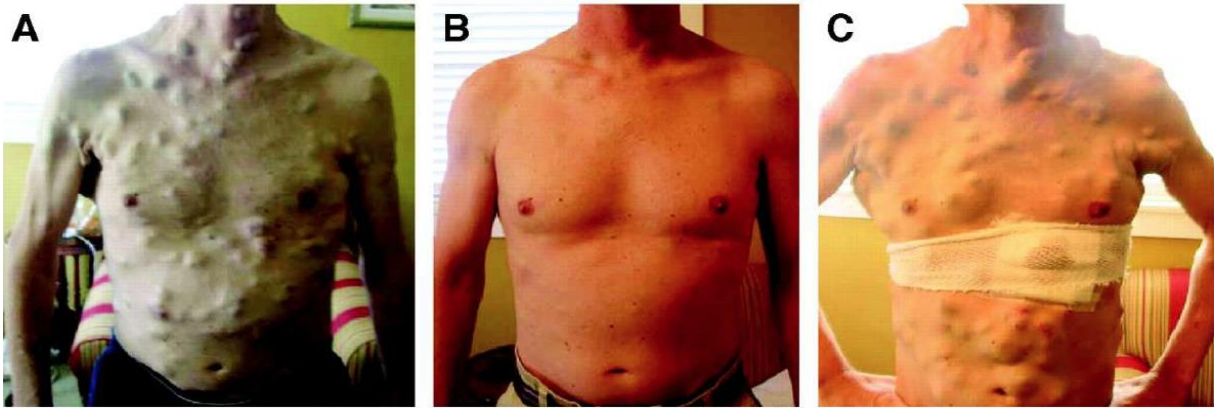

Figure 15: Patient with BRAF-inhibitor. A 38-year-old man with BRAF mutant melanoma. Pictures were taken (A) before treatment with PLX4032, (B) after 15 weeks of treatment with PLX4032, and (C) after 23 weeks of treatment, recurrence of melanoma. Adapted from [36].

1.6 Vitamin K, a cofactor for γ-glutamyl carboxylase (GGCX) to activate Gas6

A Danish scientist Henrik Dam first discovered vitamin K in the 1930s. Several vitamin K dependent protein (VKDPs) is activated by the γ-carboxylation of the glutamic acid residue in the body. Vitamin K serves as the cofactor for the enzyme γ-glutamyl carboxylase (GGCX) that catalyzes the γ-carboxylation of the glutamic acid residues. Vitamin K dependent proteins that are activated by γ-carboxylation are participated in several important biological functions such as signal transduction, vascular calcification, bone metabolism, cell proliferation, and mostly in blood coagulation [120]. Enzyme gamma-glutamyl carboxylase (GGCX) utilizes one molecule of reduced vitamin K hydroquinone (reduced form of vitamin K or KH2- active form), oxygen and carbon dioxide as cofactors and produce one molecule of oxidized vitamin K 2,3-epoxide (KO- inactive form). Simultaneously with the reaction, each glutamate on the vitamin K dependent protein is transformed to γ-carboxyglutamate by incorporation of additional carbon dioxide to the γ- carbon [121]. For reutilizing the vitamin K 2,3-epoxide, it is reduced back to vitamin k by the enzyme vitamin K epoxide reductase (VKOR) and further reduced to vitamin K hydroquinone by the enzyme vitamin K reductase (VKR). The enzymes in the vitamin K cycle are mostly protein located in endoplasmic reticulum membrane (see Figure 16) [122].

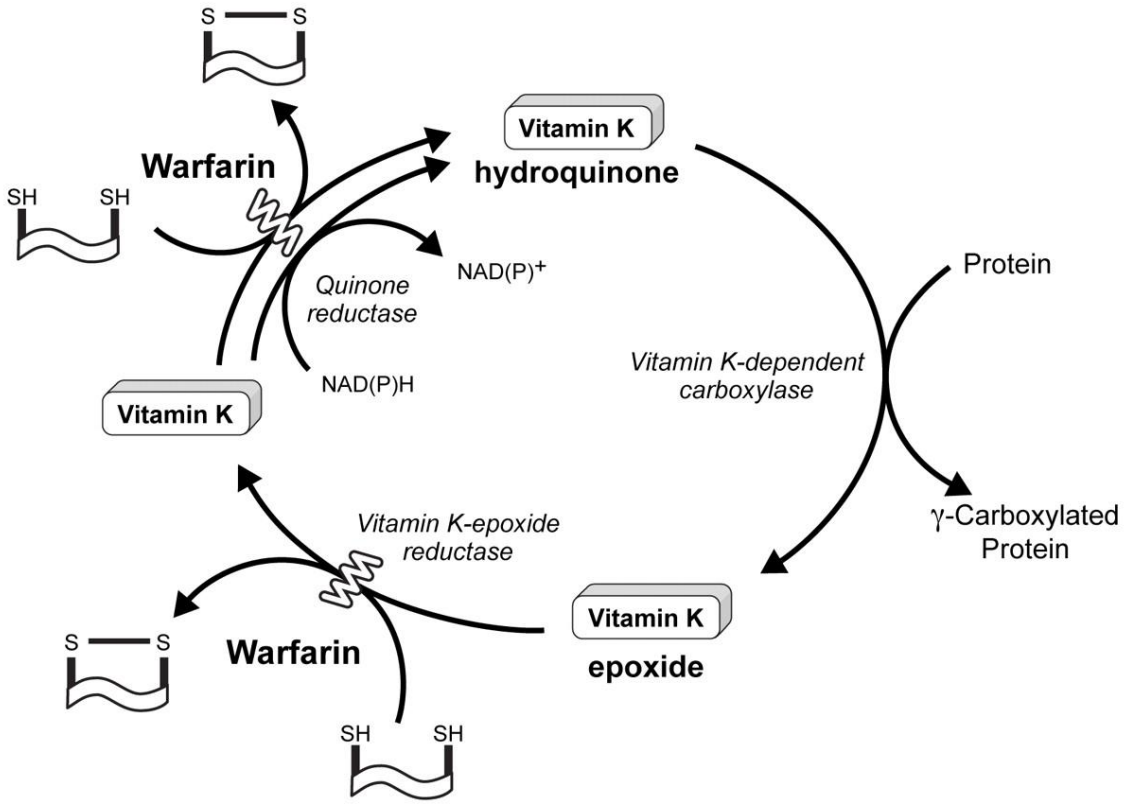

Figure 16: Vitamin K Cycle. Adapted from [121]

1.7 Warfarin is cancer reductionist

The most used anticoagulant drug in worldwide is warfarin. Around 2-10% adult population use this orally administered anticoagulant. After the administration, the body completely absorb the warfarin. The 98-99% of warfarin bound to the albumin (plasma protein) in the body. The liver mostly CYP2C9 metabolizes the warfarin completely after plasma concentration of it gets highest level after 4 hours [123, 124]. Warfarin works as the antagonist of vitamin K. It blocks the enzyme vitamin K epoxide reductase (VKOR) to convert vitamin K hydroquinone from vitamin K epoxide. As inactivation of the vitamin K cycle, the vitamin K concentration reduces in the body [125]. In the absence of vitamin K, the Gla carboxylation of the vitamin K dependent proteins will reduced. The ligand Gas6 is a vitamin K dependent protein and without vitamin k Gas6 can bind to the receptor Axl, hence cannot activate the receptor. The Axl is inhibited by the warfarin treatment is mentioned in the article by Gry Haaland named, "Association of Warfarin use with Lower Overall Cancer Incidence among Patients older than 50 Years" [126].

1.8 Axl, a regulator of melanoma progression as chemotherapeutic resistance

Researchers are trying to understand the importance of Axl in development of melanoma, their effect in metastasis and association with drug resistance. Since 50% of the melanoma is caused by *BRAF* mutation and Raf signals downstream of the MAPK pathway. However, cancer cells somehow acquire resistance against BRAF inhibitors, which means they are bypassing the signaling cascade. It is also found that, combination therapy with BRAF inhibitor and Axl inhibitor exhibits better effect suggesting that Axl is the alternative pathway that allows play a role in acquired resistance [127]. Some other researchers showed that increased cell invasion and migration followed by metastasis of melanoma linked with upregulation of Axl. Knocking down Axl or use of the inhibitor R428 (also known as BGB324 or Bemcentinib) against Axl improves disease by declining invasion and migration but less of an effect on cell proliferation [128, 129]. MITF (microphthalmia-associated transcription factor) a transcription factor that has been linked with Axl to provide acquired resistance against therapies. It is found that MITF has some effect in suppression of melanoma and inhibition of metastatic phenotype [130].

1.9 Axl and vitamin K

As previously described, Axl receptor tyrosine kinase is activated by the vitamin K dependent ligand Gas6. Upon γ-carboxylation of the Gla domain of the ligand Gas6 by vitamin K dependent enzyme GGCX, Gas6 can activate Axl. The non-carboxylated gas6 can bind to the Axl, but is unable to activate Axl and therefore the downstream signal but some reports claim it can mediate limited signal [131]. To date, link between vitamin K pathways with the therapeutic resistance of melanoma is still unclear and unexplored. The mechanism behind metastasis and therapeutic resistance may be unraveled with the understanding of vitamin K pathway gene

2 Aims of the study

The aim of this thesis is to understand if the Axl mediated signaling has any effect in cancer progression, metastasis and therapy resistance in a series of melanoma cell lines established at the Auckland Cancer Society Research Centre (ACSRC).

The specific aims of the study are:

- Characterize the expression of Axl, Gas 6 and vitamin K enzymes in a panel of 21 melanoma cell lines
- Determine whether expression of Axl, Gas6 and vitamin K enzymes are correlated with poor prognosis of melanoma patients
- Characterize the effect of vitamin K on cell migration, proliferation and spheroid formation in melanoma cell lines
- Measure the effect of the vitamin K and Axl inhibitor BGB324 on the expression of plasticity markers and other relevant genes in the melanoma cell lines.
- Apply the findings from these aims to study pathways involved in drug resistance and malignant progression using high dimensional mass cytometry (CyTOF).

3 Materials & Methods

3.1 Cell culture

3.1.1 Cell Lines

The twenty New Zealand melanoma (NZM) cell lines used for this study were obtained from surgical samples of metastatic melanoma from Professor Bruce Baguley's laboratory, the University of Auckland, New Zealand, and the CRISPR Axl knockout of NZM 17 line was obtained from Jing Kang, PhD candidate at the University of Bergen (see Table 3). Written consent was obtained from all patients under Auckland Area Health Board Ethics Committee guidelines.

Table 3*:* **Cell line panel.** Patient cell line with BRAF mutation status and the treatments they have received. Adopted from [132]

Cell line	***BRAF* V600E mutation**	**Patient Therapy**
NZM 1	Absent	Surgery and Radiotherapy
NZM 2	Absent	Surgery and Radiotherapy
NZM 3	Present	Surgery and Radiotherapy
NZM 4	Present	POC chemotherapy, 2 cycles Commenced after tissue collection
NZM 6	Present	Surgery and Radiotherapy
NZM 7	Present	Surgery and Radiotherapy
NZM 9	Absent	Surgery and Radiotherapy
NZM 11	Present	POC chemotherapy, 6 cycles Treatment commenced after tissue collection
NZM 17WT	Absent	Received vaccination before tissue collection
NZM 17AXL-/-	Absent	
NZM 20	Present	Surgery and Radiotherapy
NZM 30	Present	Surgery and Radiotherapy
NZM 34	Present	Received vaccination after tissue collection
NZM 40	Absent	POC chemotherapy, 2 cycles

		Received before tissue collection DMXAA IFN, Received vaccine Commenced after tissue collection
NZM 46	Absent	No information
NZM 55	Present	Temozolomide – one cycle. Received after tissue collection – July, 2005. Tissue collected: 10.11.2004
NZM 61	Absent	Surgery and Radiotherapy
NZM 63	Absent	DTIC chemotherapy 4 cycles Commenced after tissue collection
NZM 76	Present	No information
NZM 86	Absent	Surgery and Radiotherapy
NZM 100	Present	Surgery and Radiotherapy

3.1.2 General maintenance of NZM cell lines

NZM cell lines were cultured in α-modified minimal essential medium supplemented with insulin (5 μg/ml), transferring (5 μg/ml), and sodium selenite (5ng/ml), 100 U/ml of penicillin, 100 μg/ml of streptomycin (PS), 5% fetal bovine serum (FBS). The cell lines were cultured in a humidified low oxygen incubator (5% O_2, 5% CO_2, 37 °C) to maintain physiologically oxygen levels instead of conventional incubators with atmospheric level (21% O_2).

The cell lines were handled in a clean lamina flow hood to maintain sterility and were checked daily under a Nikon ECLIPSE TS100 microscope to monitor confluence. The cells were cultured in 75 cm^2 (T75) flasks and split in 10 cm petri dishes for RNA and protein extraction. Images of cells were captured occasionally on a Nikon D3000 microscope to monitor changes in morphology with varying growth conditions.

3.1.3 Cell thawing procedure

Cell culture medium was warmed in a 37°C water bath for 30 minutes before thawing cells from liquid N_2 storage. The cryovials that contain approximately one million cells of each NZM cell line were taken out from liquid nitrogen storage and were instantly placed into the 37°C water bath. The vials were transferred into the lamina flow hood after thawing. Before being put into the hood, the vials were wiped with 70% ethanol to avoid contamination. The cells in each vial were transferred to a 25 cm^2 (T25) flasks using 5 ml of media and the flasks were then put into a low oxygen incubator (5% O2, 5% CO2, 37 °C). The medium was exchanged with fresh medium the next day. After the cells reached 80% confluency, they were transferred into 75 cm^2 (T75) flasks for further growth.

3.1.4 Cell passaging procedure

After the cells reached a confluency of approximately 70-90% they were passaged, every 2-3 days. However, since each of the cell lines have different growth rates, some needed to be passaged more frequently to prevent overgrowth, while other cells only received fresh medium. Cell culture medium, trypsin-EDTA and PBS were pre-warmed for approximately 30 minutes in a 37°C water bath before passaging. First, medium was collected (for reseeding the non-adherent cells) and centrifuged, cells were washed with 5 ml 1×PBS, then 3 ml trypsin-EDTA was added to each 75 cm^2 (T75) flask. Flasks were placed into incubator for 2-3 minutes, the trypsinized cells were observed under a light microscope. To hasten the process of detachment, the side of the flask was agitated gently several times until the cells were completely detached. To stop trypsin activity, 3 ml of fresh serum containing medium was added and the cell suspension was transferred to 15 ml tubes and was centrifuged at 1200 rpm for 5 minutes. Then the centrifuged cells were resuspended with fresh media after the supernatant was removed. The resuspended cells were transferred into a new dish or flask. Each of the cell line's RNA and protein were extracted from three passages. For each cell line, one 75 cm^2 (T75) flask was split into two 10 cm plates (one for RNA and another for protein extraction) and one 75 cm^2 (T75) flask (for next passage). Cells were also seeded in T75 flasks for future CyTOF analysis (described in section 3.6)

3.1.5 Cell freezing

Continuous culturing of cell lines can make them more prone to genetic drift, microbial contamination, senescence and equipment failure can cause destruction of the cell lines [133]. It is therefore important to freeze the cells in liquid nitrogen for long-term storage. After reaching 70-90% confluency, the cells were washed with PBS, trypsinized (as previously described in 1.1.4) and centrifuged at 1200 rpm for 5 minutes. After centrifugation, the cells were resuspended in freezing medium (20% FBS and 10% DMSO in α-modified minimal essential medium). Cell density of 1×10^6 cells per ml was prepared and 1 ml was transferred into each cryovial. The vials were labeled with cell line names, passage number and date, transferred into a freezer box containing isopropanol, and put into -80°C overnight before transferring into liquid nitrogen for long-term storage.

3.1.6 Cell counting and quantifying viability

Counting of the cells was normally performed using the *Countess automated cell counter* from Invitrogen. If the cells had a low concentration, the counting was performed using a hemocytometer. The Countess contains a slide port where cell counting chamber slides can be inserted. 10 µl of cells suspended in media was mixed with 10 µl of trypan blue (If cells take up trypan blue, they are considered non-viable) [134]. 10 µl of the sample mixture was transferred to the chamber port on one side of the Countess Cell Counting chamber slide, which was then inserted into the instrument. Upon activation, the machine counted the live and dead cells indicating the viability percentage.

3.2 Gene expression analysis by RT-PCR

3.2.1 Cell preparation for RNA extraction

When reaching 70- 90% confluency on a 10 cm plate, cells where scraped were scraped in PBS, transferred to a 15ml tube and centrifuged at 1200 rpm for 5 minutes. The PBS was aspirated and the cells were resuspended in 1ml cold PBS, transferred to 1.5 ml Eppendorf tube, centrifuged at 1200 rpm for 5 minutes. The PBS was aspirated and the pelleted cells were transferred into -80°C freezer for further RNA extraction.

3.2.2 RNeasy Mini Kit (50) for RNA extraction

RNA was extracted using the RNEasy Mini Kit from Qiagen following the manufacturer's instructions. Cell pellets were removed from -80 freezer and gently thawed by flicking. The RNA can be degraded by vortexing, so this was avoided. After properly thawing, 600 µl buffer RLT was added in the Eppendorf tube to disrupt the cell pellet, and to lyse the cells. For proper homogenization of the cells, a motor cordless homogenizer was used. Each sample was homogenized for 25-30 sec depending on the cell pellets. Equal amount (600 µl) of 70% ethanol was added to the lysate and mixed thoroughly by pipetting. The lysate was transferred to a RNEasy spin column with 2 ml collection tubes and centrifuged at 10,000 rpm for 15s. The flow through was discarded The membrane spin column now containing bound RNA was washed with 700 µl buffer RW1 and centrifuging at 10,000 rpm for 15s. Buffer RW1 contain guanidine salt that washed away carbohydrate, fatty acid and protein. The flow-through was discarded and 500 µl of RPE buffer was added to the spin column to remove salts from the membrane and in the same manner, centrifuged at 10,000 rpm for 15s. The flow-through was discarded, 500 µl buffer RPE was added for the second wash and centrifuged at 10,000 rpm for 2 minutes. The collection tube with flow through was replaced and samples were centrifuged for 1 minute at maximum speed to collect the residual flow through. Consequently, the collection tube was replaced with a new 1.5 ml Eppendorf tube. Finally, 30 µl of RNase-free water was added to the column and centrifuged at 10,000 rpm for 1 min to elute the RNA. RNA concentration was measured with NanoDrop by reading absorbance at 260nm.

3.2.3 Re-precipitating RNA

The concentration and purity of extracted RNA can be affected by chemical contamination. Chemically contaminated RNA was re-precipitated in 10% volume of sodium acetate (3M, pH 5.2) and 2X volume of 100% ethanol and incubated overnight at -20 °C. Samples were centrifuged the next day for 40 minutes at 18,000 rpm at 4°C. The supernatant was discarded and the RNA pellet was resuspended by gently flicking in RNase free water containing 70% ethanol. After resuspension, the tubes were centrifuged at 18,000 rpm for 15 minutes at 4°C. The supernatant was decanted and the pellet resuspended in 100% ethanol and centrifuged at 18,000 rpm for 40 minutes at 4°C. Accordingly, the supernatant was discarded and the pellet were resuspended in 27 µl RNase-free water and incubated at room temperature for 10 minutes. The samples were checked for contaminants by NanoDrop analysis. The absorbance for nucleic

acid is maximum at 280 nm and minimum at 260nm. A 260/280 ratio of ~2.0 indicates that the extracted RNA is pure.

3.2.4 Synthesis of cDNA

cDNA was made with 4000 ng of RNA using High Capacity cDNA Reverse Transcription Kit in a 20 µl reaction. The master mix was made combining 4µl 10X RT buffer, 4 µl 10X RT random primers , 1.6 µl 25X dNTP Mix 100mM, 2µl reverse transcriptase and 8.4 µl water. The 20 µl sample and 20 µl of master mix were then added together and mixed properly to make it 40 µl. The mixture was transferred in the thermal cycler with the loading program 10 min at 25ºC, 120 min at 37ºC, 5 min at 85ºC and, samples were held at 4ºC (see Table 4). After making cDNA, equal volume (40 µl) of nuclease free water was added to avoid DNA degradation. The cDNAs were then ready for use in RT-PCR and the rest were stored at -20ºC (see Table 4).

Table 4: cDNA synthesis reagents and equipment.

cDNA Synthesis	
Material	**Supplier**
High-Capacity cDNA Reverse Transcription Kit	Applied Biosystems
Ambion® Nuclease-Free Water	Roche
Thermal cycler	BIO-RAD

3.2.5 Quantitative PCR (qPCR)

For gene expression analysis, probe based quantitative PCR (qPCR) also known as real time polymerase chain reaction (RT-PCR) was used. It is a powerful and sensitive tool for detecting specific mRNA quantity in samples of interest. The qPCR machine named LightCycler® 480 system (Roche) measures the intensity of the florescence emitted by the probe at each cycle of the reaction. After first cycle, the florescence intensity is not enough to detect. However, as the reaction advances, new amplicons are generated that will increase the florescence intensity as well as background intensity. The LightCycler software determines a threshold level to reduce background intensity. The point at which the reaction curve crosses the threshold level produces

Ct (threshold cycle) values that represents the number of cycle needed to detect the real florescence intensity from the sample [135].

After the synthesis of cDNA from different RNA samples, 30 µl reaction mix for each sample was made and transferred in a 384 well plate. Each of the 30 µl reaction mix contained 15 µl LightCycler® 480 Roche master mix, 1.5 µl TaqMan probe of interest, 9 µl RNase free water, 4.5 µl cDNA of interest. In a 384 well plate, each well contained 10 µl of reaction mix (see Table 6). For each sample, three technical replicates were used. For normalizing the experimental error in qPCR, two normalization technique can be used. One is the normalization to total RNA that needs reliable method for total RNA quantification and other is using housekeeping gene that is more expected method [136] GAPDH was used as it is most commonly used housekeeping gene. Other housekeeping genes including, PPIA, 18s rRNA, β-ACTIN (ACTB) and Tata Binding Protein (TBP), can be used depending on different experiment conditions for normalization. The 384 well plate with the sample and housekeeping gene was then loaded to the LightCycler® 480 system for running with the following setting as listed in (see Table 5)

Table 5: Light Cycle 480 system program settings.

PCR Stages	**Temperature** (ºC)	**Time** (mm:ss)
Pre-incubation	95ºC	10:00 mins
Amplification (40 cycles)		
Amplification-1	95ºC	00:10 secs
Amplification-2	60ºC	00:30 secs
Amplification-3	72ºC	00:01 secs
Cooling	40ºC	00:30 secs

After the completion of the 40 cycle, the Ct value or the crossing point values (CP) generated curves that represent the number of the cycles each sample needed to detect the florescence by LightCycler® 480 system. The higher the Ct value, represents lower gene expression; and the lower Ct value indicates high expression of the particular gene. These values were then taken and used to perform comparative analysis between the expressed genes with the housekeeping gene (endogenous control) represented by delta Ct. The delta Ct was measured by subtraction of delta Ct value of untreated sample from the treated sample. Changes in gene expression

between samples were calculated using the formula $2^{-\Delta\Delta Ct}$ that represents the relative expression fold change between the genes with and without treatment [137].

The analysis of Ct value using the equation:

Ct = PCR cycle

ΔCt = Ct (gene test) – Ct (endogenous control)

$\Delta\Delta C_t$ = treated (Ct (gene test) – Ct (endogenous control)) – untreated (Ct (gene test) – Ct (endogenous control))

Relative quantification (RQ) = $2^{-\Delta\Delta Ct}$

Relative quantification is fold change of the treated compared to the untreated. For example, if the RQ is 2.0, it means the gene is expressed two times more than the untreated one, if RQ is 0.2 means the expression is 80% less then untreated.

The data was collected from the LightCycler® 480 system and transferred to Microsoft Excel 2016 to determine the RQ value from the Ct value. After generating RQ values, they were presented in graphical form and analyzed using Graphpad Prism 7.

Table 6: RT PCR reagents and equipment

RT PCR	
Material	**Supplier**
LightCycler® 480 Probes Master	ThermoFisher Scientific
TaqMan® Gene Expression Assays (all probes)	ThermoFisher Scientific
Ambion® Nuclease-Free Water	Roche
LightCycler® 480 system	Roche
384 well PCR plate	ThermoFisher Scientific

3.3 Protein expression analysis by western blot

3.3.1 Cell lysate preparation

Cells grown to 70-90% confluency were washed with ice cold PBS twice, and lysed in RIPA buffer containing 1% Sodium Orthovanadate (SO), 1% protease cocktail inhibitor (PIC), 1% Phenylmethylsulfonyl fluoride (PMSF) and 1% phosphatase cocktail inhibitor (see Table 7).

After adding lysis buffer, the cells were scraped and lysates were transferred to microcentrifuge tubes and incubated on ice for 20 minutes, vortexing every 5-10 minutes. The lysates were centrifuged at 12,000 rpm for 10 mins at 4°C to pellet DNA and cellular debris. The supernatants were transferred to new tubes using a micropipette and pellets were discarded. The supernatants were then used instantly or stored at -80ºC.

Table 7: Materials used in cell lysate preparation

Material	**Supplier**
RIPA Buffer	Sigma Aldrich
PIC	Sigma Aldrich
SO	Sigma Aldrich
PMSF	Sigma Aldrich
Phosphatase inhibitor cocktail	Sigma Aldrich

3.3.2 BCA assay for determining protein concentration

For quantifying the total protein concentration in the lysate, Bicinchronic Acid (BCA) assay was performed using Pierce™ BCA Protein Assay Kit from Thermo Scientific in a 96 well plate. The standard curve was generated from the serial dilution from 0 to 2000 µg/ml of the BSA standard solution. 5 µl lysates from each sample were added to the plate and 45 µl PBS to make a 10X diluted protein sample. BCA mix was made by mixing BCA reagent A (BCA) and BCA reagent B (copper sulfate) in a 1:50 ratio. In each well, 50 µl of the BCA mix was added and placed on a shaker for 1 minute to mix properly and incubated at 37°C for 20-30min. The concentration of the samples was measured at 562 nm absorbance with the plate reader (BioTek Instruments). The absorbance values were analyzed using Microsoft Excel 2016 where the BSA standard curve was extrapolated to measure protein concentrations of each sample.

3.3.3 SDS PAGE

After measuring the sample protein concentration, the lysates were prepared for SDS PAGE (sodium dodecyl sulfate–polyacrylamide gel electrophoresis) that separates the protein by molecular mass in an electric field. The samples were diluted using PBS and sample buffer

loading dye (BIO-RAD xt sample buffer, 4x with 5% β-mercaptoethanol). Protein samples containing sample buffer were denatured by boiling at 95°C for 10 minutes.

Table 8: Materials used in SDS PAGE

Material	Supplier
xt sample buffer, 4x	BIO-RAD
Mini-PROTEAN® TGX™ Protein Gels, 20 µl 12 well Mini-PROTEAN® TGX™ Protein Gels, 15 µl 15 well	BIO-RAD
PageRuler™ Plus Prestained Protein Ladder, 10 to 250 kDa	ThermoFisher Scientific
10x Tris/Glycine/SDS buffer	BIO-RAD

Samples were separated on 4-15% gradient Mini-PROTEAN® TGX™ Protein Gels supplied by BIO-RAD (12-well with 20 µl sample loading volume or 15-well with 15 µl sample loading volume depending on experiment) in 10X Tris/Glycine/SDS buffer. 5 µg PageRuler™ Plus Prestained Protein Ladder (10 to 250 kDa from ThermoFisher Scientific) was used as a molecular marker (see Table 8). The gel was run for 1 hour at 100V.

3.3.4 Transfer of protein and immunoblotting

Following separation on SDS-PAGE, the proteins were transferred to a PVDF membrane also by electrophoresis (semi-dry). Transfer buffer in which filter papers were soaked consisted of 20% ethanol, 20% transfer buffer (Trans-Blot® Turbo™ 5x Transfer buffer by BioRad) and 60% milQ. The 0.2 µm PVDF membrane was presoaked in MeOH for 5 min. The separated proteins were transferred to the membrane for detection by antibody. The gel was removed from its chamber and was activated under UV on the ChemiDoc XRS+ (BIO-RAD). After activation, the transfer sandwich was prepared in the follow order from bottom to top: filter paper, PVDF membrane, gel and filter paper. The buffer-soaked sandwich was then placed in the Turbo transfer tank for 7 mins to transfer proteins from the gel to the membrane. The

membrane was placed in the ChemiDoc XRS+ again to verify the transfer and record the total protein content in the membrane. The membrane was blocked at room temperature with 5% non-fat dry milk or 5% BSA in TBS-Tween 0.1% (Sigma Aldrich) for an hour to avoid any unspecific binding. For detection of Axl expression, the membrane was incubated with primary anti-human Axl antibody (Polyclonal Goat IgG AF154; R&D Systems) in 2% BSA TBST at 1:1000 concentration overnight at 4°C. Axl antibody from cell signaling Axl (C89E7 Rabbit mAb) was also used. The blot was again washed three times for 5 minutes each with PBS-T and was incubated with anti-goat secondary antibody (HRP-conjugated anti-Goat IgG, anti-Rabbit IgG Secondary Antibody from Invitrogen) at 1:5000 or 1:10,000 in 5% milk or BSA at room temperature for 1 to 1.5 hour. AB885 from Abcam (Polyclonal Goat IgG) was used to identifying Gas6, diluted 1:500 in TBS-T and anti-goat secondary antibody (HRP-conjugated Anti-Goat IgG from Invitrogen) was used as secondary at 1:2000 concentration in 5% milk PBST. For detecting GGCX ab106924 from abcam raised in goat was used diluted 1: 2000 in 2% BSA and anti-goat secondary antibody (HRP-conjugated Anti-Goat IgG source wrong) diluted 1: 2000 concentration in 5% milk PBS-T.

VKORC1 was detected using ab206656 (rabbit monoclonal IgG) at 1: 1000 dilution in 5% milk TBST and HRP-conjugated Anti-Rabbit IgG Secondary Antibody (from invitrogen) at 1:10000 in 5% milk PBS-T. Anti-Vimentin antibody (ab137321) raised in rabbit (polyclonal) was used to detect vimentin at 1:50000 dilution in 2% BSA and Anti-Rabbit IgG Secondary Antibody HRP conjugated; R&D Systems was used as secondary at a concentration of 1:5000 in 5 % milk PBST. For detecting loading control alpha tubulin (Monoclonal Anti-α-Tubulin antibody produced in mouse) was used at 1:5000 concentration in 5% BSA and anti-mouse secondary antibody (goat anti-mouse IgG-HRP from invitrogen) at 1:10,000 concentration was used as secondary antibody. After incubation with secondary antibody, the blots were washed 3X 5 minutes with PBST or TBST, and the Pierce™ ECL Western Blotting Substrate (mixed 1:1) was added for 5 min. However, for stronger signal in short time for proteins with lower expression levels, Super Signal West Femto Maximum Sensitivity Substrate (mixed 1:1) was used for a few seconds to enhance the signals. The blot was exposed using ChemiDoc XRS+ (BIO-RAD) and viewed using BIO-RAD's Image Lab software (see Table 9).

Table 9. Materials used in transfer of protein and immunoblotting

Material	**Supplier**
Trans-Blot® Turbo™ Transfer System	BIO-RAD
Trans-Blot® Turbo™ Transfer Buffer	BIO-RAD
Immun-Blot® PVDF Membrane Filter paper for Turbo™ Transfer	BIO-RAD
Human Axl antibody AF154 Axl antibody, C89E7 (Rabbit monoclonal antibody)	R&D Systems Cell singling
HRP-conjugated Anti-Goat IgG Secondary Antibody HRP-conjugated Anti-Rabbit IgG Secondary Antibody	Sigma Aldrich Invitrogen
Gas6 antibody, AB885 (Polyclonal Goat IgG)	R & D system
GGCX antibody, ab106924 (Polyclonal Goat IgG)	Abcam
VKORC1 antibody, ab206656 (rabbit monoclonal IgG)	Abcam
Vimentin antibody, ab137321(rabbit polyclonal IgG)	Abcam
Alpha tubulin (Monoclonal Anti-α-Tubulin antibody produced in mouse)	Sigma Aldrich
Goat anti-mouse IgG-HRP: sc-2005	Invitrogen
Pierce™ ECL Western Blotting Substrate	ThermoFisher Scientific
SuperSignal™ West Femto Maximum Sensitivity Substrate	ThermoFisher Scientific
Blotting-Grade Blocker	BIO-RAD

3.4 Functional assays

3.4.1 Cell migration analysis using xCELLigence

Cell migration was studied by xCELLigence technology in real time. The xCELLigence electronic real-time cell-sensing assay (RTCA) DP system consists of three components. First, RTCA impedance analyzer that provide stations for three 16 well plates inside a tissue culture incubator. Second, a display monitor to assess migration using CIM plate 16 on the xCELLigence DP analyzer. Third, the 16 well CIM plates that have two chambers separated by microporous membrane made with pores on the top and gold electrodes on the bottom. The bottom of the CIM (cell invasion/ migration) microwell plates are covered with gold microelectrodes in an interdigitated pattern that measures the differences of impedance within an electrical circuit. When cell from the upper chamber passes through the 0.8 μm pore in the membrane and then adhere to the gold microelectrodes attached to the lower chamber containing chemoattractant, the computer with RTCA software generates cell index (CI) values. The cell index (CI) is the differences between the impedance at time point n and impedance in the absence of cells, divided by a nominal impedance value that is converted into a unit less parameter. This software was used for monitoring live cells as well as for analyzing the data generated. The cell number and cell size can influence the CI value. In the dual-plate (DP) format, migration was detected using the change of impedance signals generated by number of cell passes pore and attached to the electrode. It can be used to identify cell migration or invasion in short or long period of time.

The RTCA impedance analyzer was placed in an incubator (37°C, CO2 5%, O2 21%). However, cells used in the experiments were cultured in a low oxygen incubator (37°C, CO2 5%, O2 5%). The CIM-Plate is composed of two chambers, upper and lower chamber both containing 16 wells. The wells were numbered from top bottom (from A1, A2, B1, B2 ….to H1 and H2). For migration analysis, 14 wells from A1 to G2 wells of the lower chamber of the CIM-plate were filled with 160 μl medium containing 10% fetal bovine Serum (FBS) as a chemoattractant. However, the H1 and H2 were filled with serum free media (SFM) as a negative control. After filling up the lower chamber, CIM-plate 16 was assembled by placing the upper chamber on the top. The chambers were attached carefully by avoiding bubble in between the chamber. 30 μl of serum-free medium was added to the 16 wells of the upper chamber. After assembling the CIM-Plate, it was placed in the RTCA DP analyzer for 1 hour inside the incubator for background measurement. In the meantime, the cells to be used in the

Table 10: Arrangement of CIM-Plate for cell migration

A1: upper- NZM 3 (20000 cells) in FBS free medium, lower- 10%FBS medium	A2: upper-NZM3 with Vit K (20000 cells) in FBS free medium, lower-10%FBS medium
B1: upper- NZM 3 (20000 cells) in FBS free medium, lower- 10%FBS medium	B2: upper-NZM3 with Vit K (20000 cells) in FBS free medium, lower-10%FBS medium
C1: upper- NZM 3 (20000 cells) in FBS free medium, lower- 10%FBS medium	C2: upper-NZM3 with Vit K (20000 cells) in FBS free medium, lower-10%FBS medium
D1: upper- NZM 6 (20000 cells) in FBS free medium, lower- 10%FBS medium	D2: upper-NZM6 with Vit K (20000 cells) in FBS free medium, lower-10%FBS medium
E1: upper- NZM 6 (20000 cells) in FBS free medium, lower- 10%FBS medium	E2: upper-NZM6 with Vit K (20000 cells) in FBS free medium, lower-10%FBS medium
F1: upper- NZM 6 (20000 cells) in FBS free medium, lower- 10%FBS medium	F2: upper-NZM6 with Vit K (20000 cells) in FBS free medium, lower-10%FBS medium
G1: upper- NZM 3 (20000 cells) in FBS free medium, lower- 10%FBS medium	G2: upper-NZM6 with Vit K (20000 cells) in FBS free medium, lower-10%FBS medium
H1: upper- NZM 3 (20000 cells) in FBS free medium, lower- FBS free medium	H2: upper-NZM6 with Vit K (20000 cells) in FBS free medium, lower- FBS free medium

Table 11: Arrangement of CIM-Plate for cell migration

A1: upper- NZM 20 (20000 cells) in FBS free medium, lower- 10%FBS medium	A2: upper-NZM20 with Vit K (20000 cells) in FBS free medium, lower-10%FBS medium
B1: upper- NZM 20 (20000 cells) in FBS free medium, lower- 10%FBS medium	B2: upper-NZM20 with Vit K (20000 cells) in FBS free medium, lower-10%FBS medium
C1: upper- NZM 20 (20000 cells) in FBS free medium, lower- 10%FBS medium	C2: upper-NZM20 with Vit K (20000 cells) in FBS free medium, lower-10%FBS medium
D1: upper- NZM 34 (20000 cells) in FBS free medium, lower- 10%FBS medium	D2: upper-NZM34 with Vit K (20000 cells) in FBS free medium, lower-10%FBS medium
E1: upper- NZM 34 (20000 cells) in FBS free medium, lower- 10%FBS medium	E2: upper-NZM34 with Vit K (20000 cells) in FBS free medium, lower-10%FBS medium
F1: upper- NZM 34 (20000 cells) in FBS free medium, lower- 10%FBS medium	F2: upper-NZM34 with Vit K (20000 cells) in FBS free medium, lower-10%FBS medium
G1: upper- NZM 20 (20000 cells) in FBS free medium, lower- 10%FBS medium	G2: upper-NZM34 with Vit K (20000 cells) in FBS free medium, lower-10%FBS medium
H1: upper- NZM 20 (20000 cells) in FBS free medium, lower- FBS free medium	H2: upper-NZM34 with Vit K (20000 cells) in FBS free medium, lower- FBS free medium

Assay were prepared by counting. Four NZM cell lines with and without vitamin K treatment were washed with PBS and trypsinized. After trypsinization, the serum containing media was added at a 1:1 ratio to neutralize the trypsin. Then the cells were transferred into a 15ml tube for centrifugation at 800g for 5 min and after centrifuging, cells were resuspended in serum-free medium. The concentration of the cells in the serum free media was determined and was adjusted to 20,000 cells/ml by adding required amount of the same media. After incubation and background measurement, 100 µl of each cell line was added to the upper chamber to give a final of 2000 cells/well. In the bottom 4 wells, G1 and G2 were used as positive controls with serum in the lower chamber and H1, H2 used for negative control as previously explained. The CIM-plates were left in tissue culture hood for 30 minutes at room temperature to allow the cells to settle on the bottom surface of the upper chamber. Then the CIM 16 plates were placed in the RTCA DP analyzer inside the incubator and measurements were taken at intervals of 15 min for 24 hours and sometimes up to 48 hours. After 48 hours (depending on the experiment), the impedance values expressed as a CI value generated by the xCELLigence were collected as excel files and the data were analyzed by GraphPad Prism 7. All samples were run as three technical replicates. (see Table 10 & Table 11)

3.4.2 Cell proliferation & Spheroid formation assay using IncuCyte

The incuCyte®ZOOM (Essen Bioscience) system allows continuous and quantitative live cell imaging. In this system, the viable cells are measured in situ in a physiologically relevant environment inside the incubator. It has three objectives with magnifications of 4x, 10x and 20x. The system is fully automated and it takes picture of the plate at required time intervals. For the proliferation assay, the 10x magnification was used. The IncuCyte was placed in the normal incubator (37°C with 5% CO2). However, the cells were cultured in the low oxygen incubator (5% O_2, 5% CO_2, 37 °C). Thus, instead of having the plates in the IncuCyte culture conditions continuously, the pictures were taken on demand relocating the plate briefly from it's usual low oxygen culture condition to the IncuCyte for a quick scan. Cells were counted and density adjusted to 2000cells/ml. A 96 well plate (from Thermo Fisher Scientific) was mapped for 12 cell lines cultured with and without 22 uM vitamin K. 250 µl (2000cell/ml) of each sample was added in wells with 2 technical duplicates (see Table 12). The 96 well plate was placed back in the low oxygen incubator for next day picture until 5 days.

Table 12: Plate map for cell proliferation

A1	2	3	4	5	6	7	8	9	10	11	12
B	NZM4	NZM4	NZM55	NZM55	NZM20	NZM20	NZM3 vitk	NZM3 vitk			
C	NZM76	NZM76	NZM11	NZM11	NZM3	NZM3	NZM9 vitk	NZM9 vitk			
D	NZM34	NZM34	NZM9	NZM9	NZM6	NZM6	NZM6 vitk	NZM6 vitk			
E	NZM17	NZM17	NZM46	NZM46	NZM30	NZM30	NZM17 vitk	NZM17 vitk			
F	NZM76 vitk	NZM76 vitk	NZM55 vitk	NZM55 vitk	NZM4 vitk	NZM4 vitk	NZM46 vitk	NZM46 vitk			
G	NZM11 vitk	NZM11 vitk	NZM20 vitk	NZM20 vitk	NZM34 vitk	NZM34 vitk	NZM30 vitk	NZM30 vitk			
H											

For spheroid formation assay, 200 µl (2000cell/ml) of cells from the same batch were plated in ultra-low adhesion round bottom plates (Nunc™ 96-Well Polystyrene Round Bottom Microwell Plates from Thermo Fisher Scientifc) specific for spheroid formation. The plate map is demonstrated in (see Table 13). The plates were centrifuged at 12000 rpm for 15 minutes and were placed in the low oxygen incubator. Both the proliferation and spheroid formation experiments were done in parallel. Once daily for 5 days, both plates were transferred to the incuCyte®ZOOM and pictures were captured using the scan on demand command. After 5 days, a software (incuCyte®ZOOM) quantified the cell proliferation and spheroid formation assays. The software used an algorithm that analyzed and quantified phase contrast images measuring the area covered by cells and converted it to confluence over time values. Graphpad Prism 7 was used to graph the proliferation rates of the cells with and without vitamin K. However, for getting better spheroid image the magnification should change to 4x instead of 10x.

Table 13: Plate map for spheroid formation

	1	2	3	4	5	6	7	8	9	10	11	12
A	NZM76	NZM76	NZM55	NZM55	NZM9 vitk	NZM9 vitk						
B	NZM4	NZM4	NZM30	NZM30	NZM6 vitk	NZM6 vitk						
C	NZM6	NZM6	NZM3	NZM3	NZM34 vitk	NZM34 vitk						
D	NZM9	NZM9	NZM20	NZM20	NZM17 vitk	NZM17 vitk						
E	NZM11	NZM11	NZM46 vitk	NZM46 vitk	NZM20 vitk	NZM20 vitk						
F	NZM17	NZM17	NZM30 vitk	NZM30 vitk	NZM55 vitk	NZM55 vitk						
G	NZM46	NZM46	NZM4 vitk	NZM4 vitk	NZM11 vitk	NZM11 vitk						
H	NZM34	NZM34	NZM3 vitk	NZM3 vitk	NZM76 vitk	NZM76 vitk						

3.5 Phospho Axl sandwich ELISA

The enzyme-linked immunosorbent assay (ELISA) is a method that utilizes antibodies to determine and quantify the presence and status (for example phosphorylation) of specific proteins. The method was used to detect the phosphorylation of Axl RTK at the residue Tyr866 and Tyr821 in the intracellular kinase domain. Dr. Lavina Ahmed from BergenBio AS standardized the protocol used for detecting phosphorylation at two positions in sandwich ELISA; a special type of 96 well white plate (C96 fluronunc from Thermofisher) was used. The plates were coated with 100µl/well capture antibody 3,6µg/ml 5F11 against Axl (provided by BergenBio) in 200 mM Sodium carbonate/bicarbonate buffer (5,7 g Na_2CO_3 in 200 ml water plus 6,72 g $NaHCO_3$ in 800 ml, pH 9.4-9.6) (dilution 1:1000). The plate was sealed with special foil (DMSO Resistant Foil-peelable adhesive foil) and was incubated overnight in 4°C. The next day, the plates were washed by aspirating the buffer liquid. Then the plates were blocked with 5% milk in TBS buffer and were sealed with the special foil and placed in 37°C incubator for 4-5 hours. The plates were then washed two times with 0.05% TBS Tween 20 (TBST) with plate washer (from Thermo Scientific multidrop). After the last wash, the plates were dried by discarding the wash buffer completely on tissue paper. The sample lysates were sonicated and

50 µl of each sample at concentration of 1 mg/mL were added in each well. The standard for Axl was also added in five series dilution to the plate. The plates were sealed with foil and were incubated overnight at 4°C. This allows capture of total Axl from the cell lysate. On the third day, the plates were washed with 0.05% TBS Tween 20 (TBST) using the plate washer. 100µl/well pAxl 866 detection antibody at 1:10000 concentration was added in one plate and pAxl 821-18 antibody at 1:6000 concentration was added in the other plate. The antibodies were diluted in 5% milk in TBS and the plates were incubated overnight at 4°C. On the last day, the plates were washed and the secondary antibody (goat anti rabbit from Jackson's lab 111-035-144) at 1:16000 dilution was added to the plate for two hours. Finally, the plate was washed with TBST and 100µl/well ECL ELISA reagent (ThermoFisher Scientific) chemolumi (1 part liquidA: 1part liquid B) was added to develop the plates. After adding the reagent mix, the plates were shaken for 1min and read on a plate reader (CLARIOstar® High Performance Monochromator Multimode Microplate Reader from BMG LABTECH) to read the absorbance at 450-595 nm. Using an integrated software in the computer, the absorbance was collected as excel data sheet. GraphPad Prism 7 was used to make graph from the data.

3.6 Mass cytometry (CyTOF- time of flight mass spectrometry) sample preparation

Flow Cytometry is a well-established method for analyzing multiple markers on single cells [138]. Recent development of mass spectrometry leverages the precision of data analysis from flow cytometry. Cytometry by time-of-flight (CyTOF) is the fusion of the two methods. With mass cytometry, it is possible to measure more than 40 features of one single cell including antibody based determining of surface protein and intracellular protein, detecting RNA and DNA based on nucleotide amplification, and measuring cell cycle of a single cell [139]. Flow cytometry uses photon optics for detecting fluorophore generated by the sample and in contrast, the mass cytometry use chelated metal ion tag conjugated with antibody that detect in the atomic mass spectrometry [140].

3.6.1 Cisplatin labeling

Working solution of the viability reagent, cisplatin (Fluidigm) was prepared fresh on the day of the experiment by diluting the 5mM stock solution into cell media (RPMI 10% FBS) at a concentration of 1:20000. Cells were trypsinized and centrifuged at 1200 rpm for 5 minutes. After discarding the media, 5ml of the cisplatin working solution was added to each of the 15ml

tube containing the cells and incubated for 5 minutes. The cells were mixed properly by vortexing and then 5ml of cisplatin free media was added and centrifuged for 220g for 5min. The cells were then fixed with 1 ml of PFA (1.6% PFA in PBS) and after incubation for 10 minutes at room temperature, they were spun down in Eppendorf tubes, supernatant was removed, and the pellet was kept in -80C until use.

3.6.2 Barcoding

In a 96-well plate, each sample was resuspended in 200 µl of Perm Buffer and centrifuged at 300-600g for 3 minutes. The pellets were again resuspended in 195 µl of Perm Buffer and 5µL of barcoding solution (Cell-ID 20-Plex Pd Barcoding Kit from Fluidigm, contains Perm buffer and cell staining media, CSM) was added to each well and incubated for 30 min at RT. Cells were centrifuged at 300g for 4min and the pellets were gradually washed with Perm buffer and CSM (twice each).

3.6.3 Antibody staining

One sample from each of the columns were pooled into Eppendorf tubes containing CSM and permeabilized for 20min in 200µl of ice cold methanol at -20°C. The cells were washed twice in 1mL CSM and then were stained with antibody mix (antibody against the protein of interest). The pooled sample was stained into with 100µl for 1h at RT. After antibody incubation, cells were washed 3 times in CSM and ware intercalated overnight at 4°C or 30 min at RT with Iridium: 0.3µl diluted in 1ml PBS with 1.6% PFA. (Abcam). The cells were then washed twice with PBS and finally with miliQ water. The cells were resuspended in MilliQ water 10^6 cells/ ml, filtered in FACS filter tube, 100µl/ml of calibration beads were then added for normalization post data collection.

3.6.4 CyTOF measurement

The cell sample mixtures were inserted and analyzed using the CyTOF® mass cytometer (Helios from Fluidigm). The data was generated from each channel as FCS files. The FCS files were concatenated, normalized and analyzed using Cytobank (software for mass cytometry).

3.7 Statistical analysis

All the statistical analysis of this study was done using the Microsoft Excel 2016 and Graph Pad Prism 7.3. In graph Pad Prism, student t-test was implemented to compare two groups of data. For QPCR, the scales used for X and Y were linear but a Log10 scaled was also used if the values were widely spread. The Pearson correlation coefficient (Pearson's r) was used determine the linear correlation between the between two different variables. The correlation coefficient "r" measures the strength and direction of the linear relationship between data on an X-Y scatterplot. The value of Pearson's r +1 reflects a positive correlation between the variables. Whereas, the Pearson's r value -1 represents a negative correlation. The value 0 reflects no correlation. In the experiments, the values between $0.5 < r < 1$ and $-1 < r < -0.5$ are counted as significantly correlated. The R-squared vale is a statistical measure of how close the data are to the fitted regression line and this was also plotted in our graphs along with 95%confidence interval bands, curved lines adjacent to the line, which are the boundaries of all possible fitted straight regression line lines (information studied from Graphpad prism 7.3).

Statistical significant difference between the treatment and untreated groups were determined using null hypothesis and the alternative hypothesis that represents zero difference and significant difference respectively. The P value generated by the t-test differentiate the result as null or alternative hypothesis. P value (Noted in the text and figures as $*P < 0.05$, $**P < 0.01$, $***P < 0.001$, ****P < 0.0001) was considered as the statistical significant result. $*P < 0.05$ means a 5% chance that the observed result is not significant. The P value more than 0.05 was considered a non-significant result. Similarly, ****P < 0.0001 means highly significant result and the hypothesis is true. The graphs were made using the standard error of the mean (SEM) values that represents the spread of the sample mean value. One-way ANOVA was used to determine the statistical significance between two or more groups, such as with our qPCR data determining the effects of culture conditions and treatments. The two-way ANOVA was used to determine the proliferation and migration significance compared to comparing multiple time points simultaneously with different treatment.

4 Results

4.1 Expression analysis of NZM cell lines

4.1.1 Expression of Axl and Gas6 in NZM cell lines

Western blotting was used to characterize Axl and Gas6 protein expression in 20 NZM cell lines and one CRISPR Axl knockout NZM line (NZM17 Axl -/-). The method used for preparing the cell lysates for analysis is described in section 3.3. The blot showed that NZM9 and NZM17 have high Axl expression compared to the other cell lines. NZM 17 Axl-/- was used as negative control (see Figure 17). All of the NZM cell lines had Gas6 expression. NZM 30, NZM 34, NZM 46, NZM 55, NZM 61, NZM 63, NZM 100 show low Gas6 expression compared to the other lines. Antibodies used to probe Axl and Gas6 were Anti-Axl AF154 (R&D) and Anti-Gas6 (Abcam) respectively.

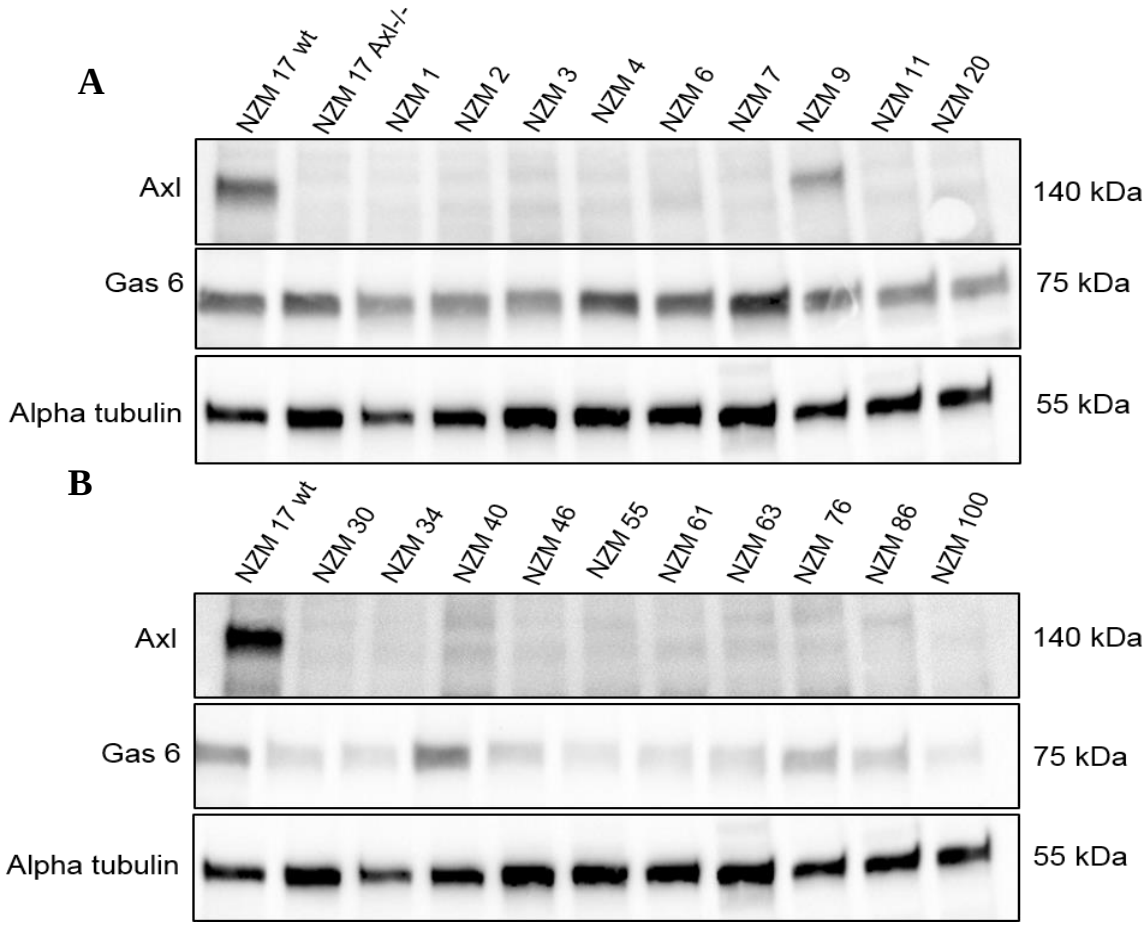

Figure 17: Western blot of Axl and Gas6 expression in the 20 NZM cell lines plus one Axl knock out line with alpha-tubulin as a loading reference. The blot representing Axl and Gas6 from NZM 1 to NZM 20 were showed in **A** and NZM 30 to NZM 100 are shown in **B**. 30 µg of protein was loaded in each gel

4.1.2 mRNA expression level of *AXL, GAS6, GGCX* and *VKORC1* in 20-melanoma cell line and their correlation with clinical outcome

qPCR was used in addition to western blotting to check Axl and Gas6 expression at mRNA level in 20 NZM cell lines, along with the expression of other genes of interest. The method used for isolating and preparing RNA for analysis is described in section 3.2. In addition, we wanted to determine any correlations between the expression levels of various Axl and vitamin K related genes with clinical outcomes of patients from whom these cell lines were derived. The levels of *AXL, GAS6, GGCX* and *VKORC1* transcripts (Figure 18 & Figure 19) were measured by qPCR. The clinical data available for us to explore included time to lymph node metastasis, distant metastasis and overall patient survival. qPCR denoted the number of DNA replication cycles taken by the genes to be expressed. The cycles were extracted and using an equation (described in 3.2.5) in Microsoft Excel the CT values were measured that show the expression of all the genes in different NZM cell lines relative to the housekeeping control. High CT values meant the expression of the particular gene was low. To determine relative expression of genes between cell lines fold change was measured against the cell line with lowest expression of the respective gene. Fold changes were then plotted against clinical outcome. However, CT values were always considered before data analysis to ensure that fold changes were biologically meaningful.

AXL expression varied among the NZM lines with CT values ranging from 17.72 to 32.29. NZM 9, NZM 17 showed highest *AXL* expression with CT value of 17.72, and 20.09 respectively, while NZM 20 showed lowest *AXL* expression with a CT value of 32.29. The CT value for NZM 100 was excluded from the result because it generated an error in the PCR reaction believed to be due to the interference of melanin bound RNA.

CT values for *GAS6* ranged from 24.77 in the NZM 17 to 33.01 in NZM 20. Among the 20 cell lines, nine showed negligible CT values over 30 indicating that expression is almost nonexistent. Expression of *GAS6* seems to be very high in a subset of cells and either very low or nonexistent in most cells (Figure not shown).

NZM 34 had highest expression of *GGCX* with CT value 24.38 and lowest expression was seen in NZM 11 with a CT value 34.6. It must be noted that as with *AXL* and *GAS6*, expression of *GGCX* in NZM 20 was also very low with CT value 25.53.

VKORC1 expression was highest with CT values 21.37 and 21.68 in NZM 55 and NZM 34 respectively in comparison to the lowest CT value 28.64 in NZM 11, matching the trend seen with *GGCX* (Figure 21). There appears to be a weak to moderate positive correlation between

the expression of between *GGCX* and *VKORC1* among these cell lines (r = 0.7, r^2 = 0.5, p=0.0004) (**Figure 18**) (Table 14)

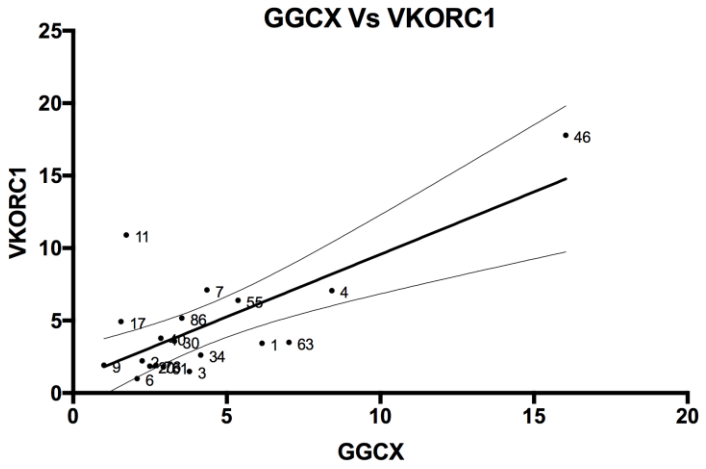

Figure 18: Correlation was between expression of *GGCX* and *VKORC1* in 20 melanoma cell lines

Table 14: The values calculated from the graph showed the Pearson r and P values that are significant.

	GGCX VS VKORC1
R	0,7305
95% Confidence Interval	0,4135 to 0,8895
r squared	0,5336
P (two-tailed)	0,0004

Values closer to 1 are considered for data that are more positively correlated. It was demonstrated that the *GGCX* and *VKORC1* have higher correlation then the others with r value of 0.7305 (Table 14). No significance was found between the expression of *GGCX* or *VKORC1* with *AXL* expression (not shown in figures).

4.1.3 Exploring the correlation between the expression *AXL, GAS6, GGCX* and *VKORC1* with the clinical outcome

Although the data was not always distributed for regression analysis it appears that the subset of lines with higher *GGCX*, Axl but not *GAS6* expression showed faster spread of the diseases and shorter overall survival (Figure 19 & Figure 20).

Regression analysis indicated a negative correlation between *GGCX* expression and overall survival, and lymph node metastasis. Patients had shorter survival, and faster spread of the disease to the lymph node and distant organs when the cells had high expression of *GGCX* (Figure 20). Although not a statistically significant there also appears to be some negative correlation between *VKORC1* expression and overall survival (Figure 21) (for Pearson's r statistics, see Table 15).

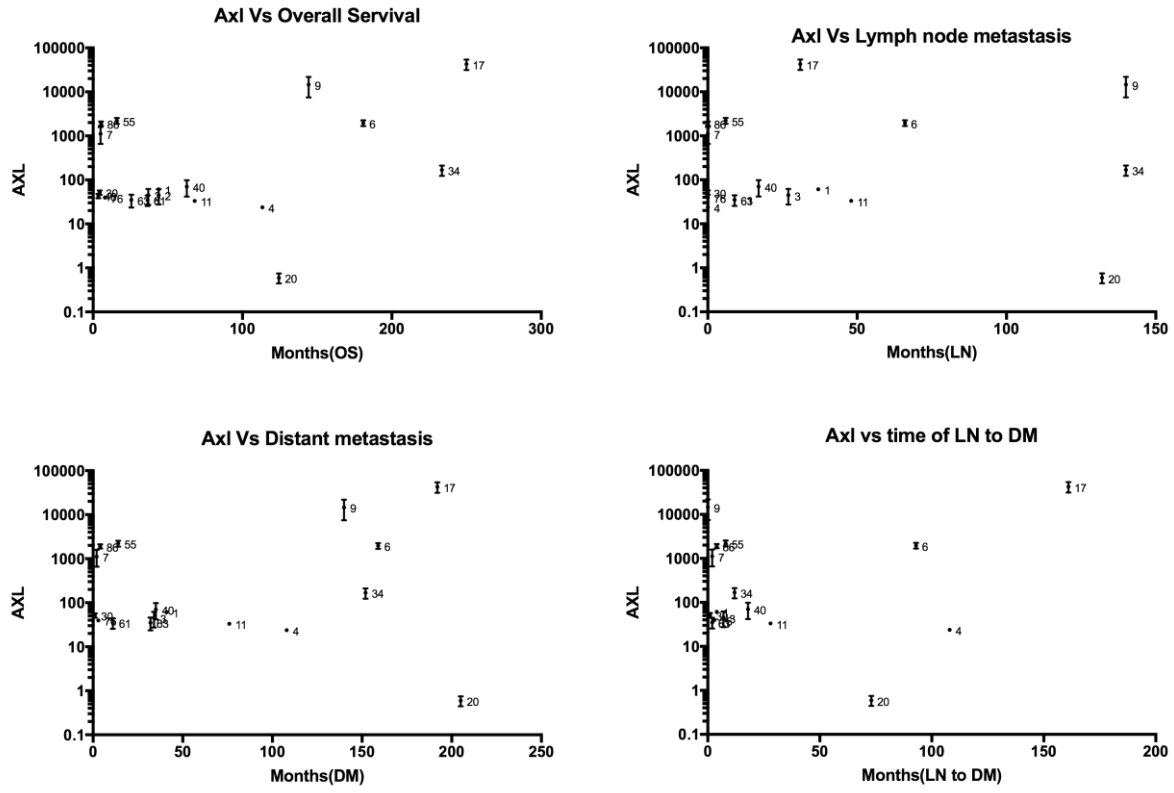

Figure 19: mRNA expression levels of *AXL* against overall survival, of the patient time to lymph node metastasis, to distant metastasis, and time from the lymph node metastasis to distant metastasis.

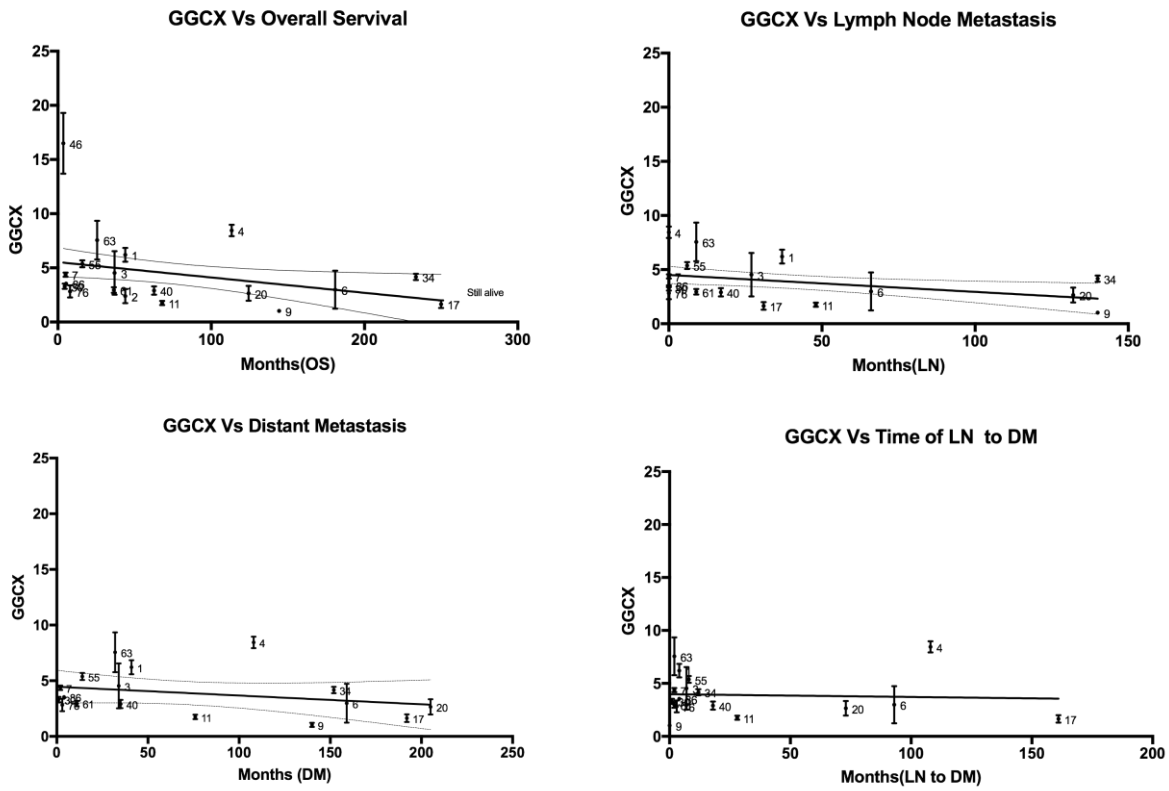

Figure 20: mRNA expression levels of *GGCX* against overall survival, of the patient time to lymph node metastasis, to distant metastasis, and time from the lymph node metastasis to distant metastasis

Table 15: The values calculated from the graph showed the Pearson r and P values that are significant.

	GGCX VS OS	**AXL VS LN to DM**	**VKORC1 VS LN**
R	-0,5177	0,6246	-0,5437
95% Confidence Interval	-0,6746 to 0,1595	0,2057 to 0,85	-0,1249 to -0,8018
r squared	0,2680	0,3901	0,2956
P (two-tailed)	0,0187	0,0074	0,0150

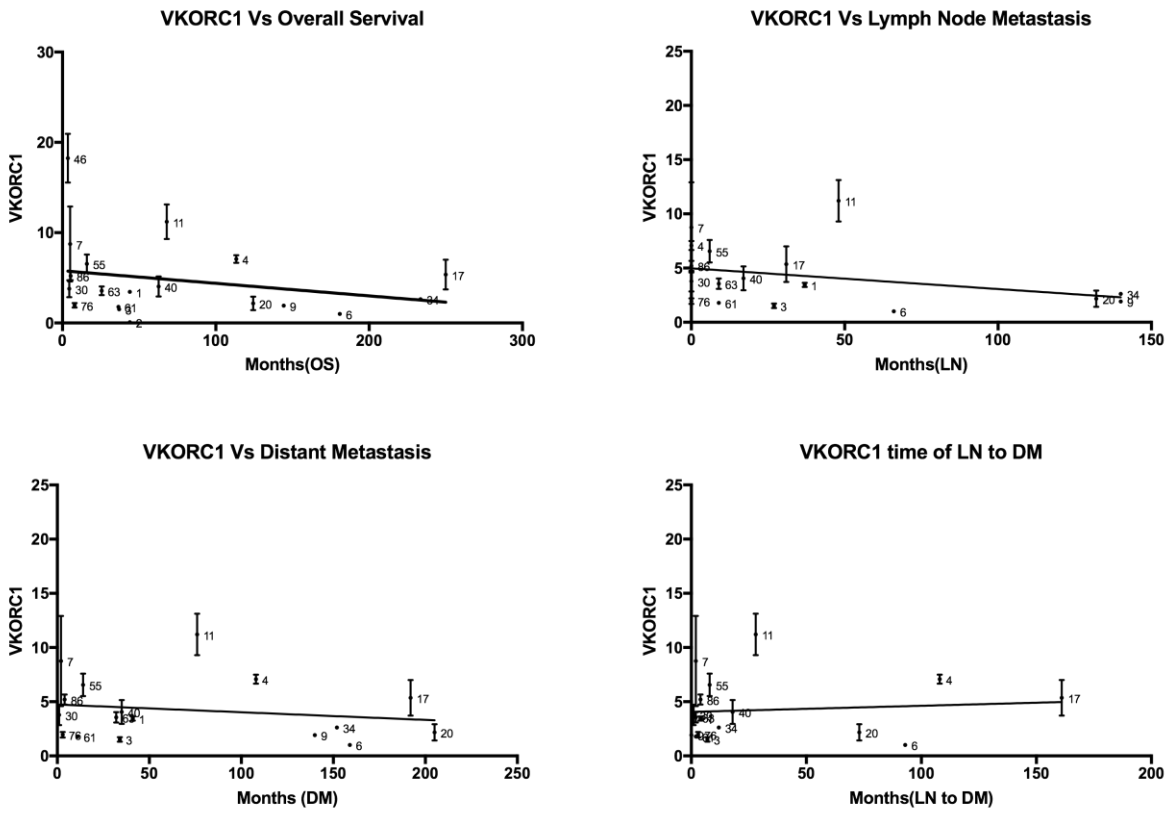

Figure 21: mRNA expression levels of *VKORC1* against overall survival, of the patient time to lymph node metastasis, to distant metastasis, and time from the lymph node metastasis to distant metastasis

4.2 The effect of culturing NZM cell lines in vitamin K

As described in the introduction of this thesis, vitamin K works as a cofactor for activating the enzyme GGCX. GGCX further promotes the activation of the Gas6 via the vitamin K dependent γ-carboxylation of its Gla domain. This involves the vitamin K dependence by converting glutamate to γ-carboxyglutamate. Gas6 activation is thought to further activate Axl [126]. In order to assess the effect of vitamin K on the NZM cell lines, 13 of the 20 cells were cultured in 22 uM vitamin K (Roche) for at least one week. 11 of these were cell lines that carried *BRAF* mutations and already part of an ongoing project in the Loren's laboratory focused on understanding resistance to BRAF inhibitors. We included one non *BRAF*-mutated cell line, NZM 46 as it had the highest expression of GGCX and hence was of interest. NZM 61 and 63 were also included as an additional two non-BRAF mutant cell lines for comparison.

Barring the addition of vitamin K, cells were cultured as usual in low oxygen incubator (5% O2, 5% CO2, 37°C) to mimic the endogenous physiological low O_2 level in tumor, which range from 2–5% [141].

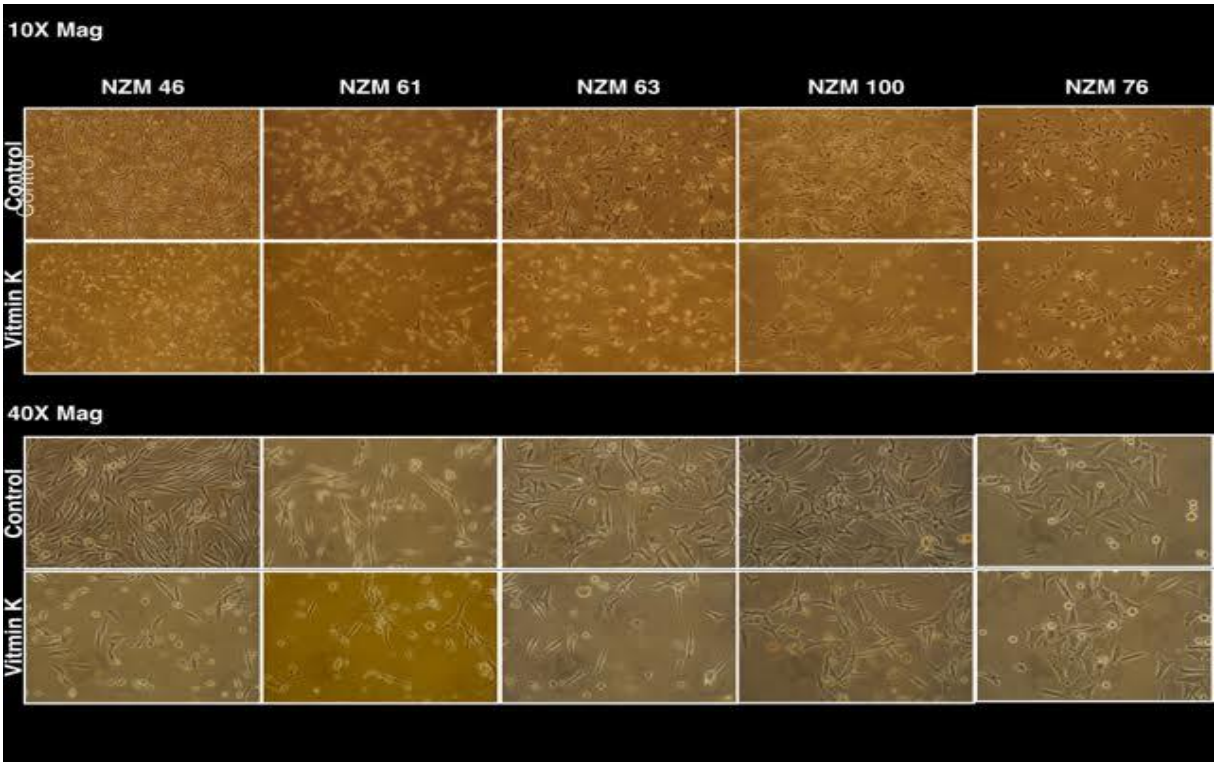

Figure 22: Images of the five NZM cell lines (100× magnification Nikon ECLIPSE TS100) selected randomly from all twenty cell lines.

The morphology of the cell lines varied with and without vitamin K (Figure 22). The cells appeared to be more epithelial-like and others more fibroblastic-like before the treatment of vitamin K (Figure 22). However, when they were treated with vitamin K, were observably more rounded or irregularly shaped. Cells cultured in vitamin K also seemed to proliferate slower and this was further investigated and described in section 4.2.1.

4.2.1 Cell culture media contained live floating cells when cultured in vitamin K

An interesting observation was that a small but noticeable number of cells appeared to become non-adherent when the NZM cells were cultured in vitamin K. These cells were first noticed as floaters in the media and assumed dead or dying cells (Figure 23). Therefore, before splitting

NZM 46, NZM 76, NZM 61, NZM 63 and NZM 100, cells from the culture medium was collected, centrifuged, and counted to analyze the live cell percentage. Counting of the cells was performed using the *Countess automated cell counter* from Invitrogen. Tryphan blue was used to determine live and dead cell (see section 3.1.6). Results from the counts showed that the cell culture medium from the vitamin K treated cells contained a significantly larger number of live cells than cells culture medium from the control group. The absolute counts and percent live cells in each sample are shown in Figure 23. These counts have been repeated and confirmed by another member of the laboratory, Dr Kjersti Davidsen.

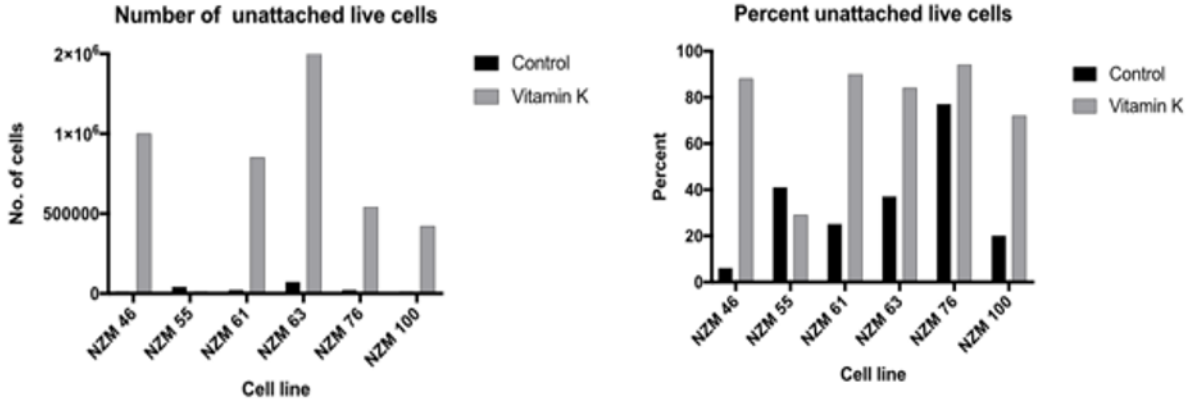

Figure 23: Cell count of the five NZM cell lines in media that are treated and untreated with vitamin K.

4.2.2 Expression of plasticity markers in NZM cell lines cultured in vitamin K and BGB324

To assess the effect of vitamin K and BGB324 at an mRNA and protein level, qPCR and western blot respectively were performed for five NZM cell lines. Expression of twelve genes was assessed in NZM3, NZM4, NZM6, NZM20, and NZM34. The cell lines were selected according to their *AXL, GAS6* and *GGCX* expression determined from the aforementioned qPCR results. The expression of genes analyzed following culture in vitamin K and BGB324 included the TAM receptors Axl and Tyro3, it's ligand Gas6, *GGCX* the enzyme for γ-carboxylation, it's transcription factor *NF1X*, plasticity markers Zeb1, Zeb2, vimentin, N-cadherin, Slug, transcription factor shown to be related to Axl, melanogenesis specific gene MITF and epithelial cell marker E-cadherin (Figure 24 & Figure 25).

4.2.2.1 **NZM 3**

Changes in the expression pattern of six of 12 genes examined were seen when NZM 3 was cultured in vitamin K, BGB324 or in a combination of both. Culturing them in vitamin K resulted in approximately two-fold significant increased transcription of *AXL*, *ZEB1*, *N-CADHERIN (CDH2)* with p value 0.005, 0.016, 0.0001 respectively (Figure 24a, 24g and 24k) and reduced transcription of *GAS6* and *E-CADHERIN (CDH1)* with p value 0.0021 and 0.0024 respectively (Figure 24b and 24l). These changes were sustained when cells cultured in vitamin K and were treated with BGB324: this included a 2.5 fold increase in expression of *AXL, ZEB1* and *N-CADHERIN* (p=0.0018, 0.0005, and 0.0001) (Figure 24a, 24g and 24k) and decreased of *GAS6* and *E-CADHERIN* (p=0.005, 0.0078) (Figure 24b, and 24l). The only difference here was a decrease in *GGCX* expression observed when cells cultured in vitamin K and were treated with BGB324 (p=0.0011, Figure 24c). With BGB324 treatment alone, only *ZEB1* expression increased (p=0.021, Figure 24g).Western blot showed a visible decrease in *VIM* expression only when the cells were treated with BGB324 alone (Figure 25). This decrease was also seen at a transcript level, although it was not statistically significant (p =0.084).

4.2.2.2 **NZM 4**

Almost all the twelve genes were transcriptionally upregulated in NZM 4 cultured in vitamin K except for *GAS6* which was downregulated (p=0.0006) and no difference seen in *MITF* expression (Figure 24b and 24d). Significant increases were found in the expression of plasticity related genes *AXL*, *GGCX*, *TYRO3*, *ZEB1*, *ZEB2*, *VIM*, *SLUG*, and *N-CADHERIN* (*CDH2)* with p value 0.0001, 0.0016, 0.008, 0.02, 0.0001, 0.003, 0.0001, 0.0035 respectively (Figure 24a, 24c, 24f-k). With BGB324 treatment in presence of vitamin K most of these genes except for *GGCX* remained upregulated, *AXL*, *TYRO3*, *ZEB1*, *ZEB2*, *VIMENTIN*, *SLUG* and *N-CADHERIN* (0.0001, 0.0148, 0.0086, 0.0038, 0.0024, 0.0019, and 0.0035 respectively) (Figure 24a, 24c, 24g-k). The expression of GAS6 mRNA decreased with BGB324 treatment in vitamin k (p=0.0012) (Figure 24b). With BGB324 treatment alone the expression of all the genes remained unchanged, except for a downregulation of *N-CADHERIN* (p= 0.0056) (Figure 24k). Western blotting showed an increased expression of *AXL* and decreased expression of *GGCX* when the cells were cultured in vitamin K but not when the vitamin K cultured cells were treated with BGB324. *GGCX* but not Axl expression levels increased with BGB324 treatment alone (Figure 25)

4.2.2.3 **NZM 6**

A downregulation of *MITF* (p=0.0006), *VIMENTIN* (p=0.035), *E- CADHERIN* (p=0.0025) and upregulation of *AXL* (p=0.0002) was found when NZM 6 in presence of vitamin K (Figure 24d, 24i, 24l, 24a). Treatment with BGB324 in vitamin K showed a similar increase in *AXL* (p=0.0004) and *SLUG* (p=0.02) and decreases *MITF, VIMENTIN, N-CADHERIN* and *E-CADHERIN* (p=0.0003, 0.02, 0.009, 0.03) (Figure 24a, 24j, 24d, 24i, 24k-l). Western blotting also showed an increased expression of Axl when cells were cultured in vitamin K regardless of the presence of BGB324 (Figure 25). Treatment with BGB324 alone showed a decrease in *GAS6*, *VIMENTIN* and *N-CADHERIN* (p=0.0001, 0.0024, 0.0034) transcripts and an increase in *ZEB1*, *ZEB2* and *SLUG* (p=0.02, 0.03, 0.04) transcripts (Figure 24b, 24i, 24k, 24g-h, 24j).

4.2.2.4 **NZM 20**

There is almost no evidence before for *AXL* expression in NZM 20 using western blot or qPCR. However, with the vitamin K treatment *AXL* (p=0.0059) as well as *SLUG* (p=0.0006) and *N-CADHERIN* (p=0.05) transcription increases and *GAS6* (p=0.02), *VIMENTIN* (p=0.02), *E-CADHERIN* (p=0.03) expression decreases (Figure 24a, 24j-k). No significant differences in transcription was found with treatment of BGB 324 in vitamin K except downregulation of *ZEB2* (p=0.004) and *VIMENTIN* (p=0.001) (Figure 24h, 24i). Downregulation of GAS6 (p=0.0001), *VIMENTIN* (p=0.006) and *N-CADHERIN* (p=0.05) was found when cells were treated with BGB324 only (Figure 24b, 24i, 24k). Western blotting showed evidence for Gas6 and strongest GGCX expression among the five cell lines examined. The western blot showed that GGCX expression remained unchanged with BGB324 treatment but decreased when the cells were cultured in vitamin K regardless of BGB324 (Figure 25).

4.2.2.5 **NZM 34**

NZM 34 showed increased *AXL, TYRO3, VIMENTIN, N-CADHERIN* transcription (p=0.0001, 0.005, 0.005, 0.003) (Figure 24a, 24f, 24i and 24k). Treatment with BGB324 did not seem to render this effect in vitamin K where a significant increases the expression of these genes continued to remain sustained along with other; *AXL, TYRO3, ZEB2, VIMENTIN, SLUG* and *N-CADHER* with p value 0.0002, 0.0001, 0.03, 0.003, 0.003, 0.03 respectively (Figure 24a, 24f, 24h-k). BGB324 treatment alone resulted in the upregulation of *ZEB2* and *SLUG* (p=0.007 and 0.05) (Figure 24h and 24j). Western blotting showed that the Axl protein expression level was strongest among the five cell lines examined and signals appeared to be too saturated to determine any changes with vitamin K or BGB324. Western blotting also showed that vimentin

expression decreased when cells were cultured in vitamin K and were remained decreased with BGB 324 treatment (Figure 25).

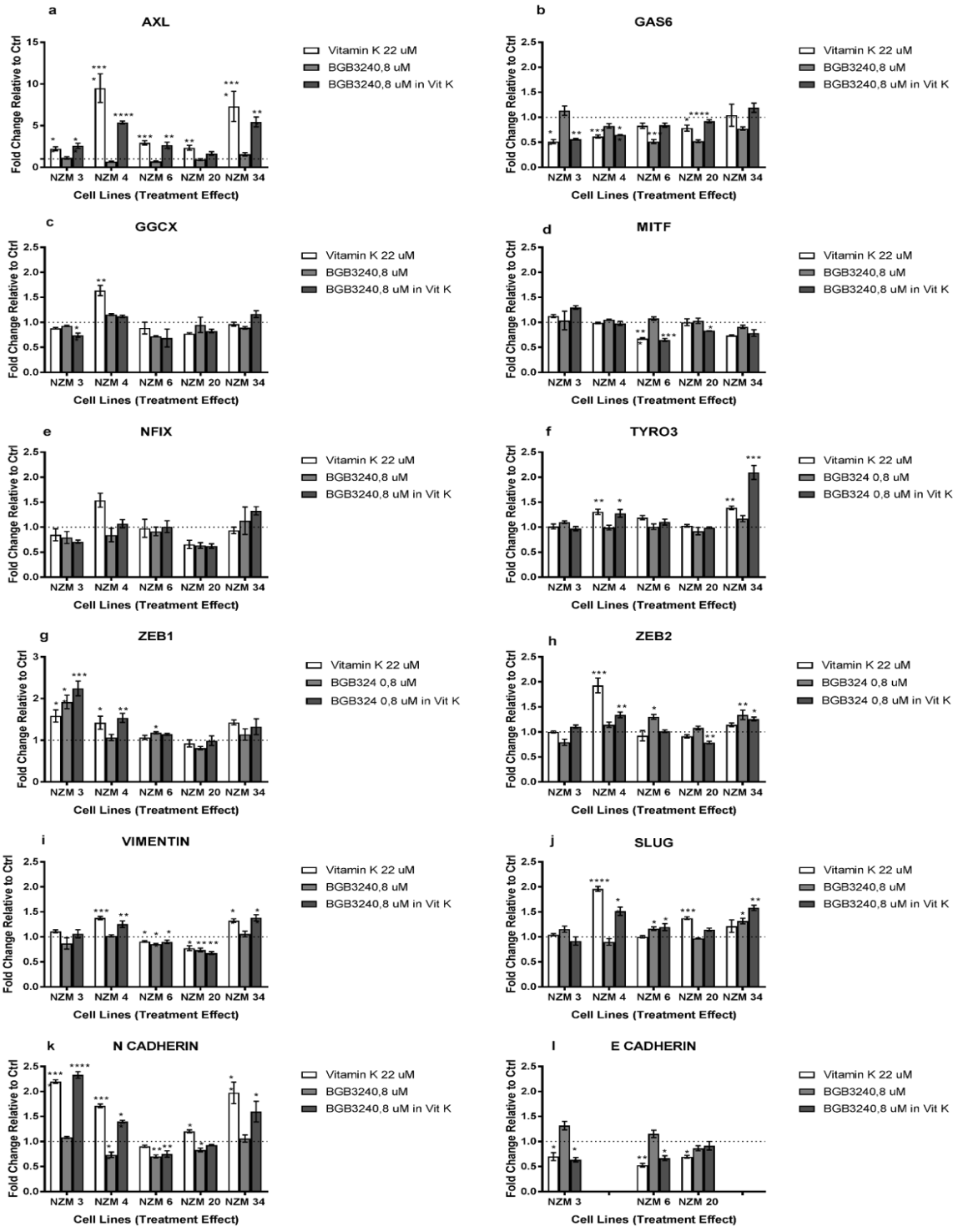

Figure 24: The validation of the fold change expression of different marker genes by qPCR. The fold change correspond to the treatment with vitamin K and BGB324 of five different cell lines. Section a,b,c represents the *Axl*, *Gas6* and *GGCX* respectively. d,e,f,g,h,i represents the plasticity markers *ZEB1*, *ZEB2*, *VIMENTIN*, *SLUG*, *E-CADHERIN*, *N-CADHERIN* respectively. j and k are transcription factors *NF1X*, *MITF*, however, *TYRO3* is a TAM receptor. The number of stars on the top of the bar means the significance. For example *p<0.05, **p<0.01 and *** p<0.001 and **** p<0.0001.

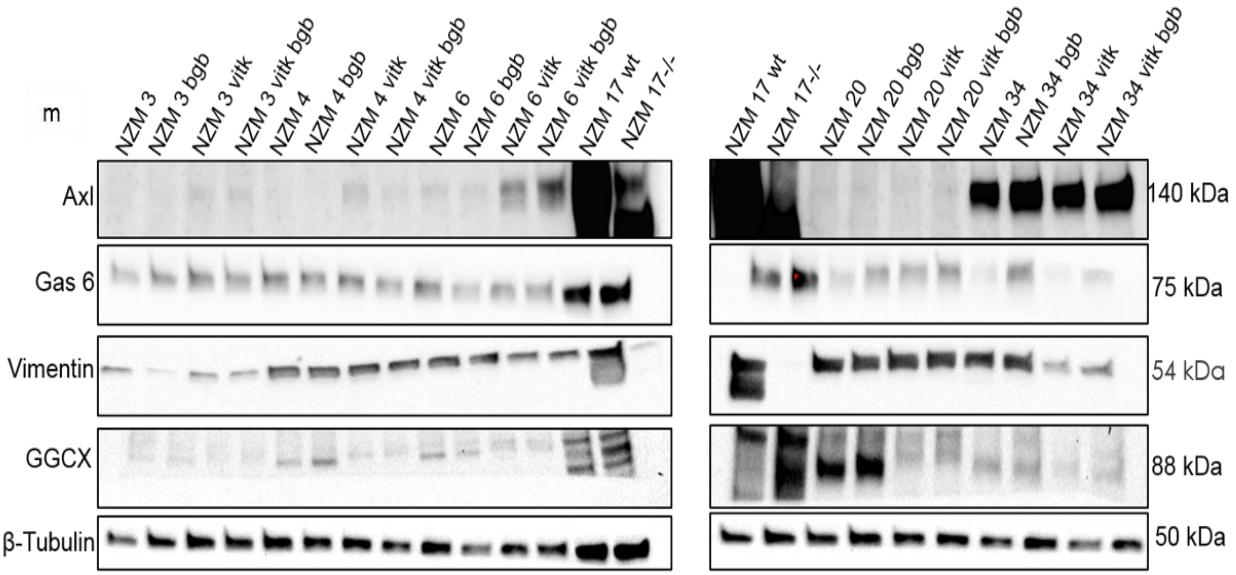

Figure 25: The western blot represents the effect of vitamin K and BGB324 in protein level.

4.3 Functional assays

4.3.1 The effect of vitamin K on melanoma cell proliferation

The proliferation rate of twelve NZM cell lines was measured using the IncuCyte® Live Cell Analysis system as described in section 3.4.2. The machine was available for use in a normal incubator (21% O2, 5% CO2, 37ºC) but as previously noted NXM cells are cultured under low oxygen (5% O2, 5% CO2, 37ºC). In order to maintain the culture conditions but still monitor proliferation, the plate was removed from the low O_2 incubator and placed into the IncuCyte for 2-4 minutes to capture images on demand. Picture was taken every day for 5 days. Cell density was determined by the IncuCyte software which assessed density based on confluence. Sine the same algorithm was to be translated to all the cell lines, confluence was thought to be a more appropriate measure than cell count as different cells lines had different sizes and shapes. Graphs representing confluence were drawn on the GraphPad Prism7 software using those values generated by the IncuCyte software.

Figure 26 represents the proliferation rate of the 12 NZM cell lines cultured with and without vitamin K. It was found that all the cell lines except NZM 11 and NZM 17 had decreased proliferation in Vitamin K. NZM 4, NZM 76, NZM 6 had decreased proliferation when cultured in vitamin K ($p < 0.0001$). In contrast, NZM 3 and NZM 11 showed an increase in proliferation when cultured in vitamin K ($p = 0.048$, $p=0.035$ respectively) but this was relatively not as significant (Figure 26).

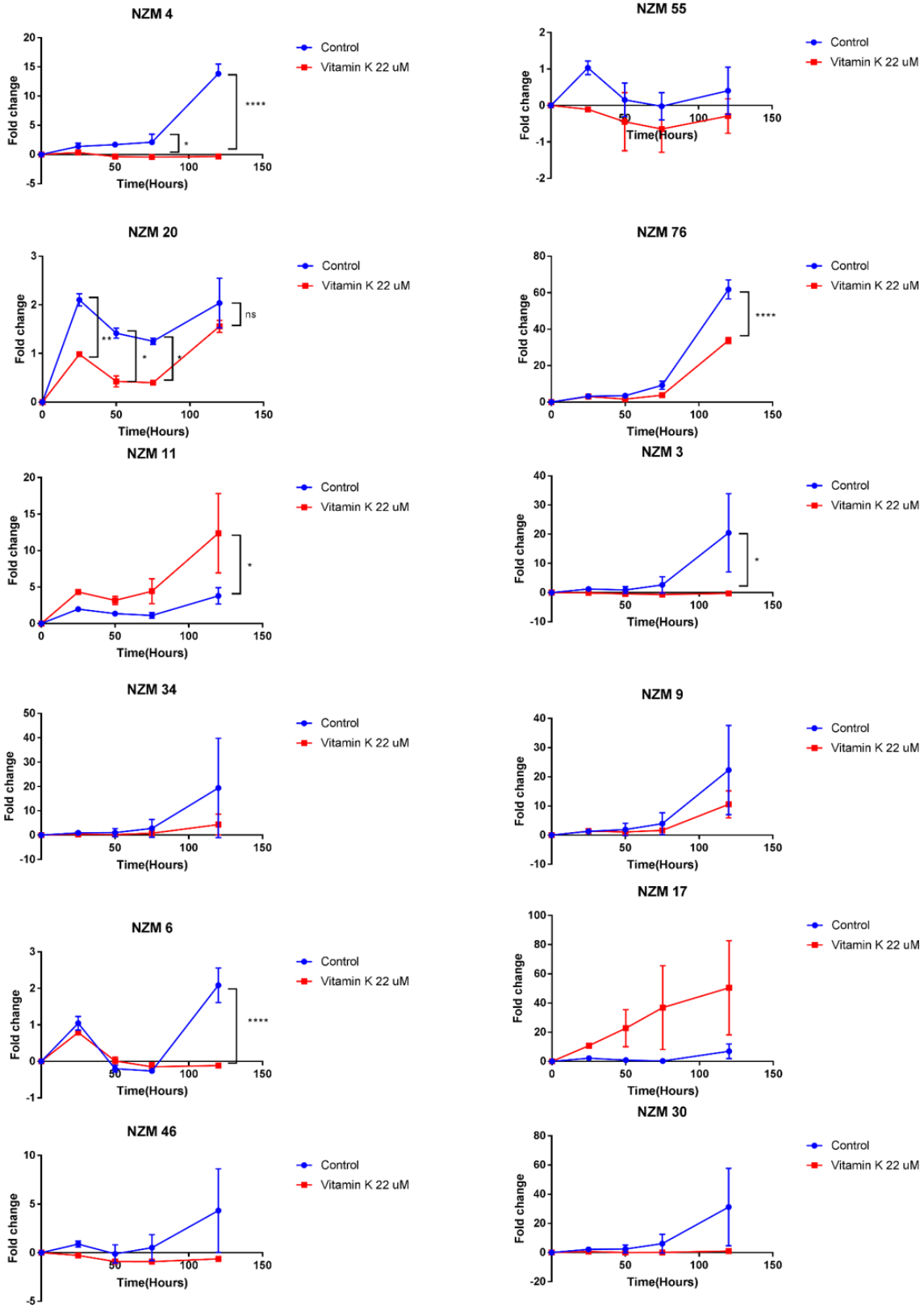

Figure 26: Proliferation rate of NZM cell lines cultured with the vitamin K. Cell confluence over 5 days as measured by the developed algorithms on the IncuCyte software. The P values were measured using Prism7. *P < 0.05, **P < 0.01, ***P < 0.001, ****P<0.0001 represents statistically significant differences. The X-axis shows the time (120 hours) of proliferation and Y-axis represents fold change. The P values are shown at different time point inside the figures.

4.3.2 Migration analysis of NZM cell lines cultured in vitamin K

Cell migration assays were performed in the xCELLigence system located in a normal oxygen incubator (21% O2, 5% CO2, 37ºC). The plates were placed in the xCELLigence for over 25 hours to investigate the effect of vitamin K in four NZM cell lines. Within 25 hours values representing the number of migrating cells were generated by the xCELLigence software using cell index (CI) at a 15 minutes intervals.

After 25 hours, the CI values generated likely represnted proliferation rather than migration. Within the 25 hour duration, it was found that the NZM 3 and NZM 20 in vitamin K migrated significantly faster (p=0.0204 and 0.0001 respectively). No significant differences in migration were determined in NZM 6 and NZM 34 regardless of the presence of vitamin K (**Figure 27**).

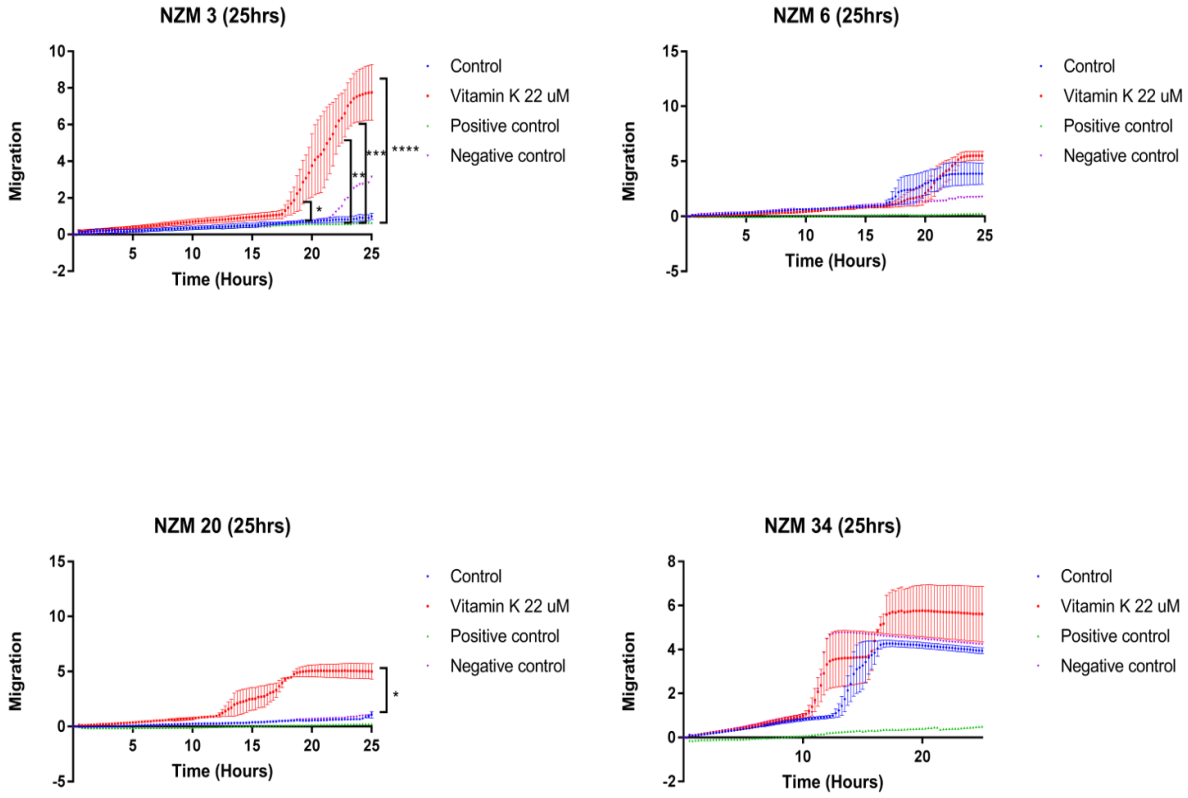

Figure 27: Migration rate of cells cultured with the vitamin K. The red and blue lines indicate CI of cells cultured with and without vitamin K respectively. The P values significance difference overtime of the NZM 3 cell lines and the p value for NZM 20 after 25 hours were represented. However, NZM 6 and NZM 34 did not show any significance (no showed in figure). Representative graphs shown from two biological repeats. The X-axis and Y-axis corresponds time and migration respectively. *P < 0.05, **P < 0.01, ***P < 0.001, ****P<0.0001 represents statistically significant differences.

4.3.3 Spheroid formation NZM cell lines cultured in vitamin K

Spheroid formation was examined using the IncuCyte® Live Cell Analysis system system in the same manner as described in section 3.4.2 where the assay was run under low oxygen conditions but the plate was relocated to the IncuCyte system once a day where 3-4 minutes were used to capture one image per well at 10X magnification for 5 days. Cells were plated in duplicates as described in methods. The spheroid forming cells were determined by monitoring the cell ability and rate to form spheroids. Cell culture medium and vitamin K was replaced every two days.

Images of spheroids at each time point are shown in spheroid formation assay. NZM 17, NZM 6, NZM 76, NZM 9, NZM 4, NZM 11 NZM 55 with vitamin K appeared to start forming spheroid faster as presented by the loss of cell aggregate like appearance to a smoother texture representing curvature and more regularly rounded edges respectively. The NZM 55 and NZM 17 in particular formed spheroids much faster in vitamin K from day 2. NZM 34, NZM 30, NZM 3 and NZM 20, NZM 46 did not show any obvious differences in spheroid formation with the vitamin K. (Figure 28, Figure 29 & Figure 30).

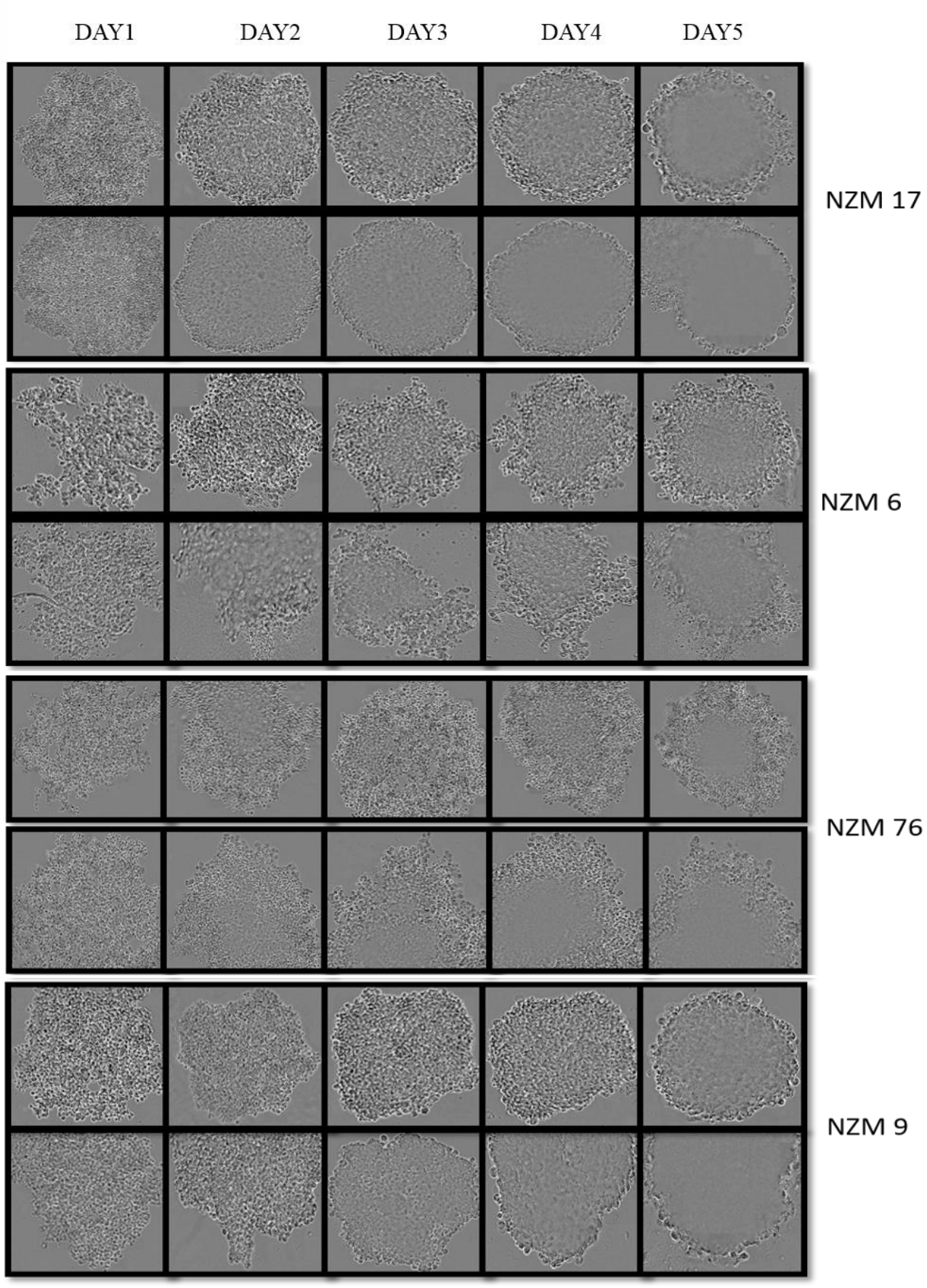

Figure 28: Spheroid formation assay for five days of NZM 17, NZM 6, NZM 76, and NZM 9 cell lines without (all top row) and with vitamin K (all bottom row)

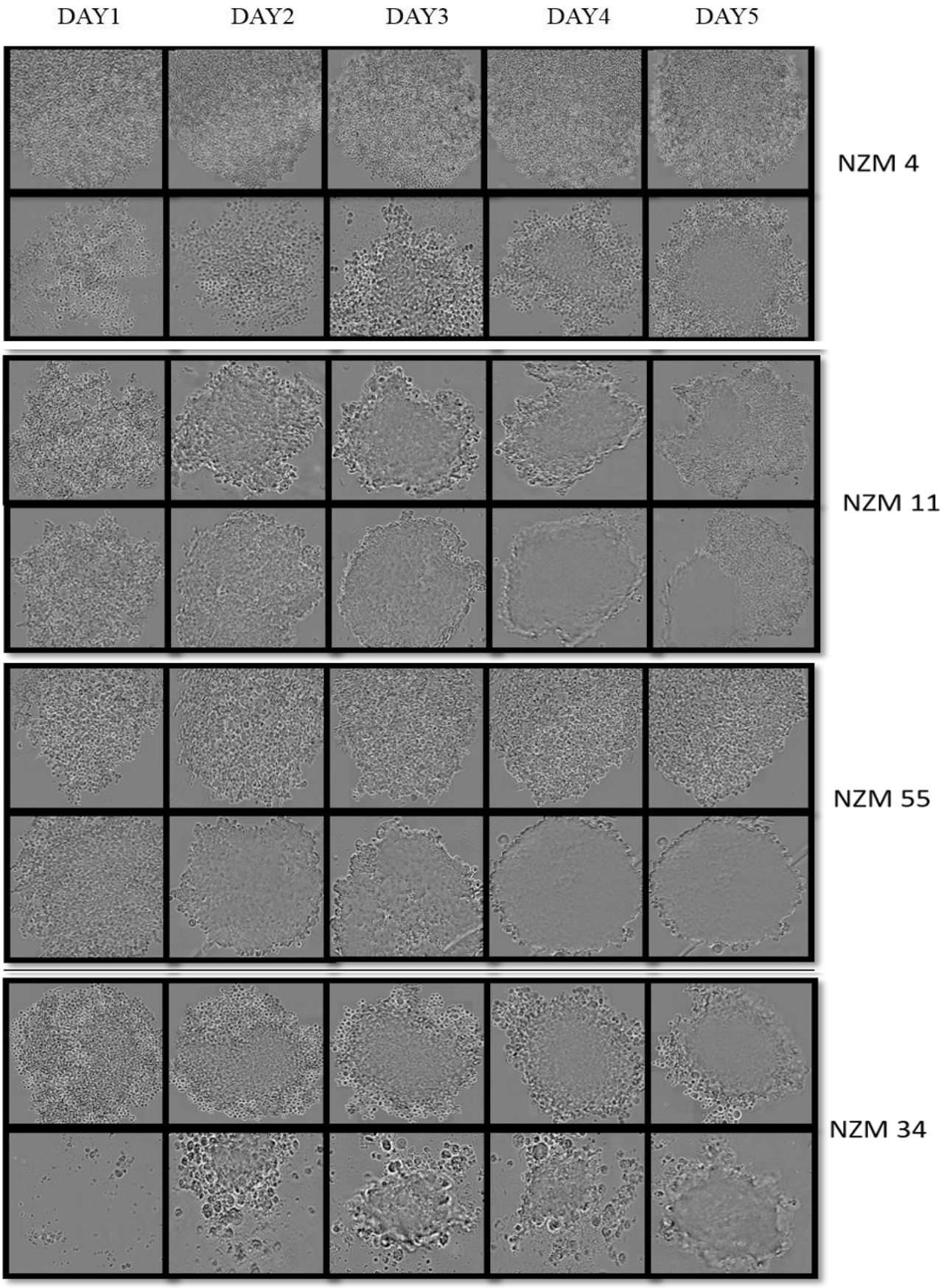

Figure 29: Spheroid formation assay for five days of NZM 4, NZM 11, NZM 55, and NZM 34 without (all top row) and with vitamin K (all bottom row)

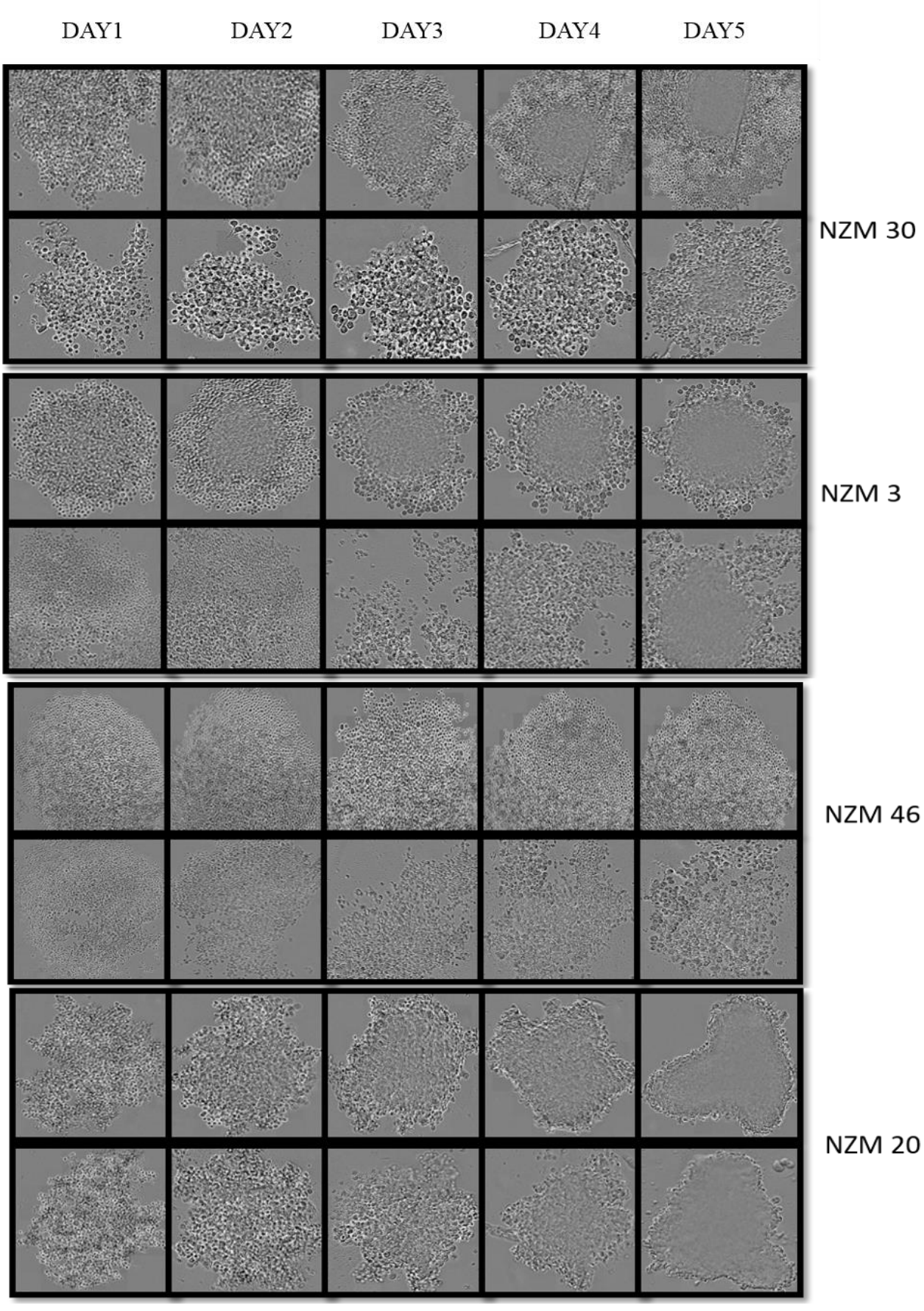

Figure 30: Spheroid formation assay for five days of NZM 30, NZM 3, NZM 46, and NZM 20 without (all top row) and with vitamin K (all bottom row)

4.4 High dimensional Mass cytometry trial run of NZM 7 treated with vitamin K

A current ongoing project in the Prof. Loren's laboratory is to underestand intracellular signalling cascades using mass cytometry. All 21 NZM lines mentioned in this thesis cultured in various conditions including vitamin K and BGB324 have been prepared for CyTOF analysis as descibed in section 3.6. A trial run on the Helios cyTOF system (Fluidigm) has been carried out with NZM 7 cell line cultured with and without vitamin K (but no floating cells had been collected at this point) to analyze phosphorylation and expression levels of 25 proteins (Figure 31). The signalling panel included heavy metal linked antibodies against human proteins p-SHP2, cleaved Caspase3, p-Stat3, p-Stat5, PD-L1, p-Stat6, p-EGFR, p-Stat1, p-AKT, Vimentin, p-38, E-cadherin, p-MAPKAPK2, p-Erk1-2, p-PLCγ2, IFNγ, p-NFkB, YAP, Axl, p-S6, CD-44, p-Creb, CD-133, GFP, EGFR ("p" indicating phosphorylation). The panel was previously designed by PhD candidate Maria Lie, Dr Kjerstii Davisen and Dr. Stacey D'mello from the Prof. Lorens laboratory with specific research interests in their mind. The results showed a minor change in expression levels of various proteins when cells were cultured with vitamin K. The largest differences in upregulation were seen in Axl , vimentin and p-S6 , calculated transformed ration of median value of 0.26, 0.29, 0.24 respectively. However, p-Erk1-2, pNF-kB, p-PLCγ2 showed down regulation in the vitamin K treated with ratio 0.24, 0.22, 0.18 respectively (**Figure 32**). This was a pilot study and further optimization is needed to validate the result and optimize antibody concentrations.

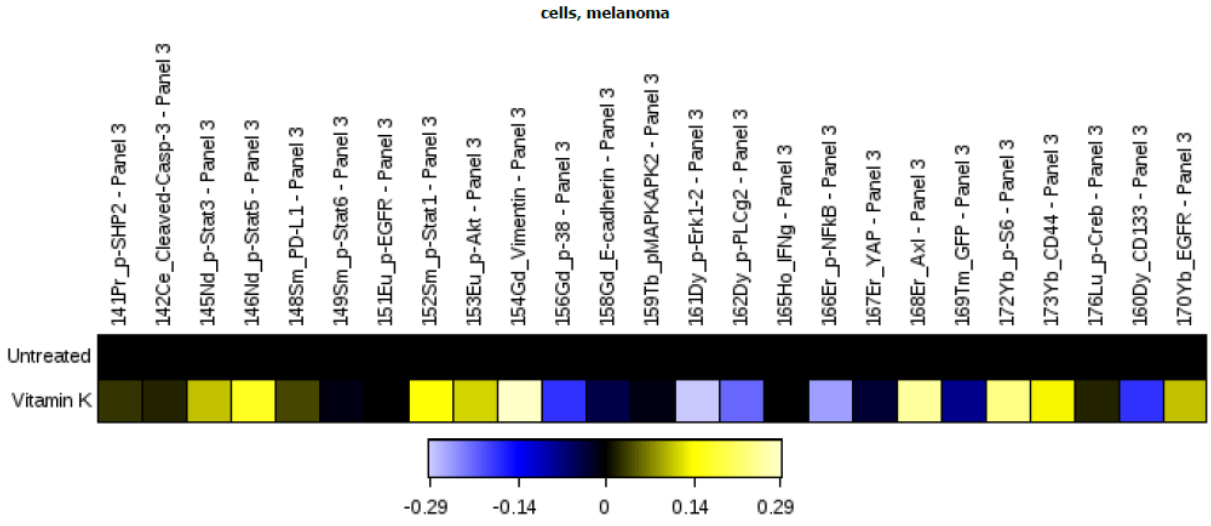

Figure 31: Heat map of the 25 protein expression explained previously. The top row represents the untreated and the bottom row represents the treated proteins with vitamin K.

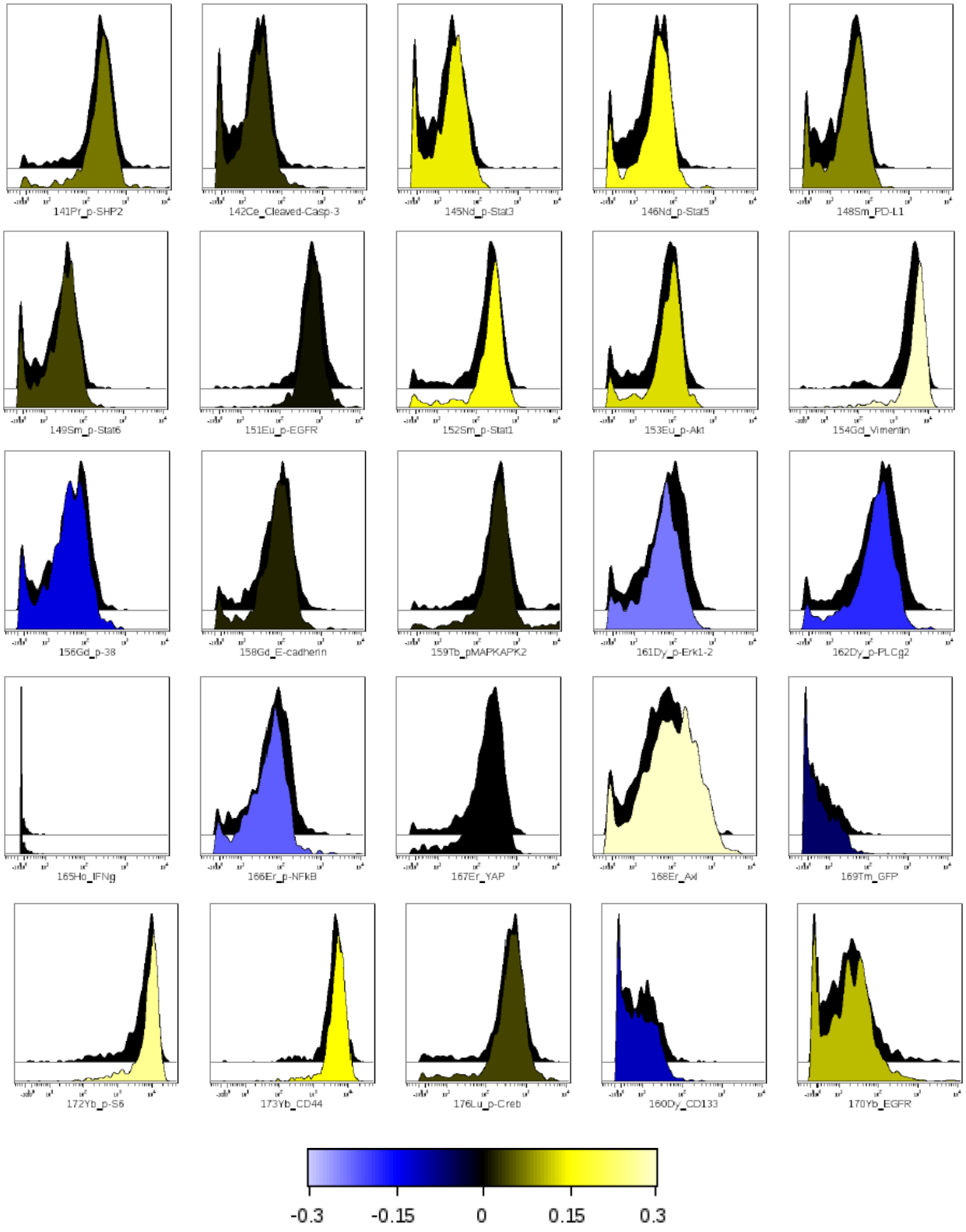

Figure 32: Histograms comparing protein expressions between NZM 7 treated with (front) or without vitamin K (back), colored according to transformed ratio of medians using the first row as control. The data is transformed using an arcsinh transformation with a cofactor of five. 25 different proteins named in the X-axis of the histogram were analyzed to see the expression difference with and without vitamin K of the NZM7 cell lines.

5 Discussion

Malignant melanoma is a highly aggressive cancer with high prevalence of somatic mutation (400 mutations/Mb). The somatic mutations are mostly caused by the exposure to carcinogens such as UV radiation. 70% of all melanomas harbors *BRAF^{V600E}*, *NRAS, GNAQ, GNA11, MEK1, KIT (MAP2K1), CTNNB1* mutations. These mutations are either driver mutation or passenger mutations that consist the bigger potion of the 400 mutation/Mb burden. This huge mutational burden makes the malignant melanoma harder to treat with conventional therapies [12, 142]. Targeted therapies such as BRAF inhibitors show promising improvements in the beginning but over time patients acquire resistance [143]. Abnormal expression of different tyrosine kinase receptors has been associated with drug resistance. Drug resistance is acquired by altering of the signaling pathway regulated by these RTKs [144]. In this study, cell lines derived from metastatic melanoma of New Zealand patients were used to study disease progression and resistance to therapy at a molecular level.

5.1 Expression of Axl and Gas6 in NZM cell lines

Expression of Axl RTK and its ligand Gas6 at a protein and RNA level were determined by western blot and qPCR. The western blot showed high expression of Axl in melanoma cell lines NZM 17, NZM 9 but was not sensitive enough to detect lower levels of Axl seen from our qPCR results. Gas6 was seen to be expressed at the protein level in most of the cell lines although up on close consideration we later questioned the integrity of the antibody used here. Most interestingly, a signal was detected at approximately 210- 220 KDa that suggested the existence of Gas6 prebound with Axl. The molecular weight of Gas6 is 75 kDa but when probing for Gas6 by western blot additional high molecular weight bands were seen in all samples at approximately 200-kDa position (Figure 33). The molecular weight of Axl is around 120 kDa. One possible explanation is that these bands may be a result of Gas6 pre-bound to Axl on the cellular surface. This has been previously reported in the Lemke group who were the discoverers of the TAM receptors. They report that the Axl RTK usually exists in a state where Gas6 is pre-bound and that phosphatidylserine is needed for the activation of the receptor in this state [79]. In addition, they also report that when Axl is knocked down, Gas6 protein is not detectable but transcription remains unchanged. This suggests that since Gas6 is a secreted soluble ligand, its detection in the cell may be lost when it does not bind to Axl [79]. However, we do not observe this change in our CRISPR Axl knockout cell line (Figure 17). Another

student tested this antibody (ab885 from Abcam) and she showed that this antibody was not able to detect recombinant human Gas6 purchased from R&D, which made its specificity questionable [145]. An alternative antibody (MAB885) against human Gas6 was not able to detect Gas6 in cell lysates but successful detected the recombinant human Gas6. Among 20 cell lines, 9 of them (NZM 1, NZM 2, NZM 3, NZM 7, NZM 11, NZM 20, NZM 30, NZM 55 and NZM 61) have very high CT value representing Gas6 expression. This again suggests that the western blot signals are not specific for Gas6.

Previous studies have shown that Axl exists not only as a transmembrane receptor, but also in soluble form consisting of the cleaved extracellular domain (soluble Axl, sAXL) with a molecular weight of 80 KDa, detectable in the growth medium. Other studies showed that sAXL competes for Gas6 binding with the Axl receptor [146, 147]. Cell culture medium was collected during our experiments and this is currently being examined for the presence of sAXL and Gas6 in free or bound form. Immunoprecipitation and ELISA methods could also be used in the future to capture these proteins determine their interaction.

At an mRNA level, all cell lines except NZM 20 expressed Axl with CT value less than 30. In agreement with the western blot results, NZM 17 and NZM 9 showed highest expression of Axl among the 20 lines. Expression of Axl in these two cell lines were over a thousand fold higher than the other cell lines and we therefore needed to use a log scale to represent the data (Figure 19). This high expression might be explained by gene amplification. Moreover, a study by Shaffer et al. recently showed a large variation in transcription levels of certain genes, including *AXL* in melanoma cells. Distinct cell in single population expressing high *AXL* levels acquire drug resistance [148]. One might speculate that cell lines with high *AXL* expression have a higher propensity to acquire drug resistance.

Our results show a discrepancy between the qPCR and western blot expression data suggests regulation of expression at a posttranscriptional level. The microRNAs miR-34a and miR-34c reported to target AXL mRNA. Deletion of the miR-34 binding site in the *AXL* 3′ UTR region of the mRNA reinstated Axl protein levels [149].The presence of these miRNAs could be determined using qPCR. It is also possible that only a small subset of cells express Axl expression and that this is averaged out and hence not detectable by western blotting [148]. Analysis by CyTOF may therefore be necessary to characterize Axl expression.

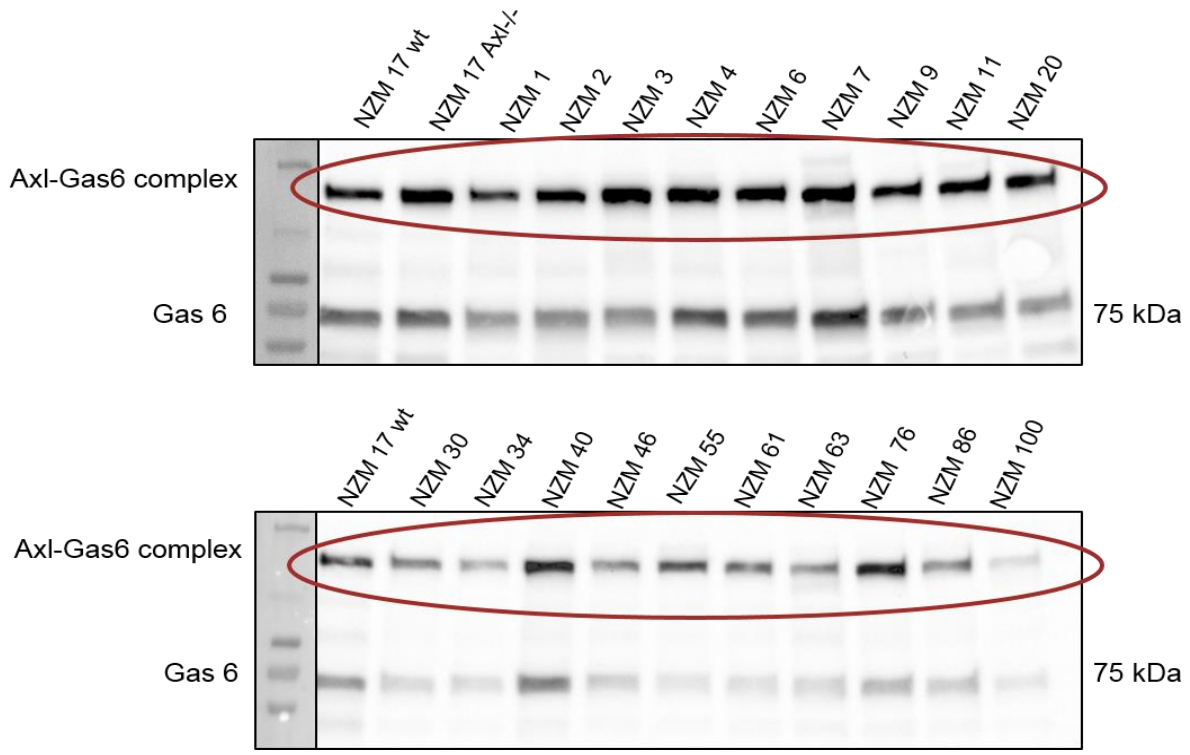

Figure 33: Higher molecular weight bands at approximately 200kDa. Possibly Axl-Gas6 complex.

5.2 GGCX but not Axl and Gas6 expression showed correlation with poor patient prognosis

As previously noted, the vitamin K dependent γ-carboxylation of Gas6 by GGCX facilitates its activation (section 1.6) which is hypothesized to increase Axl activation and signaling [86]. Previous published work has shown that the overexpression of Gas6 and Axl correlates with increased cancer invasion, metastasis and poor patient prognosis in a number of cancer types [150] including glioblastoma [106]. A recent study has demonstrated a decrease in cancer incidence in patients treated with warfarin. Warfarin inhibits the recycling of vitamin K epoxide to vitamin K (described in 1.7) [126]. However, the expression of *GGCX* and other vitamin K cycle enzyme *VKORC*1 has not been previously explored in the context of cancer. In light of these findings, we used qPCR to investigate whether the expression of *GGCX* and other vitamin K cycle enzymes had any association with clinical outcome in the melanoma cell lines. Our qPCR results demonstrated that although *AXL* and *GAS6* expression did not correlate with clinical outcome, expression of *GGCX* correlated to some extent with shorter overall survival ($r = -0.5177$, $p<0.03$). It is therefore likely that Gas6 γ-carboxylation and subsequent Axl phosphorylation might also be associated with survival. It is also therefore not surprising that

except for some correlation with lymph node to distant metastasis no correlation was observed between the expressions of Axl or Gas6 with clinical outcome (Figure 36) but rather that the activation status of these two molecules are more relevant in this context. In order to further support this finding, Axl activation and signaling downstream are currently being investigated using ELISA and CYTOF respectively. Gas6 γ-carboxylation is being determined using western blotting and mass spectrometry.

The Broad Institute Cancer Cell Line Encyclopedia (CCLE) was used to investigate correlation between genes of interest in melanoma using previously deposited RNAseq data. *GGCX* expression was profiled in 40 different cancer types where melanomas appeared in the top 4 (Figure 34). Previous reports have shown that expression *AXL* inversely related to *MITF* expression and this correlated with metastatic melanoma progression and drug resistance [48]. Low *MITF/AXL* ratio has been associated with increased drug resistance in melanoma. This trend was reflected in scatter plots created from the Broad Institute database where *MITF* negatively correlated with *AXL* expression in the 63 melanoma samples. Interestingly, a negative correlation was also observed between *MITF* and *NFIX*, the transcription factor of *GGCX* (Graph A & B Figure 35) [151].

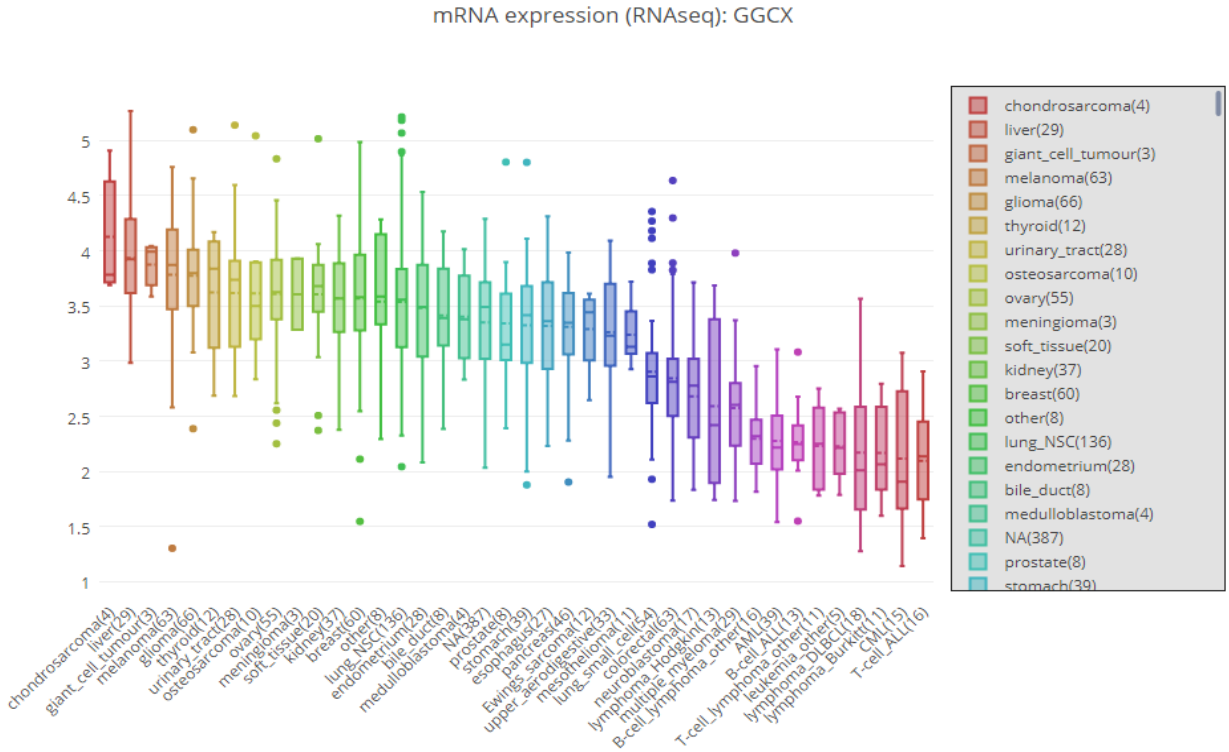

Figure 34: The GGCX expression in 40 different cancer types.

There is also evidence for a positive correlation between *NFIX* and *AXL* expression (Graph C Figure 35). These associations point to a link between the Axl and vitamin K systems. Although these correlations of *NFIX* with *AXL* and *MITF* are not apparent with *GGCX* (Graph D Figure 35), this may be dependent on the vitamin K present in the system. As seen from this thesis and others in this group [145] *GGCX* expression decreased with the presence of vitamin K, as does *GAS6* expression. In light of this it is interesting to note the negative correlation between *GGCX* and *GAS6* expression in the 64 melanoma samples and recall that the decrease in *GAS6* expression seen in this study in the presence of vitamin K. The correlation between *AXL* and *GAS6* expression in these melanoma samples is also noteworthy, here as in our data there also appears to be a subset of samples with high *GAS6* expression that have high and low *AXL* expression (Graph E & F Figure 35).

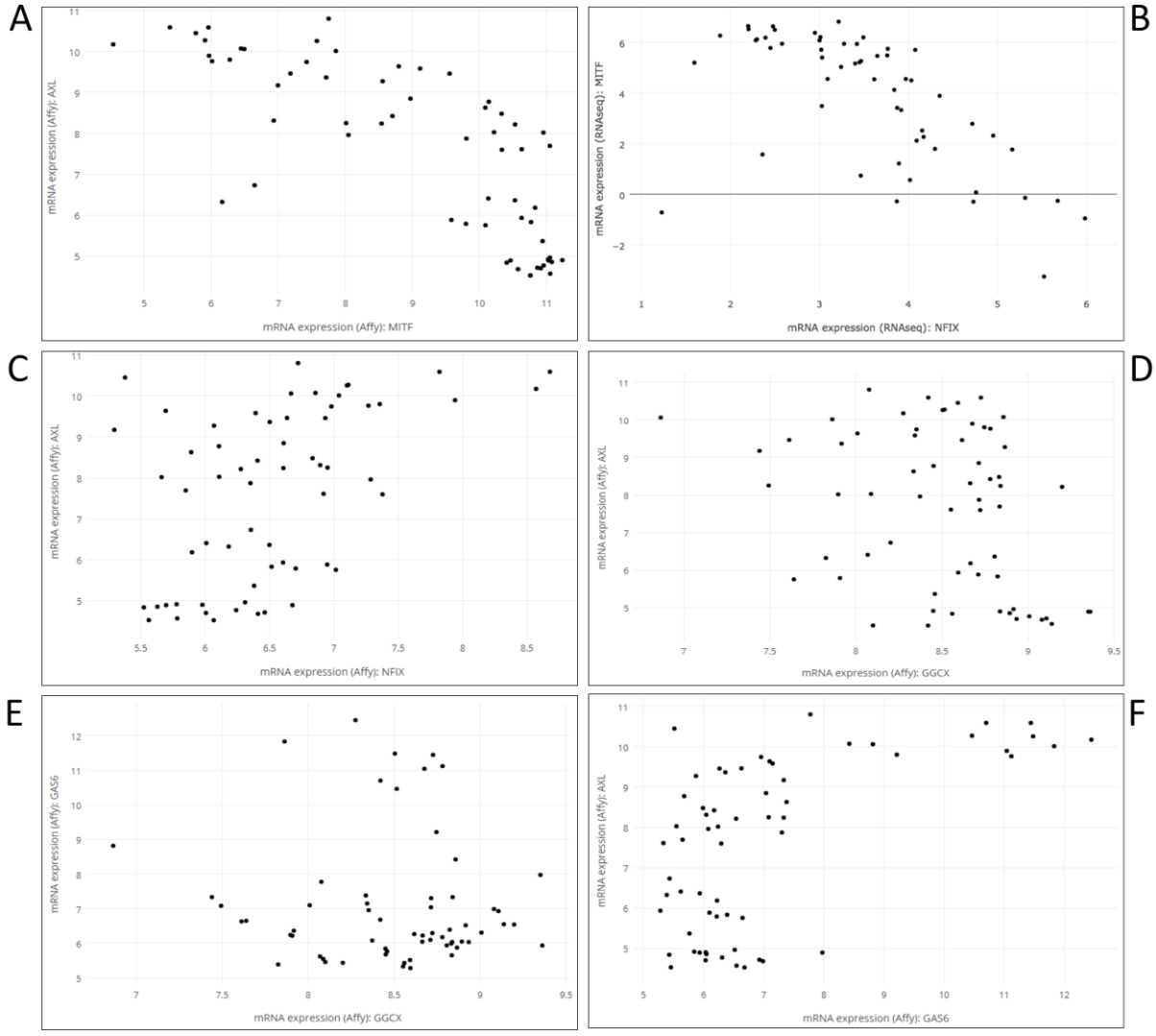

Figure 35: Scatter plot from deposits at the Broad Institute showing correlation between different gene expression levels in melanoma samples from 63 patients [152].

5.3 The effect of vitamin K on morphology and gene expression in melanoma cell lines

The importance of the effect of vitamin K on Axl activation was highlighted by Haaland et al [126]. Following from this we treated the melanoma cell lines with 22μM vitamin K (decided upon from previous studies in blood coagulation-refer to the Blood paper). It was hard to confirm the complete absence of vitamin k in the control cell culture conditions but lack of γ-carboxylation of proteins in these cells was demonstrated by blot by another member of the Prof. Loren's laboratory [145]. We first observed that the cells appeared morphologically different when cultured in vitamin K, with a fibroblast-like rounded membrane rather than a classic dendritic morphology of a melanoma cell. A number of cells rounded and peeled off the culture surface and many cells appeared to be floating in cell culture media. These floating cells were confirmed to be alive (Figure 22). One research group has described this as a highly migratory amoeboid phenotype and in the context of cancer; this represents mesenchymal-amoeboid transition. The amoeboid phenotype has been described as rounded and irregular shape, with almost no focal adhesion [153]. Another group distinguish glioblastoma multiform cells into adherent cells and floating aggregates called neurospheres and demonstrated that mice injected with floating cells died 10 days faster than the mice with injected with adherent cells [154].

Axl activation by its ligand Gas6 may be influenced by the presence of vitamin K. Vitamin K works as the cofactor for enzyme *GGCX*, which as previously described carboxylates the Gla domain of Gas6 to activate it (see section 1.6). Thus it is likely that Axl is more frequently or strongly activated in the presence of vitamin K [86] and this might drive the observed phenotype of amoeboid transition. Future studies using these Axl knock out cell lines and inhibitors are needed to confirm that this effect is Axl mediated.

Our study further focused on five NZM cell lines with variable expression levels of *AXL*. The selected cell lines were cultured with and without vitamin K and treated with BGB324 a selective inhibitor of Axl kinase activity. Culturing cells in medium supplemented with vitamin K resulted in gene expression changes. These effects were maintained when the cells were treated with BGB324 only if vitamin K was present. For example, *AXL, ZEB1, SLUG* and *N-CADHERIN* were upregulated in a number of cell lines cultured with vitamin K and remained increased with BGB324 and vitamin K. We hypothesize that when cells were cultured with vitamin K, Gas6 is carboxylated and activates Axl cell signaling. As BGB324 blocks Axl signaling it appears that the presence of excess vitamin K may overcome some of the effect, based on the observed expression gene patterns.

We did not see evidence for epithelial to mesenchymal transition (EMT) in all cell lines. This included plasticity markers like vimentin, Zeb1, Zeb2, Slug, N-cadherin that are known to be associated with Axl [100, 155]. Melanoma are not an epithelial type of cancer and are perhaps already in a mesenchymal state as can be seen from high *VIM* expression in almost all the cell lines (Figure 24). However we did see a further upregulation of vimentin and Slug with vitamin K treatment in NZM 4 and NZM 34 that have high expression Axl with vitamin K but also NZM 3, a cell line with almost no Axl expression. This indicates possibility of vitamin K mediated EMT that is mediated independently of Axl. N-cadherin is another mesenchymal marker found to be upregulated in cancer [156] that we see increase with the vitamin K but not with BGB324 treatment.

NFIX a transcription factor master regulator of the cancer metastasis linked to the upregulation of *GGCX* in lung cancer [151]. No changed in expression of *NFIX* were observed with vitamin K or BGB324 suggesting that the effects we see are directly on genes of interest. No significant difference in *MITF* transcripts was observed with vitamin K and BGB324 treatment but due to the complex posttranslational regulation of *MITF* and its isoforms, expression at the protein level should be investigated [48]. In the trial run of NZM 7 cell line using CyTOF, also found the upregulation of Axl, Vimentin and phospho-ribosomal protein S6 kinase (p-S6) and downregulation pErk1-2, pNF-kB, p-PLCγ2 with vitaminK treatment. Although it must be noted the expriment was done once as a trial run and further optmisation of parameters are needed.

5.4 The effect of vitamin K on cell migration, proliferation and spheroid formation

Assays were conducted to investigate the vitamin K on cell migration, proliferation and spheroid formation, NZM cell lines were generally found to proliferate slower, but migrate and form spheroid faster when cultured in vitamin K. Bilamdzic et al showed that the faster spheroids forming cancer cells have more invasive capacity [157]. After that, several contradictory papers show that spheroid formation either induces cancer progression or inhibits tumor growth. In spheroids, the individual cells are not distinguishable by low resolution microscopy such as that of the IncuCyte. Studies have shown that cells in a spheroid make adherens junction using E-cadherin which makes them less mesenchymal as well as less invasive [158]. However, the vitamin K effects on spheroid formation remain unclear. In our study, it is apparent that the vitamin K has some effect on spheroid formation. Cells cultured in

3D stay in close proximity creating an anaerobic condition tumor microenvironment leading to increased hypoxic response element (HIF-1 and HIF2). The increase formation of HIF1 and HIF2 mediate the upregulation of Axl [116, 159]. The vitamin K treated cell lines might have higher Axl expression than the untreated cells casing them to form spheroids faster. Expression of Axl in the fast forming spheroids can be determined by western blot or even CyTOF.

In our study, we demonstrated that the NZM cell lines cultured in vitamin K proliferate slower. A previous study in human hepatocellular carcinoma (HCC) showed the addition of synthetic vitamin K in the cell culture media reduces the cell growth and proliferation. They also mention that the vitamin K have distinct pathway of growth inhibition than the TGF-β1 mediated inhibition mechanism [160]. Other studies on muscle cells explain the importance of vitamin K in muscle cell proliferation [161]. Previous studies mostly reported the effect of vitamin D in cancer metastasis. One study demonstrates the inhibition of colorectal cancer cell proliferation by vitamin K2. They explains the mechanism of vitamin k2 blocking the EGFR mediated signaling pathway followed by cell proliferation of cancer cells [162].

We observed that cells cultured in vitamin K migrate faster. Previous studies have reported the involvement of TAM receptors in cancer cell migration. It was showed that the Axl upregulation correlates with the overexpression of the migration-associated genes like cell adhesion molecules (VCAM1, ICAM1 and E-selectin), integrins (ITGA and ITGB), neuropilins (NRP1 and NRP2) [163]. Since vitamin K is impotant for Axl activation, it was expected to increased cell migration with vitamin K treatment. One study demonstrated the BGB324 treatment reduces the WM1366 melanoma cell migration potential by 50% [164].

6 Concluding remarks

In this study, we have characterized the expression of Axl Gas6, other plasticity and vitamin K related genes in a large panel of 20 cell lines derived from patients with metastatic melanoma. We have looked at whether these genes could be important diagnostic or prognostic markers, and whether vitamin K allows melanoma cells to develop plasticity and chemo-resistant phenotype.

Although we need to look at a larger sample size in the futurw, there is some indication that expression of the vitamin K dependent enzyme GGCX, correlated with poor prognosis.

We also found that in addition to observing morphological differences, cells cultured in vitamin K alone did have an effect on the expression of Axl, its associated genes as well as other plasticity markers, and this effect was abrogated by BGB324. However BGB324 was not able to abrogate this effect if the cells were cultured in vitamin K suggesting acquisition of a resistant phenotype.

In addition, function studies indicated that vitamin K tended to reduce melanoma cell proliferation, but increased rates of cell migration and spheroid formation, both indications of plasticity phenotype. Further work using the Axl inhibitors and knockout experiments are needed to confirm whether these functional effects are Axl mediated or whether a new pathway facilitating the effect of vitamin K is to be explored. Nevertheless, we can conclude an effect of vitamin K that warrants further investigation. Studies on various pathways using CyTOF are currently underway in the Prof. Lorens laboratory with one pilot run reported in this thesis.

7 Future perspective

In our study, we indicate that the expression of GGCX correlate with poor prognosis in melanoma. However, Axl and Gas6 do not share the same association in melanoma. It is likely that the expression profiles of these genes are different *in vitro* and have changed over the long periods in culture. It is likely more useful to look at expression of these genes in resected tumors rather than cell lines. This is a possibility considering the current melanoma trial with BGB324 - combination therapy at Haukeland University Hospital. As previously mentioned, mass cytometry (CyTOF) analysis is also being carried out on all 20 the cell lines to assess their signaling profiles in vitamin K, the effect of the Axl inhibitor BGB324 in this context and also the effects on signaling when these cells are made resistant to BRAF inhibitors. Future perspectives also include using CyTOF to study tumour immune interrelations under these conditions.

We also want to measure vitamin K concentration in the media, systemically in humans and in organs of mouse models. This is currently underway in collaboration with NEFES and Haukeland University Hospital.

In the future, it would also be useful to isolate and analyze the floating cells in the media after vitamin K treatment and for their expression profiles to be determined separately.

A more comprehensive and high throughput approach to studying transcription is also needed and samples from all these cell lines with various treatments are currently being prepared for RNA sequencing.

We found that vitamin K not only effected expression profiles of cells but also their proliferation, and migration and spheroid formation ability. However, we need to determine whether this effect is Axl mediated. This might be done by inhibiting or knocking out Axl using BGB324 or CRISPR technology respectively.

Finally, *in vitro* effects must be validated *in vivo* and this too is currently underway in the Prof. Lorens laboratory. *In vivo* analysis will also help us to gain insight into the effect these conditions have on immune interaction and evasion.

Other future directions include quantification and validation of bands in western blots, validation of spheroid formation assays using 4x magnification rather than 10X on the IncuCyte, Validation of migration studies in low oxygen and determining the effects on the

phospho status of Axl and the γ-carboxylation status of Gas6 using immunoprecipitation by ELISA or western blot. Co-immunoprecipitation might also be used to study the interstation of Axl with Gas6 and other proteins.

Several studies showed using mass spectrometry that the auto phosphorylation of Axl upon ligand Gas6 binding can be occur in several site. Almost six sites were demonstrated at the autophosphorylation site that have no downstream effect. The mostly active phosphorylation site of Axl are the Y779, Y821, Y866 and these sites are the docking site for critical signaling cascades [165, 166]. Sandwich ELISA based assays looking at the effects of vitamin K and BGB 324 on Axl phosphorylation at position of Y821 and Y866 were attempted but data has not been not shown here because further optimization is required.

8 Supplementary Figures

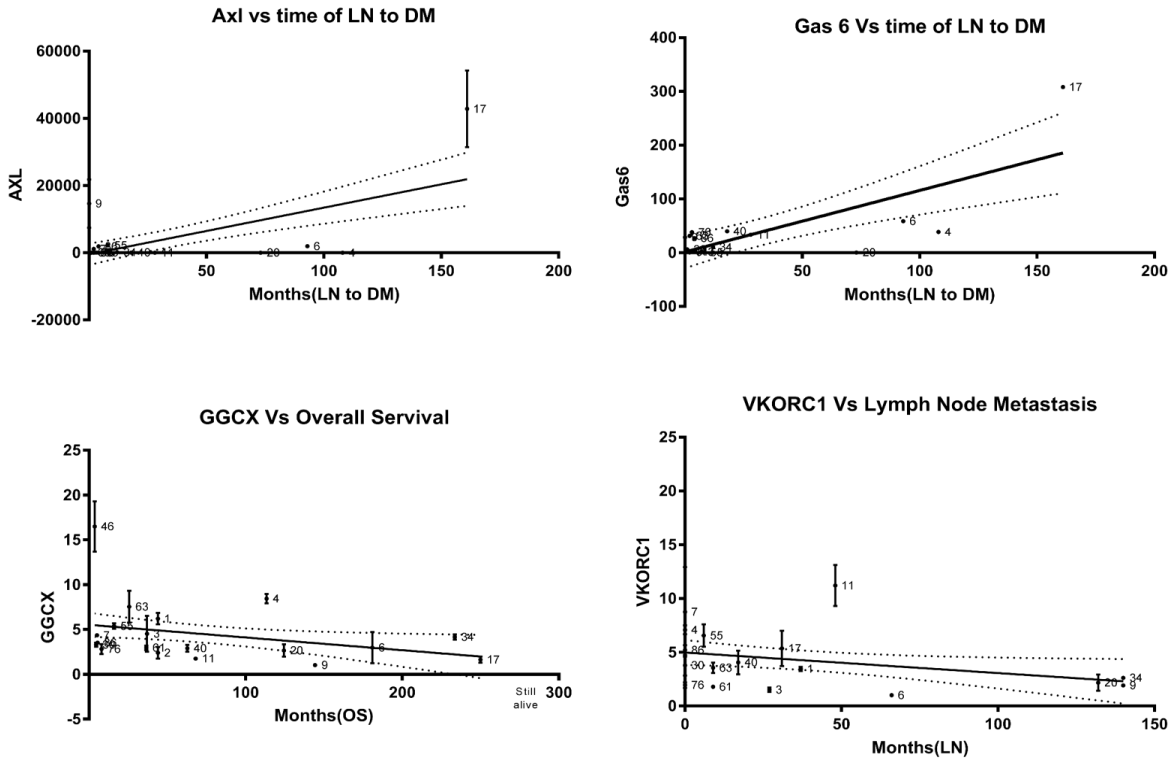

Figure 36: The correlation of clinical outcome with expression of *AXL, GAS6, GGCX* and *VKORC1*. The graphs showing only the significant results. The significance was determined using the Pearson r value. The r value between 0.5 < r < 1 and -1< r < -0.5 are counted as statistically significant.

9 References

1. Hanahan, D. and R.A. Weinberg, *The hallmarks of cancer.* Cell, 2000. **100**(1): p. 57-70.
2. Hanahan, D. and R.A. Weinberg, *Hallmarks of cancer: the next generation.* Cell, 2011. **144**(5): p. 646-74.
3. Ferlay, J., et al., *Cancer incidence and mortality worldwide: sources, methods and major patterns in GLOBOCAN 2012.* Int J Cancer, 2015. **136**(5): p. E359-86.
4. Lo, J.A. and D.E. Fisher, *The melanoma revolution: from UV carcinogenesis to a new era in therapeutics.* Science, 2014. **346**(6212): p. 945-9.
5. Dagogo-Jack, I. and A.T. Shaw, *Tumour heterogeneity and resistance to cancer therapies.* Nat Rev Clin Oncol, 2018. **15**(2): p. 81-94.
6. Lawrence, M.S., et al., *Mutational heterogeneity in cancer and the search for new cancer-associated genes.* Nature, 2013. **499**(7457): p. 214-218.
7. Burrell, R.A., et al., *The causes and consequences of genetic heterogeneity in cancer evolution.* Nature, 2013. **501**(7467): p. 338-45.
8. Weigelt, B. and J.S. Reis-Filho, *Histological and molecular types of breast cancer: is there a unifying taxonomy?* Nat Rev Clin Oncol, 2009. **6**(12): p. 718-30.
9. Prahallad, A., et al., *Unresponsiveness of colon cancer to BRAF(V600E) inhibition through feedback activation of EGFR.* Nature, 2012. **483**(7387): p. 100-3.
10. Pao, W. and J. Chmielecki, *Rational, biologically based treatment of EGFR-mutant non-small-cell lung cancer.* Nat Rev Cancer, 2010. **10**(11): p. 760-74.
11. Logothetis, C.J., *Re: intratumor heterogeneity and branched evolution revealed by multiregion sequencing.* Eur Urol, 2013. **64**(1): p. 170.
12. Alexandrov, L.B., et al., *Signatures of mutational processes in human cancer.* Nature, 2013. **500**(7463): p. 415-21.
13. Davies, H., et al., *Mutations of the BRAF gene in human cancer.* Nature, 2002. **417**(6892): p. 949-54.
14. Pollock, P.M., et al., *High frequency of BRAF mutations in nevi.* Nat Genet, 2003. **33**(1): p. 19-20.
15. Tsao, H., et al., *Melanoma: from mutations to medicine.* Genes Dev, 2012. **26**(11): p. 1131-55.
16. Siegel, R., D. Naishadham, and A. Jemal, *Cancer statistics, 2012.* CA Cancer J Clin, 2012. **62**(1): p. 10-29.
17. World Health Organization. *How common is skin cancer?* 2013; Available from: http://www.who.int/uv/faq/skincancer/en/index1.html.
18. Lens, M.B. and M. Dawes, *Global perspectives of contemporary epidemiological trends of cutaneous malignant melanoma.* Br J Dermatol, 2004. **150**(2): p. 179-85.
19. Montagna, W. and K. Carlisle, *The architecture of black and white facial skin.* J Am Acad Dermatol, 1991. **24**(6 Pt 1): p. 929-37.
20. Gibbs, S., et al., *Melanosome capping of keratinocytes in pigmented reconstructed epidermis--effect of ultraviolet radiation and 3-isobutyl-1-methyl-xanthine on melanogenesis.* Pigment Cell Res, 2000. **13**(6): p. 458-66.
21. Ali, Z., N. Yousaf, and J. Larkin, *Melanoma epidemiology, biology and prognosis.* EJC Suppl, 2013. **11**(2): p. 81-91.
22. Cancer Registry of Norway, *Cancer in Norway 2016 - Cancer incidence, mortality, survival and prevalence in Norway*. 2017, Cancer Registry of Norway: Oslo.
23. Ferlay, J., et al., *Cancer incidence and mortality patterns in Europe: estimates for 40 countries in 2012.* Eur J Cancer, 2013. **49**(6): p. 1374-403.
24. Geisler, J., et al., *Malignant melanoma--diagnosis, treatment and follow-up in Norway.* Tidsskr Nor Laegeforen, 2013. **133**(20): p. 2154-9.
25. Gandini, S., et al., *Meta-analysis of risk factors for cutaneous melanoma: I. Common and atypical naevi.* Eur J Cancer, 2005. **41**(1): p. 28-44.

26. Green, A.C., S.C. Wallingford, and P. McBride, *Childhood exposure to ultraviolet radiation and harmful skin effects: epidemiological evidence.* Prog Biophys Mol Biol, 2011. **107**(3): p. 349-55.
27. Balch, C.M., et al., *Final version of the American Joint Committee on Cancer staging system for cutaneous melanoma.* J Clin Oncol, 2001. **19**(16): p. 3635-48.
28. Mohr, P., et al., *Staging of cutaneous melanoma.* Ann Oncol, 2009. **20 Suppl 6**: p. vi14-21.
29. Jaworek-Korjakowska, J. and P. Kleczek, *Automatic Classification of Specific Melanocytic Lesions Using Artificial Intelligence.* Biomed Res Int, 2016. **2016**: p. 8934242.
30. Agarwala, S.S., et al., *Temozolomide for the treatment of brain metastases associated with metastatic melanoma: a phase II study.* J Clin Oncol, 2004. **22**(11): p. 2101-7.
31. Hodi, F.S., et al., *Improved survival with ipilimumab in patients with metastatic melanoma.* N Engl J Med, 2010. **363**(8): p. 711-23.
32. Johnson, D.B. and J.A. Sosman, *Therapeutic Advances and Treatment Options in Metastatic Melanoma.* JAMA Oncol, 2015. **1**(3): p. 380-6.
33. Schadendorf, D., et al., *Pooled Analysis of Long-Term Survival Data From Phase II and Phase III Trials of Ipilimumab in Unresectable or Metastatic Melanoma.* J Clin Oncol, 2015. **33**(17): p. 1889-94.
34. O'Donnell, J.S., et al., *Resistance to PD1/PDL1 checkpoint inhibition.* Cancer Treat Rev, 2017. **52**: p. 71-81.
35. Bhatia, S., S.S. Tykodi, and J.A. Thompson, *Treatment of metastatic melanoma: an overview.* Oncology (Williston Park), 2009. **23**(6): p. 488-96.
36. Wagle, N., et al., *Dissecting therapeutic resistance to RAF inhibition in melanoma by tumor genomic profiling.* J Clin Oncol, 2011. **29**(22): p. 3085-96.
37. Villanueva, J., et al., *Acquired resistance to BRAF inhibitors mediated by a RAF kinase switch in melanoma can be overcome by cotargeting MEK and IGF-1R/PI3K.* Cancer Cell, 2010. **18**(6): p. 683-95.
38. Girotti, M.R., et al., *Inhibiting EGF receptor or SRC family kinase signaling overcomes BRAF inhibitor resistance in melanoma.* Cancer Discov, 2013. **3**(2): p. 158-67.
39. Tsao, H., M.B. Atkins, and A.J. Sober, *Management of cutaneous melanoma.* N Engl J Med, 2004. **351**(10): p. 998-1012.
40. Robert, C., et al., *Anti-programmed-death-receptor-1 treatment with pembrolizumab in ipilimumab-refractory advanced melanoma: a randomised dose-comparison cohort of a phase 1 trial.* Lancet, 2014. **384**(9948): p. 1109-17.
41. Chapman, P.B., et al., *Improved survival with vemurafenib in melanoma with BRAF V600E mutation.* N Engl J Med, 2011. **364**(26): p. 2507-16.
42. Hauschild, A., et al., *Dabrafenib in BRAF-mutated metastatic melanoma: a multicentre, open-label, phase 3 randomised controlled trial.* Lancet, 2012. **380**(9839): p. 358-65.
43. Flaherty, K.T., et al., *Improved survival with MEK inhibition in BRAF-mutated melanoma.* N Engl J Med, 2012. **367**(2): p. 107-14.
44. Flaherty, K.T., et al., *Combined BRAF and MEK inhibition in melanoma with BRAF V600 mutations.* N Engl J Med, 2012. **367**(18): p. 1694-703.
45. Andreassen, R.C., *The role of MITF in the regulation of CDKN2A in melanoma*, in *Department of Bioscience*. 2017, UNIVERSITY OF OSLO Norway.
46. James Frederick , P.-C., MMSc, *New Clinical Trial Underway for Treatment of Advanced Melanoma*, in *Melanoma News Today*. 2017: Dallas, TX 75206.
47. Wan, P.T., et al., *Mechanism of activation of the RAF-ERK signaling pathway by oncogenic mutations of B-RAF.* Cell, 2004. **116**(6): p. 855-67.
48. Muller, J., et al., *Low MITF/AXL ratio predicts early resistance to multiple targeted drugs in melanoma.* Nat Commun, 2014. **5**: p. 5712.
49. Lai, K.O. and N.Y. Ip, *Methods to Study the Signal Transduction of the Surface Receptor Tyrosine Kinase TrkB in Neurons.* Methods Mol Biol, 2018. **1722**: p. 211-222.
50. Butti, R., et al., *Receptor tyrosine kinases (RTKs) in breast cancer: signaling, therapeutic implications and challenges.* Mol Cancer, 2018. **17**(1): p. 34.

51. Lemmon, M.A. and J. Schlessinger, *Cell signaling by receptor tyrosine kinases.* Cell, 2010. **141**(7): p. 1117-34.
52. Blume-Jensen, P. and T. Hunter, *Oncogenic kinase signalling.* Nature, 2001. **411**(6835): p. 355-65.
53. Chen, M.K. and M.C. Hung, *Regulation of therapeutic resistance in cancers by receptor tyrosine kinases.* Am J Cancer Res, 2016. **6**(4): p. 827-42.
54. Chen, M.K. and M.C. Hung, *Proteolytic cleavage, trafficking, and functions of nuclear receptor tyrosine kinases.* Febs j, 2015. **282**(19): p. 3693-721.
55. Hollenhorst, P.C., *RAS/ERK pathway transcriptional regulation through ETS/AP-1 binding sites.* Small GTPases, 2012. **3**(3): p. 154-8.
56. Hitomi, M. and D.W. Stacey, *Cyclin D1 production in cycling cells depends on ras in a cell-cycle-specific manner.* Curr Biol, 1999. **9**(19): p. 1075-84.
57. Holt, K.H., et al., *Phosphatidylinositol 3-kinase activation is mediated by high-affinity interactions between distinct domains within the p110 and p85 subunits.* Mol Cell Biol, 1994. **14**(1): p. 42-9.
58. Cantley, L.C., *The phosphoinositide 3-kinase pathway.* Science, 2002. **296**(5573): p. 1655-7.
59. Dasari, A. and W.A. Messersmith, *New strategies in colorectal cancer: biomarkers of response to epidermal growth factor receptor monoclonal antibodies and potential therapeutic targets in phosphoinositide 3-kinase and mitogen-activated protein kinase pathways.* Clin Cancer Res, 2010. **16**(15): p. 3811-8.
60. Song, G., G. Ouyang, and S. Bao, *The activation of Akt/PKB signaling pathway and cell survival.* J Cell Mol Med, 2005. **9**(1): p. 59-71.
61. Yuan, T.L. and L.C. Cantley, *PI3K pathway alterations in cancer: variations on a theme.* Oncogene, 2008. **27**(41): p. 5497-510.
62. Linger, R.M., et al., *TAM receptor tyrosine kinases: biologic functions, signaling, and potential therapeutic targeting in human cancer.* Adv Cancer Res, 2008. **100**: p. 35-83.
63. Graham, D.K., et al., *The TAM family: phosphatidylserine sensing receptor tyrosine kinases gone awry in cancer.* Nat Rev Cancer, 2014. **14**(12): p. 769-85.
64. Tsou, W.I., et al., *Receptor tyrosine kinases, TYRO3, AXL, and MER, demonstrate distinct patterns and complex regulation of ligand-induced activation.* J Biol Chem, 2014. **289**(37): p. 25750-63.
65. Anderson, H.A., et al., *Serum-derived protein S binds to phosphatidylserine and stimulates the phagocytosis of apoptotic cells.* Nat Immunol, 2003. **4**(1): p. 87-91.
66. Angelillo-Scherrer, A., et al., *Deficiency or inhibition of Gas6 causes platelet dysfunction and protects mice against thrombosis.* Nat Med, 2001. **7**(2): p. 215-21.
67. Paccez, J.D., et al., *The receptor tyrosine kinase Axl in cancer: biological functions and therapeutic implications.* Int J Cancer, 2014. **134**(5): p. 1024-33.
68. Liu, E., B. Hjelle, and J.M. Bishop, *Transforming genes in chronic myelogenous leukemia.* Proc Natl Acad Sci U S A, 1988. **85**(6): p. 1952-6.
69. O'Bryan, J.P., et al., *axl, a transforming gene isolated from primary human myeloid leukemia cells, encodes a novel receptor tyrosine kinase.* Mol Cell Biol, 1991. **11**(10): p. 5016-31.
70. McCloskey, P., et al., *GAS6 mediates adhesion of cells expressing the receptor tyrosine kinase Axl.* J Biol Chem, 1997. **272**(37): p. 23285-91.
71. Neubauer, A., et al., *Expression of axl, a transforming receptor tyrosine kinase, in normal and malignant hematopoiesis.* Blood, 1994. **84**(6): p. 1931-41.
72. Melaragno, M.G., et al., *Gas6 inhibits apoptosis in vascular smooth muscle: role of Axl kinase and Akt.* J Mol Cell Cardiol, 2004. **37**(4): p. 881-7.
73. Stenhoff, J., B. Dahlback, and S. Hafizi, *Vitamin K-dependent Gas6 activates ERK kinase and stimulates growth of cardiac fibroblasts.* Biochem Biophys Res Commun, 2004. **319**(3): p. 871-8.
74. Hafizi, S. and B. Dahlback, *Gas6 and protein S. Vitamin K-dependent ligands for the Axl receptor tyrosine kinase subfamily.* Febs j, 2006. **273**(23): p. 5231-44.

75. Migdall, J.G., DK, *AXL (AXL receptor tyrosine kinase).* Atlas of Genetics and Cytogenetics in Oncology and Haematology, 2010-02.
76. Braunger, J., et al., *Intracellular signaling of the Ufo/Axl receptor tyrosine kinase is mediated mainly by a multi-substrate docking-site.* Oncogene, 1997. **14**(22): p. 2619-31.
77. Schmidt, T., et al., *Macrophage-tumor crosstalk: role of TAMR tyrosine kinase receptors and of their ligands.* Cell Mol Life Sci, 2012. **69**(9): p. 1391-414.
78. Levin, P.A., et al., *Axl Receptor Axis: A New Therapeutic Target in Lung Cancer.* J Thorac Oncol, 2016. **11**(8): p. 1357-1362.
79. Lew, E.D., et al., *Differential TAM receptor-ligand-phospholipid interactions delimit differential TAM bioactivities.* Elife, 2014. **3**.
80. Hasanbasic, I., I. Rajotte, and M. Blostein, *The role of gamma-carboxylation in the anti-apoptotic function of gas6.* J Thromb Haemost, 2005. **3**(12): p. 2790-7.
81. Kirane, A., et al., *Warfarin Blocks Gas6-Mediated Axl Activation Required for Pancreatic Cancer Epithelial Plasticity and Metastasis.* Cancer Res, 2015. **75**(18): p. 3699-705.
82. Mark, M.R., et al., *Characterization of Gas6, a member of the superfamily of G domain-containing proteins, as a ligand for Rse and Axl.* J Biol Chem, 1996. **271**(16): p. 9785-9.
83. Jin, Y., et al., *Gas6/AXL Signaling Regulates Self-Renewal of Chronic Myelogenous Leukemia Stem Cells by Stabilizing beta-Catenin.* Clin Cancer Res, 2017. **23**(11): p. 2842-2855.
84. Whitty, A., *A Particularly Discriminating Receptor.* Cell Syst, 2015. **1**(1): p. 14-5.
85. Lemke, G. and T. Burstyn-Cohen, *TAM receptors and the clearance of apoptotic cells.* Ann N Y Acad Sci, 2010. **1209**: p. 23-9.
86. Meyer, A.S., A.J. Zweemer, and D.A. Lauffenburger, *The AXL Receptor is a Sensor of Ligand Spatial Heterogeneity.* Cell Syst, 2015. **1**(1): p. 25-36.
87. Korshunov, V.A., *Axl-dependent signalling: a clinical update.* Clin Sci (Lond), 2012. **122**(8): p. 361-8.
88. Hafizi, S. and B. Dahlback, *Signalling and functional diversity within the Axl subfamily of receptor tyrosine kinases.* Cytokine Growth Factor Rev, 2006. **17**(4): p. 295-304.
89. Goruppi, S., et al., *Gas6-mediated survival in NIH3T3 cells activates stress signalling cascade and is independent of Ras.* Oncogene, 1999. **18**(29): p. 4224-36.
90. Adam, L., et al., *Regulation of microfilament reorganization and invasiveness of breast cancer cells by kinase dead p21-activated kinase-1.* J Biol Chem, 2000. **275**(16): p. 12041-50.
91. Allen, M.P., et al., *Novel mechanism for gonadotropin-releasing hormone neuronal migration involving Gas6/Ark signaling to p38 mitogen-activated protein kinase.* Mol Cell Biol, 2002. **22**(2): p. 599-613.
92. Honda, H., et al., *Serial analysis of gene expression reveals differential expression between endometriosis and normal endometrium. Possible roles for AXL and SHC1 in the pathogenesis of endometriosis.* Reprod Biol Endocrinol, 2008. **6**: p. 59.
93. Brown, M., et al., *Gene of the month: <em>Axl</em&gt.* Journal of Clinical Pathology, 2016. **69**(5): p. 391.
94. Rothlin, C.V., et al., *TAM receptors are pleiotropic inhibitors of the innate immune response.* Cell, 2007. **131**(6): p. 1124-36.
95. Alvarez, J.V., et al., *Signal transducer and activator of transcription 3 is required for the oncogenic effects of non-small-cell lung cancer-associated mutations of the epidermal growth factor receptor.* Cancer Res, 2006. **66**(6): p. 3162-8.
96. Li, Y., et al., *Axl as a potential therapeutic target in cancer: role of Axl in tumor growth, metastasis and angiogenesis.* Oncogene, 2009. **28**(39): p. 3442-55.
97. Zhao, W., Y. Li, and X. Zhang, *Stemness-Related Markers in Cancer.* Cancer Transl Med, 2017. **3**(3): p. 87-95.
98. Raysi Dehcordi, S., et al., *Stemness Marker Detection in the Periphery of Glioblastoma and Ability of Glioblastoma to Generate Glioma Stem Cells: Clinical Correlations.* World Neurosurg, 2017. **105**: p. 895-905.

99. Garg, M., *Epithelial-mesenchymal transition - activating transcription factors - multifunctional regulators in cancer.* World J Stem Cells, 2013. **5**(4): p. 188-95.
100. Vuoriluoto, K., et al., *Vimentin regulates EMT induction by Slug and oncogenic H-Ras and migration by governing Axl expression in breast cancer.* Oncogene, 2011. **30**(12): p. 1436-48.
101. Zhang, Z., et al., *Activation of the AXL kinase causes resistance to EGFR-targeted therapy in lung cancer.* Nat Genet, 2012. **44**(8): p. 852-60.
102. Liu, L., et al., *Novel mechanism of lapatinib resistance in HER2-positive breast tumor cells: activation of AXL.* Cancer Res, 2009. **69**(17): p. 6871-8.
103. Dufies, M., et al., *Mechanisms of AXL overexpression and function in Imatinib-resistant chronic myeloid leukemia cells.* Oncotarget, 2011. **2**(11): p. 874-85.
104. Sainaghi, P.P., et al., *Gas6 induces proliferation in prostate carcinoma cell lines expressing the Axl receptor.* J Cell Physiol, 2005. **204**(1): p. 36-44.
105. Shieh, Y.S., et al., *Expression of axl in lung adenocarcinoma and correlation with tumor progression.* Neoplasia, 2005. **7**(12): p. 1058-64.
106. Hutterer, M., et al., *Axl and growth arrest-specific gene 6 are frequently overexpressed in human gliomas and predict poor prognosis in patients with glioblastoma multiforme.* Clin Cancer Res, 2008. **14**(1): p. 130-8.
107. Zhang, Y., et al., *Knockdown of AXL receptor tyrosine kinase in osteosarcoma cells leads to decreased proliferation and increased apoptosis.* Int J Immunopathol Pharmacol, 2013. **26**(1): p. 179-88.
108. van Ginkel, P.R., et al., *Expression of the receptor tyrosine kinase Axl promotes ocular melanoma cell survival.* Cancer Res, 2004. **64**(1): p. 128-34.
109. Melaragno, M.G., Y.W. Fridell, and B.C. Berk, *The Gas6/Axl system: a novel regulator of vascular cell function.* Trends Cardiovasc Med, 1999. **9**(8): p. 250-3.
110. Rankin, E.B., et al., *AXL is an essential factor and therapeutic target for metastatic ovarian cancer.* Cancer Res, 2010. **70**(19): p. 7570-9.
111. Xu, J., et al., *Axl gene knockdown inhibits the metastasis properties of hepatocellular carcinoma via PI3K/Akt-PAK1 signal pathway.* Tumour Biol, 2014. **35**(4): p. 3809-17.
112. Sawabu, T., et al., *Growth arrest-specific gene 6 and Axl signaling enhances gastric cancer cell survival via Akt pathway.* Mol Carcinog, 2007. **46**(2): p. 155-64.
113. Paolino, M., et al., *The E3 ligase Cbl-b and TAM receptors regulate cancer metastasis via natural killer cells.* Nature, 2014. **507**(7493): p. 508-12.
114. Berclaz, G., et al., *Estrogen dependent expression of the receptor tyrosine kinase axl in normal and malignant human breast.* Ann Oncol, 2001. **12**(6): p. 819-24.
115. Holland, S.J., et al., *Multiple roles for the receptor tyrosine kinase axl in tumor formation.* Cancer Res, 2005. **65**(20): p. 9294-303.
116. Rankin, E.B., et al., *Direct regulation of GAS6/AXL signaling by HIF promotes renal metastasis through SRC and MET.* Proc Natl Acad Sci U S A, 2014. **111**(37): p. 13373-8.
117. Tai, K.Y., et al., *Axl promotes cell invasion by inducing MMP-9 activity through activation of NF-kappaB and Brg-1.* Oncogene, 2008. **27**(29): p. 4044-55.
118. Brand, T.M., et al., *AXL mediates resistance to cetuximab therapy.* Cancer Res, 2014. **74**(18): p. 5152-64.
119. Zhao, Y., et al., *Differential expression of Axl and correlation with invasion and multidrug resistance in cancer cells.* Cancer Invest, 2012. **30**(4): p. 287-94.
120. Tie, J.K., et al., *Functional study of the vitamin K cycle in mammalian cells.* Blood, 2011. **117**(10): p. 2967-74.
121. Tie, J.K. and D.W. Stafford, *Functional Study of the Vitamin K Cycle Enzymes in Live Cells.* Methods Enzymol, 2017. **584**: p. 349-394.
122. Shearer, M.J. and P. Newman, *Recent trends in the metabolism and cell biology of vitamin K with special reference to vitamin K cycling and MK-4 biosynthesis.* J Lipid Res, 2014. **55**(3): p. 345-62.

123. Ouirke, W., et al., *Warfarin prevalence, indications for use and haemorrhagic events.* Ir Med J, 2007. **100**(3): p. 402-4.
124. Takahashi, H. and H. Echizen, *Pharmacogenetics of warfarin elimination and its clinical implications.* Clin Pharmacokinet, 2001. **40**(8): p. 587-603.
125. Gage, B.F. and L.J. Lesko, *Pharmacogenetics of warfarin: regulatory, scientific, and clinical issues.* J Thromb Thrombolysis, 2008. **25**(1): p. 45-51.
126. Haaland, G.S., et al., *Association of Warfarin Use With Lower Overall Cancer Incidence Among Patients Older Than 50 Years.* JAMA Intern Med, 2017. **177**(12): p. 1774-1780.
127. Zuo, Q., et al., *AXL/AKT axis mediated-resistance to BRAF inhibitor depends on PTEN status in melanoma.* Oncogene, 2018.
128. Sensi, M., et al., *Human cutaneous melanomas lacking MITF and melanocyte differentiation antigens express a functional Axl receptor kinase.* J Invest Dermatol, 2011. **131**(12): p. 2448-57.
129. Tworkoski, K., et al., *Phosphoproteomic screen identifies potential therapeutic targets in melanoma.* Mol Cancer Res, 2011. **9**(6): p. 801-12.
130. Cohen-Solal, K.A., H.L. Kaufman, and A. Lasfar, *Transcription factors as critical players in melanoma invasiveness, drug resistance, and opportunities for therapeutic drug development.* Pigment Cell Melanoma Res, 2018. **31**(2): p. 241-252.
131. Rajotte, I., I. Hasanbasic, and M. Blostein, *Gas6-mediated signaling is dependent on the engagement of its gamma-carboxyglutamic acid domain with phosphatidylserine.* Biochem Biophys Res Commun, 2008. **376**(1): p. 70-3.
132. D'mello, S.A.N., *An Investigation into GRIN2A Mutations in Human Melanoma*. 2015, University of Auckland: New Zealand.
133. Jang, T.H., et al., *Cryopreservation and its clinical applications.* Integr Med Res, 2017. **6**(1): p. 12-18.
134. Cadena-Herrera, D., et al., *Validation of three viable-cell counting methods: Manual, semi-automated, and automated.* Biotechnol Rep (Amst), 2015. **7**: p. 9-16.
135. Joyce, C., *Quantitative RT-PCR. A review of current methodologies.* Methods Mol Biol, 2002. **193**: p. 83-92.
136. Dheda, K., et al., *Validation of housekeeping genes for normalizing RNA expression in real-time PCR.* Biotechniques, 2004. **37**(1): p. 112-4, 116, 118-9.
137. Rao, X., et al., *An improvement of the 2^(-delta delta CT) method for quantitative real-time polymerase chain reaction data analysis.* Biostat Bioinforma Biomath, 2013. **3**(3): p. 71-85.
138. Finak, G., et al., *Standardizing Flow Cytometry Immunophenotyping Analysis from the Human ImmunoPhenotyping Consortium.* Sci Rep, 2016. **6**: p. 20686.
139. Spitzer, M.H. and G.P. Nolan, *Mass Cytometry: Single Cells, Many Features.* Cell, 2016. **165**(4): p. 780-91.
140. Janes, M.R. and C. Rommel, *Next-generation flow cytometry.* Nat Biotechnol, 2011. **29**(7): p. 602-4.
141. Pittman, R.N., *Oxygen gradients in the microcirculation.* Acta Physiol (Oxf), 2011. **202**(3): p. 311-22.
142. Reddy, B.Y., D.M. Miller, and H. Tsao, *Somatic driver mutations in melanoma.* Cancer, 2017. **123**(S11): p. 2104-2117.
143. Holderfield, M., et al., *Targeting RAF kinases for cancer therapy: BRAF-mutated melanoma and beyond.* Nat Rev Cancer, 2014. **14**(7): p. 455-67.
144. Nazarian, R., et al., *Melanomas acquire resistance to B-RAF(V600E) inhibition by RTK or N-RAS upregulation.* Nature, 2010. **468**(7326): p. 973-7.
145. Luong, Y.J., *Identification of Inhibitors of Vitamin K-Dependent Gamma-Carboxylation*, in *Centre of Pharmacy, Department of Biomedicine*. 2018, University of Bergen: Bergen, Norway.
146. Costa, M., P. Bellosta, and C. Basilico, *Cleavage and release of a soluble form of the receptor tyrosine kinase ARK in vitro and in vivo.* J Cell Physiol, 1996. **168**(3): p. 737-44.

147. Ekman, C., J. Stenhoff, and B. Dahlback, *Gas6 is complexed to the soluble tyrosine kinase receptor Axl in human blood.* J Thromb Haemost, 2010. **8**(4): p. 838-44.
148. Shaffer, S.M., et al., *Rare cell variability and drug-induced reprogramming as a mode of cancer drug resistance.* Nature, 2017. **546**: p. 431.
149. Mudduluru, G., et al., *Regulation of Axl receptor tyrosine kinase expression by miR-34a and miR-199a/b in solid cancer.* Oncogene, 2011. **30**(25): p. 2888-99.
150. Song, X., et al., *Overexpression of receptor tyrosine kinase Axl promotes tumor cell invasion and survival in pancreatic ductal adenocarcinoma.* Cancer, 2011. **117**(4): p. 734-43.
151. Rahman, N.I.A., et al., *NFIX as a Master Regulator for Lung Cancer Progression.* Front Pharmacol, 2017. **8**: p. 540.
152. Institute, B., *Cancer Cell Encyclopedia*. 2018, The Broad Institute of MIT & Harvard: USA.
153. Chilla, A., et al., *Mature and progenitor endothelial cells perform angiogenesis also under protease inhibition: the amoeboid angiogenesis.* J Exp Clin Cancer Res, 2018. **37**(1): p. 74.
154. Strong, A.D. and R.L. Daniels, *Live-cell calcium imaging of adherent and non-adherent GL261 cells reveals phenotype-dependent differences in drug responses.* BMC Cancer, 2017. **17**.
155. Asiedu, M.K., et al., *AXL induces epithelial-to-mesenchymal transition and regulates the function of breast cancer stem cells.* Oncogene, 2014. **33**(10): p. 1316-24.
156. Yang, J., et al., *Twist, a master regulator of morphogenesis, plays an essential role in tumor metastasis.* Cell, 2004. **117**(7): p. 927-39.
157. Bilandzic, M. and K.L. Stenvers, *Assessment of Ovarian Cancer Spheroid Attachment and Invasion of Mesothelial Cells in Real Time.* J Vis Exp, 2014(87).
158. Stadler, M., et al., *Exclusion from spheroid formation identifies loss of essential cell-cell adhesion molecules in colon cancer cells.* Scientific Reports, 2018. **8**(1): p. 1151.
159. Nalwoga, H., et al., *Strong Expression of Hypoxia-Inducible Factor-1alpha (HIF-1alpha) Is Associated with Axl Expression and Features of Aggressive Tumors in African Breast Cancer.* PLoS One, 2016. **11**(1): p. e0146823.
160. Wang, Z., et al., *The growth inhibitory effects of vitamins K and their actions on gene expression.* Hepatology, 1995. **22**(3): p. 876-82.
161. Ronning, S.B., et al., *Vitamin K2 improves proliferation and migration of bovine skeletal muscle cells in vitro.* PLoS One, 2018. **13**(4): p. e0195432.
162. Bai-Chun Liu, Y.S., Feng Li, Li-Juan Wei, Jun-An Li, *Vitamin K2-induced inhibition of colorectal cancer cell proliferation and its underlying mechanisms.* international Journal of Clinical and Experimental Pathology, 2016. **Volume 11, Number 4:1841-2269;2018**.
163. Uribe, D.J., et al., *The receptor tyrosine kinase AXL promotes migration and invasion in colorectal cancer.* PLoS One, 2017. **12**(7): p. e0179979.
164. Fleuren, E.D., et al., *The role of AXL and the in vitro activity of the receptor tyrosine kinase inhibitor BGB324 in Ewing sarcoma.* Oncotarget, 2014. **5**(24): p. 12753-68.
165. Pao-Chun, L., et al., *Cytoplasmic ACK1 interaction with multiple receptor tyrosine kinases is mediated by Grb2: an analysis of ACK1 effects on Axl signaling.* J Biol Chem, 2009. **284**(50): p. 34954-63.
166. Fridell, R.A., H.P. Bogerd, and B.R. Cullen, *Nuclear export of late HIV-1 mRNAs occurs via a cellular protein export pathway.* Proc Natl Acad Sci U S A, 1996. **93**(9): p. 4421-4.